PB 84-209402

REPORT NO.
UCB/EERC-84/02
APRIL 1984

EARTHQUAKE ENGINEERING RESEARCH CENTER

DYNAMIC RESPONSE BEHAVIOR OF XIANG HONG DIAN DAM

by

R. W. CLOUGH
K.-T. CHANG
H.-Q. CHEN
R. M. STEPHEN
G.-L. WANG
Y. GHANAAT

Report to the National Science Foundation on
Research conducted under the U.S.-China Protocol for
Scientific and Technical Cooperation in Earthquake Studies

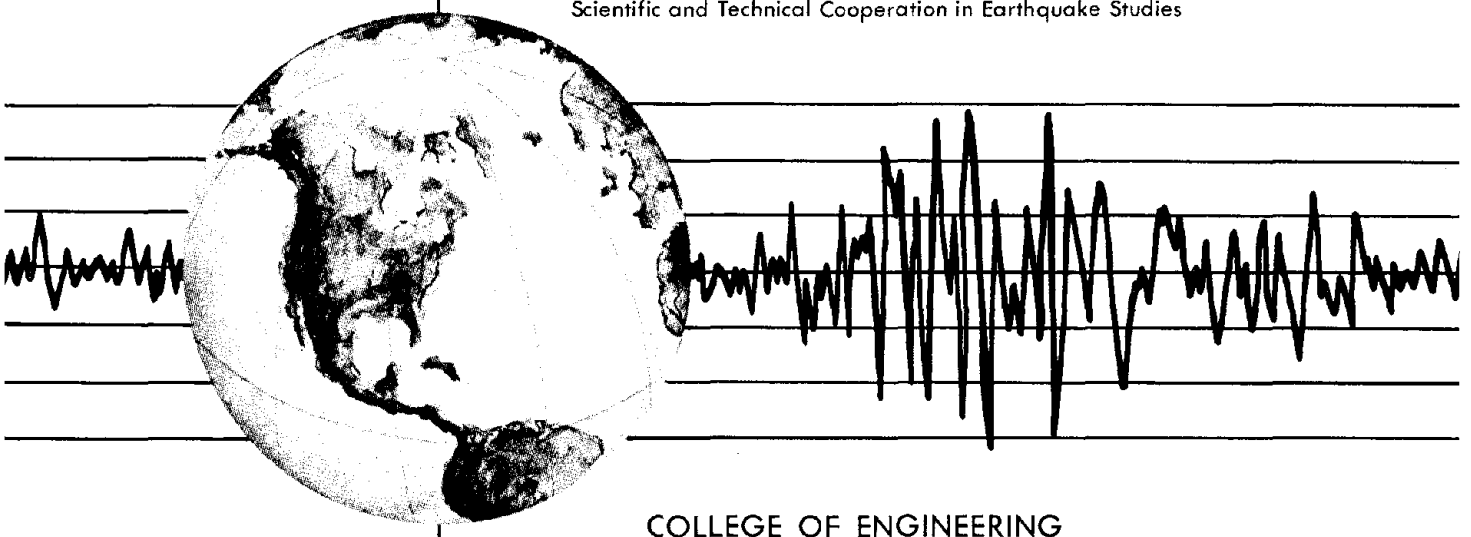

COLLEGE OF ENGINEERING

UNIVERSITY OF CALIFORNIA · Berkeley, California

For sale by the National Technical Information Service, U.S. Department of Commerce, Springfield, Virginia 22161.

See back of report for up to date listing of EERC reports.

DISCLAIMER

50272-101

REPORT DOCUMENTATION PAGE	1. REPORT NO. NSF/CEE - 84017	2.	3. Recipient's Accession No. PB84 209402
4. Title and Subtitle: DYNAMIC RESPONSE BEHAVIOR OF XIANG HONG DIAN DAM			5. Report Date: April, 1984 6.
7. Author(s): R. Clough, K.-T. Chang, H.-Q. Chen, R. Stephen, G.-L. Wang, & Y. Ghanaat			8. Performing Organization Rept. No. UCB/EERC-84/02
9. Performing Organization Name and Address: Earthquake Engineering Research Center, University of California, 1301 South 46th Street, Richmond, CA 94804			10. Project/Task/Work Unit No. 11. Contract(C) or Grant(G) No. (C) (G) CEE-8214198
12. Sponsoring Organization Name and Address: National Science Foundation, 1800 "G" Street NW, Washington, DC 20050			13. Type of Report & Period Covered 14.

15. Supplementary Notes

16. Abstract (Limit: 200 words) This study of Xiang Hong Dian Dam is the first phase of a U.S.-China cooperative project on "Interaction Effects in the Seismic Response of Arch Dams" and was carried out by the Scientific Research Institute of Water Conservancy and Hydroelectric Power and Tsinghua University, Beijing, and the Earthquake Engineering Research Center, University of California, Berkeley.

The purpose of this study was to evaluate and improve the mathematical models used to represent the foundation rock and the reservoir. Measurements were made of the vibration behavior of Xiang Hong Dian Dam, a single curvature arch located in Anhui Province, China. Vibrations were excited by rotating mass shakers and also by ambient vibration effects in the environment; measured vibration mode shapes and frequencies were then compared with a finite element model analysis of the dam, reservoir, and foundation rock.

The study showed that (1) a foundation rock model extending a distance equal to the dam height in all directions from the dam-rock interface is sufficient to represent the interaction, (2) the reservoir can be modelled adequately by a mesh of incompressible liquid elements extending upstream a distance three times the dam height. Using these interaction models excellent agreement was obtained between the experimental and analytical vibration properties, after the modulus of elasticity of the concrete had been adjusted properly.

17. Document Analysis a. Descriptors

b. Identifiers/Open-Ended Terms

c. COSATI Field/Group

18. Availability Statement: Release Unlimited	19. Security Class (This Report)	21. No. of Pages 168
	20. Security Class (This Page)	22. Price

DYNAMIC RESPONSE BEHAVIOR OF XIANG HONG DIAN DAM

by

Ray W. Clough; K.-T. Chang
Huo-Qun Chen; Roy M. Stephen
Guang-Lung Wang; Yusof Ghanaat

A Report on Research Conducted under the
U.S.-China Protocol
for Scientific and Technical Cooperation in
Earthquake Studies

Report No. UCB/EERC-84/02

Earthquake Engineering Research Center
University of California
Berkeley, California

April 1984

ABSTRACT

This study of Xiang Hong Dian Dam is the first phase of a cooperative research project on "Interaction Effects in the Seismic Response of Arch Dams" being carried out under the U.S.-China Protocol for Scientific and Technical Cooperation in Earthquake Studies. The cooperating organizations are the Scientific Research Institute of Water Conservancy and Hydroelectric Power and Tsinghua University, of Beijing, and the Earthquake Engineering Research Center of the University of California, Berkeley.

In this study, measurements were made of the vibration behavior of Xiang Hong Dian Dam, a single curvature arch located in Anhui Province, China; the vibrations were excited both by rotating mass shakers and also by ambient vibration effects in the environment. The measured vibration mode shapes and frequencies were then compared with results obtained analytically using a finite element model of the dam, the reservoir, and the foundation rock. The purpose of the study was to evaluate and improve the mathematical models used to represent the foundation rock and the reservoir.

The essential results of the study are (1) a foundation rock model extending a distance equal to the dam height in all directions from the dam-rock interface is sufficient to represent the interaction, (2) the reservoir can be modelled adequately by a mesh of incompressible liquid elements extending upstream a distance three times the dam height, and (3) using these interaction models excellent agreement was obtained between the experimental and analytical vibration properties, after the modulus of elasticity of the concrete had been adjusted properly. Further research is needed to determine if these conclusions also may be applied to other arch dams.

PUBLICATION NOTE

This report is being published simultaneously by the Scientific Research Institute for Water Conservancy and Hydroelectric Power of Beijing and by the Earthquake Engineering Research Center of the University of California, Berkeley. The report produced by each organization is provided with the standard cover for that organization.

TABLE OF CONTENTS

TABLE OF CONTENTS (Cont'd) Page

TABLE OF CONTENTS (Cont'd) Page

LIST OF TABLES

LIST OF TABLES (Cont'd)

LIST OF FIGURES

Chapter 1

INTRODUCTION

1.1 BACKGROUND

A concrete arch dam impounding a large reservoir presents a major potential hazard to downstream centers of population, especially if the dam is located in an active seismic region. Therefore, even though there is no record that a major arch dam ever has suffered significant damage during an earthquake, it is essential to develop and verify procedures for calculating the earthquake performance of proposed designs or existing dams.

In principle, an arch dam is a typical form of structural system suitable for analysis by standard finite element procedures, using available general purpose structural analysis computer programs. However, two features of an arch dam greatly complicate its structural performance. First, such a structure is extremely stiff and massive, and it imposes significant deformations on its foundation even though an arch dam will be built only on a stiff, strong rock base. These deformations are important even under static load, but they have a much greater influence on the dynamic response during an earthquake. The second complicating feature of any concrete dam system is the water in the reservoir. Under static conditions this merely subjects the dam to an easily determined load, but during an earthquake the mass of the water provides significant inertial resistance to the dynamic response, and thus influences both the frequency characteristics and the intensity of the resulting response.

Analytical procedures to account for the effects of both types of interaction have been included in earthquake response calculations of concrete dams for several decades. Typically the reservoir interaction has been represented by an added mass applied to the face of the dam[1],

although more recent research has suggested that the compressibility of the reservoir water should be considered as well as its mass[2]. Foundation interaction was modeled traditionally by flexibility coefficients defined for the interface between the dam concrete and the foundation rock[3]; however, with the introduction of the finite element method it has become customary to include a block of foundation rock directly in the mathematical model of the dam-foundation system[4]. It is the purpose of the research program described in this report to make a quantitative evaluation of the best analytical procedures for taking account of these interaction mechanisms by correlation of vibration measurements made on arch dams in the field with predictions based on mathematical analyses. It should be noted that field measurements of the vibration properties of arch dams have been made many times in the past, and these measured results often have been correlated with evaluated results[5]. However, none of these previous field experimental studies have been directed primarily towards the effects of reservoir or foundation interaction, or toward verifying the analytical procedures used to represent these effects.

1.2 ORGANIZATION OF THE RESEARCH PROJECT

The present study was initiated in 1982 as a three year cooperative research project entitled "Interaction Effects in the Seismic Response of Arch Dams", administered under the U.S.-China Protocol for Scientific and Technical Cooperation in Earthquake Studies. The cooperating institutions are the Earthquake Engineering Research Center (EERC) of the University of California at Berkeley, acting for the United States, and the Scientific Research Institute of Water Conservancy and Hydroelectric Power (SRIWCHP) together with Tsinghua University, both of Beijing, acting

for China. Professor R. W. Clough of the University of California and Vice President K. T. Chang of Tsinghua University were the Principal Investigators. Funding for the EERC part of the research was provided by the U.S. National Science Foundation, and funding for the SRIWCHP part was provided by the Ministry of Water Conservancy and Electric Power of China.

1.3 SCOPE OF THE INVESTIGATION

The complete investigation included making detailed vibration measurements of two arch dams in China, one of single curvature, the other of double curvature. The measured results from both dams are compared with analytical predictions obtained using the most refined mathematical procedures; conclusions are drawn concerning the validity of current procedures for modeling the interaction effects, and recommendations are made of the most effective analysis techniques.

The present report describes the investigation carried out on the first of the two dams studied in China: Xiang Hong Dian Dam in Anhui Province. The report is presented in four main chapters dealing with: Experimental Investigation, Analytical Study, Correlation of Experimental and Analytical Results, and Static and Earthquake Response Behavior. In a final section, conclusions drawn from the study of this first dam are summarized.

1.4 ACKNOWLEDGMENTS

Although the study of Xiang Hong Dian Dam was done under the nominal supervision of Professors Chang and Clough, it actually was a large team effort with major contributions made by many individuals. Among the principal participants, the following must be mentioned. The field work was done under the direct supervision of Mr. H.-Q. Chen, Vice-Head of Earthquake Engineering at SRIWCHP. Mr. Chen also supervised the reduction

of the field data taken by the PRC team and the preparation of a draft report on the experimental study. The U.S. part of the field investigation was supervised by Mr. R. M. Stephen, Principal Development Engineer of the University of California, Berkeley, and he also managed the reduction and processing of the U.S. experimental data. Mr. G. P. Lu Deputy Director of Scientific Research Institute for Water Conservancy of Anhui Province (SRIWCAP), also took part in this study, and he also was responsible for the SRIWCAP field investigation team. Mr. G. L. Wang, Visiting Research Engineer at EERC, on leave from the Department of Hydraulic Structures, Tsinghua University, did most of the analytical studies under the guidance of Dr. Y. Ghanaat, Consultant to the project; in addition Dr. Ghanaat made the necessary modifications of the ADAP program and also supervised the correlation of analytical and experimental results.

Chapter 2

EXPERIMENTAL INVESTIGATION

2.1 TEST STRUCTURE

After thorough review of single curvature arch dams in China, Xian Hong Dian Dam was selected as the vehicle for the first experimental study in this project. This is a relatively simple non-overflow gravity arch structure located in the middle reach of the Pi River in Jinzhai County of Anhui Province, as shown in Fig. 2.1. The Scientific Research Institute of Water Conservancy of Anhui Province (SRIWCAP) took an active part in the field measurement program. The photograph, Fig. 2.2, gives a general view of the dam and reservoir. The rock foundation at the dam site is mainly composed of magmatic rock with some tuff and breccia. It is located in a moderately active seismic zone where the maximum design earthquake intensity corresponds to MM III(i.e., intensity VIII in the Modified Mercalli Scale). The dam construction was completed in July 1958; the field measurements described in this report were carried out in August 1982.

As shown in the photograph, Fig. 2.3, the dam is constructed in a U-shaped valley, with a crest length-to-height ratio of 3.75. The maximum height above the river channel is 87.5 m (287.1 ft), the crest stands at 143.4 m above sea level, and the crest length is 361.0 m (1184.4 ft). Figure 2.4 gives a plan and a section view of the structure. It is 5.0 m (16.4 ft) thick at the crest and 39.0 m (128.0 ft) thick at the base, giving a maximum thickness to height ratio of 0.45. The radius of the extrados is constant at 180.0 m (590.6 ft); the intrados radius varies from 175.0 m (574.2 ft) at the crest to 141.0 m (462.6 ft) at the base, with a maximum central angle of 115°. The dam body consists of 25 blocks separated by

vertical contraction joints; except for the two abutment blocks, at the upstream face the length of the blocks is 14.0 m (45.9 ft). As may be seen in Figs. 2.3 and 2.4, four walkways are located on the downstream face, at elevations 127.0 m, 113.5 m, 100.0 m, and 86.5 m above sea level. The design level of the reservoir is 139.1 m, its surface is 1400 km^2, and the stored volume is 2,630 million cu. meters. A plan view of the reservoir is shown in Fig. 2.5.

2.2 TEST EQUIPMENT

The vibration properties of the dam were measured using both forced vibrations generated by rotating mass shakers as well as ambient vibrations. The vibration behavior was measured by velocity meters located at many points on the dam and by sensitive seismometers located on the foundation rock. In addition hydrodynamic pressures were measured in the reservoir during the forced vibration tests. The principal features of the various items of experimental equipment are summarized in this section.

2.2.1 Eccentric Mass Shakers

The rotating mass shakers used in this research program were recently designed and built at the SRIWCHP in Beijing; Fig. 2.6 is a photograph of a typical unit. As many as four of these units can be operated simultaneously, with one of them serving as the "master" in the control system and with the other "slave" units synchronized to operate in phase with the master or 180° out of phase. The frequency of the exciters is indicated digitally and can be controlled to 0.5% accuracy in each of three ranges: 0.5 to 5.0 Hz, 1.0 to 10 Hz, and 2.5 to 25 Hz. Figure 2.7 shows the shaker control units in operation in the instrumentation house. The phase difference between the exciters is controlled to less than 5

degrees; shifting between in-phase and out-of-phase operation of the slave units may be accomplished while they are in operation.

The force capacity of each shaker unit is 4000 kg. The exciting force depends on the speed of operation and the mass eccentricity, as indicated by the graph of Fig. 2.8. The mass eccentricity is provided by weights placed in baskets counter-rotating about two vertical shafts, as may be seen in Fig. 2.6. The large baskets seen in the photograph are used for low frequency operation; for testing at high frequencies, these baskets are removed and small baskets (not visible in the photo) are used instead.

2.2.2 Measurement Systems

The radial and tangential components of the forced vibration response of the dam were sensed by two sets of velocity meters, provided by SRIWCHP and SRIWCAP, respectively. A group of these velocity meters, designated Model 65, is shown in Fig. 2.9, prior to being positioned on the dam. Their natural frequency is 1 Hz and the damping ratio is set at 0.7 critical; sensitivity of the instrument is about 370 volt-sec/meter. Signal conditioners, Models GZ-5 and 701-5, were used to control and amplify each set of six velocity meters. In general, for this study the amplifiers were set in the integrating mode so that the resulting signal was proportional to displacement.

Five photorecording oscillographs, Model SC-16 and SC-18, and two magnetic tape recorders, Model SONY-14 and TEAC R 280C were used to record the signals from the velocity meters. The frequencies of the oscillograph galvanometers are 400 or 800 Hz. A common time mark was recorded simultaneously in all five oscillographs.

To measure the vibrations of the foundation rock during the forced vibration tests and also to measure ambient vibrations of the dam, very sensitive Kinemetrics Ranger seismometers Model SS-1 were employed. Figure 2.10 shows a Ranger seismometer in position on the rock at the dam abutment. Eight of these units were used in this study, four with a calibration of 165 volt-sec/meter and the others with 137 volt-sec/meter. Separate Kinemetric signal conditioner units, Model SC-1, were used to amplify and control each group of four seismometers; the nominal maximum gain in each channel was 100,000. The amplified analog signals were converted to digital form and recorded on magnetic tape using a Kinemetrics Digital Data System, Model DDS-1103.

Another piece of equipment that greatly facilitated the field measurement work was the Rockland Spectrum Analyzer Model 512-18. The analog signal from any of the transducers could be fed into this unit, where it was digitized on line and then processed digitally by a Fast Fourier Transform program to obtain the Fourier amplitude spectrum of the incoming signal. The resulting response spectrum of the dam motions gave a direct indication of its natural frequencies.

Hydrodynamic pressure measurements were made at the face of the dam during the forced vibration testing, using three Kistler Model 206 Piezotron low pressure, high sensitivity transducers. Each of these piezoelectric gages was connected to a Piezotron coupler and the output was fed to a Validyne integrating amplifier, Model AM49. With the amplifier set to its highest gain, the output sensitivity was about 0.08 psi/volt. Signals from these gages also were recorded on the Kinemetrics Digital Data System mentioned above.

2.2.3 Locations of Shakers and Transducers

During the test, the four shaking machines were deployed along the dam crest, each oriented to exert its force in the local radial direction. The arrangement of the four units were symmetrical, at distances of 46.7 and 92.8 meters each side of the center line of the dam (Block 13) as shown in Fig. 2.11. The "master" unit was mounted at Block 16 and the other three were located at Blocks 7, 10, and 19.

The velocity transducers were positioned on the dam crest and on the four downstream face walkways. A total of 57 velocity gage stations were used; on the right side of the dam; these were located at the crest and at the top walkway near the center of all blocks. At other levels on the right side of the dam and at all levels on the left side they were located only in the odd numbered blocks. One additional velocity meter station was located at crest level on the right abutment rock to provide correlation with data obtained on rock with other instruments.

The Ranger seismometer stations were established on the foundation rock of the right abutment except for one unit that was positioned next to the velocity meter at the crest of Block 3; this unit also was intended to provide correlation between measurements made with the two different types of gages. In general, the rock stations first were located at each level as close to the end of the dam as possible; then additional stations were established at the same levels at distances of 5 to 10 meters from the dam. A total of 14 Ranger stations were established including the one on the crest of the dam. In addition, four pressure gage stations were established on the right side of the center line; at each of these stations the pressure was to be measured at three water depths: 5m, 15m, and 25m, however, because of gage malfunction some of these measurements were not made.

The locations of the velocity gages, of the Ranger seismometers and of the pressure gages all are indicated on Fig. 2.12. Because there were more recording stations than instruments for each type of instrument, it was necessary to repeat the tests several times with the instruments moved to different locations. The tests had to be run four times to obtain all the Ranger seismometer readings.

2.3 EXPERIMENTAL PROCEDURES AND RESULTS

The fundamental dynamic properties of the dam that were measured in this test program were the vibration frequencies, the mode shapes, modal damping ratios and the distribution of hydrodynamic pressures during the forced vibration. Procedures used to determine each of these types of quantities and the results obtained are described in the following sections.

2.3.1 Vibration Frequencies

The ambient vibrations resulting from wind and wave action provided the simplest means of evaluating the vibration properties of the dam. For this purpose, ambient motions were measured in both radial and tangential directions by the Ranger seismometers located at 11 stations equally spaced across the crest of the dam. Three minute samples of data in each direction were recorded in digital form by the Kinematics recorder from each of the 11 transducer stations. Then after the tapes were returned to Berkeley, these digital records were converted to Fourier amplitude spectra by a Fast Fourier Transform computer program. The final result of this procedure is the relative amplitude of vibration in each direction at each gage station evaluated at frequency increments of 0.0244 Hz. A graph of these relative amplitudes plotted against the frequency is called a displacement frequency response curve. The ambient displacement frequency

response curve derived from data obtained at the crest of Block 12 is shown in Fig. 2.13. Of course the frequencies at which the peak responses are observed represent the natural vibration frequencies; these peak frequencies indicated in Fig. 2.13 are listed in Table 2.1.

Essentially the same concept is involved in the forced vibration determination of the natural frequencies, except that the vibratory motion is induced by the shaker system and thus is obtained for only one frequency at a time. Consequently, the relative motion observed for different frequencies at any selected point on the dam, or for different points on the dam at any selected frequency, can be observed directly on the oscillograph records, and there is no need to apply a Fourier transform analysis. To determine the peak response frequencies, the oscillograph records from several velocity meters located at the dam crest were monitored as the exciting frequency of the shaking machines was increased by increments. Near each resonance peak in the response curves, where the slope was changing rapidly with frequency, the frequency steps were made as small as the speed controller permitted (<0.05 Hz) in order to define the peak response frequency accurately; for frequencies far from resonance, the steps were made relatively large. Each time the frequency was set to a particular value, sufficient time was allowed for the response amplitude to stabilize before the traces were recorded; at the same time, the frequency was read from the digital counter of the control system and it was written on the chart. After the oscillograph records were returned from the field, the displacement amplitude at each frequency was read and normalized to a constant value of exciting force. These normalized amplitudes were then plotted versus frequency to obtain the forced vibration displacement frequency response curves. The curves obtained using symmetric and anti-symmetric excitation are presented

in Figs. 2.14 and 2.15, respectively. The corresponding forced vibration peak response frequencies are listed in Table 2.1, together with the ambient vibration results.

It is interesting to note that the forced and ambient frequency response curves show similar peaks for the frequency range up to about 7 Hz, but that an additional peak is seen on the ambient curve at 7.13 Hz which is not present on the forced vibration curve. This demonstrates a basic limitation of the forced vibration test procedure: the arrangement of the shaker system may not significantly excite some true vibration mode. Further comments concerning this "missing mode" will be made in the discussion of the analytical results.

Another point to be noted is that the reservoir surface level changed from 122.45 to 127.43 m during the test program, due to nearly continuous heavy rainfall. This 5 m raising of the water level caused significant increase in the reservoir added mass and led to noticeable reduction in the vibration frequencies. Thus, it is necessary to note the reservoir level in any listing of the vibration frequencies; this point will be discussed later in the correlation of experimental and analytical results (Chapter 4).

2.3.2 Mode Shapes

The vibration mode shapes were obtained easily from the ambient vibration measurements because the Fourier amplitude spectra indicate directly the relative displacement amplitude at each frequency. Thus, the vibration shape for each modal frequency was obtained by merely observing the relative amplitude recorded at each Ranger seismometer station at the peak response frequencies. Corrections were made for differences in sensitivity of the seismometers by applying the relative sensitivity factors indicated by measurements made with all instruments

positioned at the same point on the dam. It will be noted that the ambient vibration mode shapes (shown in Figs. 2.31 to 2.36 and discussed later in this section) were obtained only at the dam crest because it was assumed that the ambient motions at other levels would not be large enough to be recorded effectively.

In concept, the procedure for determining mode shapes from the forced vibration tests was similar except that it was necessary to take readings of the relative response amplitudes only at the peak response frequencies already determined. Operating the shakers continuously at each such frequency, response amplitudes were measured at all stations on the dam and in the foundation rock. As mentioned earlier, it was necessary to move the transducers several times to observe the response at all stations; in order to ensure consistent results, one reference transducer was retained in the same location as the others were moved, then all measured values were adjusted to correspond to a constant reference amplitude.

The radial and tangential displacement patterns for the dam obtained in this way from the forced vibration tests are plotted in Figs. 2.16 to 2.25 for the 10 forced vibration frequencies listed in Table 2.1. It will be noted that the displaced shapes are plotted for the crest and for the four walkway levels in each figure. It also should be noted that these shapes are induced by the exciters acting at the crest; that is, they are forced response shapes and are not entirely equivalent to the corresponding free vibration mode shapes, although they generally are quite similar. Additional information about these shapes is given in Figs. 2.26 to 2.30, in which the radial displacement pattern is plotted over the height of three typical blocks for each specified forcing frequency. It is significant that no change of sign of the displacement

is seen over the height of any block, even for the highest frequency that is plotted. The magnitude of the applied shaking forces, and the resulting radial displacement amplitudes at the crest for each of these forcing frequencies are listed in Table 2.2.

Corresponding radial displacements measured by the Ranger seismometers on the abutment rock for the first four forced vibration frequencies are listed in Table 2.3. These seismometer stations were located at the crest and at the four walkway levels; at most levels two measurements are listed, one on the rock essentially at the concrete interface and the other at a distance of 5 to 10 m from the end of the dam. The table lists these horizontal distances together with the measured response displacement. As was mentioned earlier, parallel readings were made at the crest of Block 3 with a Ranger seismometer and a PRC velocity meter so that the amplitude of motion in the abutment rock (Table 2.3)could be correlated with that observed on the dam (Table 2.2). These parallel readings at Block 3 in the radial and the tangential directions for each of the test frequencies are listed in Table 2.4; also listed is the proportionality factor that would convert the PRC reading to the U.S. value. Study of this table shows that the two types of transducers give essentially the same results for the first three frequencies. Considering that the PRC velocity meters were operating near their threshold of sensitivity, the agreement between the two sets of data is remarkable. Because the measured abutment rock motions are significant only in comparison with values calculated from the mathematical model, plots of these abutment motions are presented and discussed later in the correlation between analysis and experiment.

The normalized values of radial displacements obtained from ambient vibration measurements are listed in Table 2.5 for the first six ambient vibration peak frequencies. These ambient vibration shapes are plotted

in Figs. 2.31 to 2.36; for comparison, the corresponding forced vibration shapes for the first five frequencies (equivalent to Figs. 2.16 to 2.20) also are plotted in the same figures. As was noted earlier, the mode with an ambient frequency of 7.13 Hz was not identified in the forced vibration test; for this reason the calculated sixth mode shape is plotted for comparison with the ambient vibration mode shape in Fig. 2.36. This "missing mode" in the forced vibration test will be discussed later in connection with the analytical investigation. Study of the results of the forced and the ambient vibration test procedures shows that the two methods give surprisingly similar mode shapes and frequencies. This demonstrates the great merit of the ambient vibration procedure because it is much faster and less expensive than the forced vibration method. Moreover, the ambient vibration shapes may be closer to the true free vibration shapes because they are not distorted by the shaker forces applied at the dam crest; and as noted in this example the ambient procedure may identify modes that are missed in a forced vibration test. However, it should be noted that the interaction measurements that are the essential part of this research project can be obtained only by the forced vibration procedure.

2.3.3 Damping Ratios

Damping ratios were determined for each forced vibration frequency using the half-power method applied to the normalized displacement frequency response curves. The formula used may be written

$$\xi_n = \frac{\Delta f_n}{2 f_n}$$

where ξ_n = modal damping ratio

f_n = modal frequency

Δf_n = width of modal response curve.

The width Δf_n is defined as the difference between the frequencies at the two points on the response curve with amplitude 0.707 times the peak response amplitude for mode "n". Strictly speaking, this formula is valid only for determining the damping ratio of a single-degree-of-freedom system; however, it gives a good indication of the modal damping ratio for a multiple-degree-of-freedom system if its frequencies are well separated so there is little interference from adjacent response peaks. Results of this damping ratio analysis from the forced vibration displacement frequency response curves are listed in Table 2.6.

2.3.4 Hydrodynamic Pressures

To measure the hydrodynamic pressures during the forced vibration tests, the pressure gages were suspended by their waterproof electrical cables from the crest of the dam. At first it was intended to suspend the three gages at depths of 5, 15, and 25 m, respectively, moving them successively to stations located at the centers of Blocks 7, 9, and 11. Unfortunately, first one and then a second gage suffered short circuits due to water leakage, hence only one gage was available during much of the test program and data was not obtained at all depths at each station.

The pressure readings were recorded by the Kinemetrics digital tape recorder, and were processed after the tapes were returned to Berkeley in the same way as the Ranger seismometer readings on the abutment rock. The hydrodynamic pressure amplitudes measured at the various gage points are listed in Table 2.7; in addition they are plotted in comparison with the predicted pressure values in the correlation section of this report.

Chapter 3

ANALYTICAL STUDY

3.1 ADAP COMPUTER PROGRAM

3.1.1 General Comments

The essential feature of this cooperative research program is the correlation of analytically predicted performance with the dynamic response measured during field tests of the dam. Thus, it is necessary to have an effective analysis procedure that is capable of evaluating the effects of foundation and reservoir interaction on the structural response to harmonic excitation. Although in principle many general purpose finite element analysis programs might be adapted to this purpose, it was decided from the beginning to use the program ADAP[6] (Arch Dam Analysis Program) because it was specifically developed for analysis of static and dynamic response of concrete arch dams. The original program was written at the EERC as a research project funded by the U.S. Bureau of Reclamation. General features of ADAP, as it was developed originally and as it subsequently has been improved, are described briefly in this section. More specific details about the program as it was applied to the analysis of XHD dam are presented in the following sections of this chapter.

3.1.2 Element Types

The ADAP program makes use of special "thickshell" (THKSHL) and "3D-shell" (3DSHEL) elements to model the curved surfaces in the body of an arch dam. The thickshell elements are derived by an isoparametric formulation using quadratic geometric and displacement interpolation functions in the dam face directions, but only linear interpolation in the thickness direction. "Reduced integration" is employed through the thickness to allow for the effects of shear distortion...eight nodes are

defined at the edges of the element mid-surface, each having five degrees of freedom--the deformation degree of freedom through the thickness having been replaced by a zero stress constraint in this direction. The dam body also could be modeled by the 3D-shell elements, which are based on the same type of isoparametric interpolation functions, but retain the complete set of 16 nodes, 8 each at the corners and mid-edges of the exterior faces. Each of these nodes has three translational degrees of freedom so special "transition" elements also are provided to permit assembly of the different types of elements; the transition elements may have nodes either at the outer surfaces or at the mid-surface on any edge. Also included in the basic element library is an eight-node "brick" element (designated 3D) based on linear isoparametric interpolation in all three axes. These elements generally are used to model the foundation rock, but they also can be used to model the dam body--using three elements through the thickness.

3.1.3 Program Capabilities

The program includes a mesh generator capability for the dam body, which provides an element system for any three-centered arch based on specified arch center coordinates, radii, and central angles. Similarly, the finite element system to model an appropriate block of foundation rock also can be generated automatically based on the essential dam abutment coordinates.

In the original version, ADAP was capable of evaluating static stresses and displacements due to dead weight of the concrete and hydrostatic pressures, as well as to specified distributions of temperature change within the dam concrete. It also was capable of calculating the vibration mode shapes and frequencies of the dam-foundation system, and of calculating its response to arbitrary earthquake input--applied in each of three

global axes and specified either as a time-history accelerogram or as a response spectrum. In a subsequent development[7], interaction effects with an incompressible reservoir were added to the dynamic analysis. The reservoir can be modeled by added masses derived either by an extension of the Westergaard concept[1] which accounts for the curved surfaces of the arch dam, or by a finite element modeling of the reservoir. The elements used in the reservoir model have a 16 node configuration similar to those used to model the dam, so the reservoir added masses can be combined directly with the mass matrix for the dam.

An additional analytical capability has been added to ADAP during the present investigation--it can now evaluate the response to specified harmonic forces applied to the dam at any designated points. Thus, the mathematical model can simulate directly forced vibration tests as they are done in the field, and can evaluate the resulting amplitudes of displacements at selected reference points or of hydrodynamic pressures at the face of the dam (or in the reservoir).

3.2 IDEALIZATION OF XIANG HONG DIAN DAM

In this investigation, the entire dam system consisting of the concrete body, the foundation rock, and the reservoir water was modeled by finite element meshes that conformed to the specified geometry of the actual components in the field. The modeling of each component is described in the following sections.

3.2.1 Dam Body

The basic concept of the mesh generator used to idealize the dam body is that all nodes are arranged on horizontal sections (designated as the mesh elevations) and on vertical planes projected upward from the intersection of the mesh elevations with the canyon wall. These vertical and

horizontal sections are identified first on the "reference surface"; this consists of vertical cylindrical surfaces (typically three circular cylinders) that pass through the upstream edge of the dam crest. Then the coordinates of the nodes on the upstream and downstream faces are obtained by radial projection from the reference surface.

This modelling concept is very suitable for Xiang Hong Dian Dam (XHD) because it is a simple gravity arch of single curvature with a vertical upstream face; moreover its contraction joints between blocks are vertical. Preliminary studies indicated that 6 mesh elevations would provide an adequate model of this dam, leading to a total of 30 concrete elements--18 3DSHEL elements adjacent to the canyon face and 12 THKSHL elements for the interior regions. The arrangement of these elements projected on the X-Z plane is shown in Fig. 3.1, while Fig. 3.2 gives a perspective view of the elements in the dam body.

3.2.2 Foundation Rock

The mesh generator program for the foundation rock permits development of finite element rock models with three degrees of refinement. The foundation mesh is constructed on planes cut into the canyon walls in the direction normal to the dam-rock contact surface at the interface node locations. Figure 3.3 shows the traces of these normal planes as they intersect the X-Z plane of the XHD dam coordinate axes. On each of these normal planes, a semi-circle is drawn from the dam-rock interface with a radius equal to 1 or 1.5 times the height of the dam. Six nodes equally spaced around this semi-circle define the boundary of the foundation rock. Preliminary analyses indicated that the coarsest mesh (i.e., foundation mesh type-1, with a radius equal to the dam height) is appropriate for modelling the foundation rock of the XHD dam, because it provides adequate

accuracy with minimal computer costs. Figure 3.4 shows the mesh arrangement of the foundation rock associated with the right part of the dam; the entire foundation model consisted of 80 eight-node brick elements (3D). The rock beyond this foundation zone was assumed to be rigid, so all boundary nodes of the foundation block were fixed in position.

3.2.3 Reservoir

In order to establish the finite element model of the reservoir, it first was necessary to determine the upstream extent of the system to be included in the analysis. Based on the topography of the reservoir bottom and on previous parametric studies, a reach extending 300 m upstream of the dam face (i.e., about three times the height of the dam) was selected for the reservoir model; Fig. 3.5 is a map showning the topography of the XHD reservoir bottom and the extent of the finite element model.

It should be noted that the reservoir model subroutine includes a mesh-generator capability based on the concept that the reservoir is bounded by a cylindrical surface obtained by translating the canyon wall-concrete interface upstream (i.e., in the Y axis direction). The reservoir elements are then arranged in successive "layers" with the nodes on successive sections located to correspond with the interface nodes; the number of layers to be used in any case may be specified arbitrarily. In the case of XHD dam, however, the topography of the reservoir was not of this cylindrical form, so the nodal coordinates of the reservoir had to be specified directly as input data. Figure 3.6 shows the liquid finite element mesh at the nodal sections labeled L = 15 m, 65 m, 130 m and 300 m in Fig. 3.5 as well as at the dam interface. The four layers of elements

defined by these sections were found to give adequate accuracy, but the additional section at L = 620 m was used in some preliminary studies. Boundary nodes at the reservoir-rock interface and at the upstream face of the model were assumed to be fixed; hydrodynamic pressures at the top surface were assumed to be zero (i.e., wave action was neglected).

Because the reservoir is seldom filled to the crest of the dam, the top nodes of the reservoir elements must be established at the specified reservoir level and do not coincide with the concrete dam crest nodes. Therefore the accelerations that control the pressures developed at the nodes of the top layer of liquid elements (and accordingly the added mass of these elements) must be determined by special procedures. In this subroutine, the accelerations are determined at the integration points of the liquid elements using the displacement interpolation functions defined for the concrete elements.

3.2.4 Material Properties

The material properties used in preliminary studies of XHD dam were supplied by the Scientific Research Institute of Water Conservancy of Anhui Province (SRIWCAP), as follows. For the dam concrete, the Young's modulus used in static analyses was $E_s = 2.0 \times 10^6$ T/m^2 (2.84×10^6 psi) and in dynamic analyses it was $E_d = 4.0 \times 10^6$ T/m^2 (5.68×10^6 psi). For the foundation rock, the Young's modulus was 2.6×10^6 T/m^2 (3.69×10^6 psi) for both static and dynamic analyses. The Poisson's ratio for both concrete and rock was set to 0.2. The unit weight of the concrete was 2.4 T/m^3 (150 pcf), but it was assumed to be zero for the foundation rock (i.e., a massless foundation was assumed). The unit weight of the reservoir water was taken to be 1.0 T/m^3 (62.4 pcf) and it was assumed to be incompressible. No temperature change data was available, so thermal

stresses were not considered in the static analysis.

As is described in the section on correlation of analysis and experiment, the elastic moduli of the rock and concrete were adjusted later to give the best possible agreement between measured results and analytical predictions.

3.3 ANALYTICAL PROCEDURES

3.3.1 Static Analysis

The static analysis was performed by solving the following equation of static equilibrium:

$$\underline{K}\,\underline{U} = \underline{R} \tag{3.1}$$

where $\underline{K}$ is the stiffness matrix of the dam-foundation system, and $\underline{U}$ and $\underline{R}$ are vectors, respectively, of displacements and loads corresponding to nodal point degrees of freedom. For the Xiang Hong Dian Dam, the load vector included the combination of gravity load and hydrostatic pressure components, only. Temperature change was not considered in this static analysis; ignoring the thermal stresses may be considered to be equivalent to assuming that the stresses induced by temperature change have been eliminated by subsequent creep effects. Once $\underline{K}$ and $\underline{R}$ were assembled, Eq. 3.1 was solved for the global displacements $\underline{U}$ using Gaussian elimination applied to the symmetric banded stiffness matrix $\underline{K}$.

3.3.2 Dynamic Analysis - General Comments

The dynamic behavior of the dam-reservoir-foundation system is expressed by the system equations of motion which express the dynamic equilibrium; thus they are equivalent to Eq. 3.1 but with the addition of the dynamic resisting forces due to inertia and damping, as follows:

$$\underline{M}\,\ddot{\underline{U}} + \underline{C}\,\dot{\underline{U}} + \underline{K}\,\underline{U} = \underline{R}(t) \tag{3.2}$$

in which $\underline{M}$ is the mass matrix of the dam-reservoir system, $\underline{C}$ is the viscous damping matrix, and $\dot{\underline{U}}$ and $\ddot{\underline{U}}$ are the nodal velocity and acceleration vectors representing the first and second time derivatives of the displacement vector. The first step in the dynamic analysis was the evaluation of the added mass of the reservoir water, which is combined in $\underline{M}$ with the mass of the dam concrete. As was noted earlier, the foundation rock is assumed to be massless, so it does not contribute to $\underline{M}$.

Because the finite element model of the entire dam-reservoir-foundation system involves hundreds of degrees of freedom, it is desirable to transform Eq. 3.2 to a more efficient set of coordinates than the nodal displacements. The vibration mode shapes are a very efficient means of describing the dynamic response; if the response is linear, generally only a few modes are needed to express the essential dynamic behavior. Thus the second step in the dynamic analysis of XHD dam was the evaluation of its mode shapes and frequencies.

In the present case, the modal coordinates have an additional important advantage: because it is assumed that the damping matrix $\underline{C}$ provides proportional damping, the transformed equations of motion are uncoupled, so the dynamic response may be calculated separately for each modal coordinate and the total response obtained by mode-superposition. The dynamic excitation vector, $\underline{R}(t)$, in Eq. 3.2 represented two different types of input in the present study--earthquake ground motions and harmonic excitation provided by the rotating mass shakers attached to the dam crest. In the following sections, the procedures used in evaluating the added mass of the reservoir, the system mode shapes and frequencies, the modal excitation functions, and the modal responses are each discussed

in sequence.

3.3.3 Added Mass of the Reservoir

Because the objectives of this research project required that only the best available analytical procedures be used for correlation with the experimental results, only the finite element reservoir analysis capability of ADAP was used to represent the reservoir interaction. The formulation of this analysis subroutine (called RSVOIR) is presented in Reference 7; a brief summary of the procedure is presented here for completeness. In modeling the interaction mechanism, it is assumed that the hydrodynamic pressure in the reservoir is governed by the wave equation:

$$\nabla^2 P\ (x,y,z,t) = \frac{1}{c^2}\ \ddot{P}\ (x,y,z,t) \tag{3.3}$$

where c is the velocity of sound in water. In the formulation used in ADAP, the reservoir water is assumed to be incompressible, therefore, the velocity of sound becomes infinite and the RHS of Eq. 3.3 vanishes. Boundary conditions for the reservoir are given by

$$\frac{\partial P}{\partial n_s} = -\rho\, \ddot{U}^t_{n_s} \tag{3.4}$$

where n_s is the outward normal direction from the reservoir-boundary interface and $\ddot{U}^t_{n_s}$ is the total normal acceleration of the fluid at the boundary.

Following the Galerkin procedure, the discretized equivalent of Eq. 3.3 is

$$\int_V \underline{N}^T\ (\nabla^2 \bar{P})dV = 0 \tag{3.5}$$

where $\underline{N}$ is a row vector of arbitrary weighting functions, and $\bar{P}$ is an approximate expression of the pressure distribution in the reservoir. In this analysis, the pressure distribution in the reservoir will be

expressed by the finite element concept, dividing it into fluid elements and expressing the pressure within each element by the nodal pressure $p^{(e)}$, multiplied by interpolation function $\underline{N}^{(e)}$, i.e.

$$\bar{p}^{(e)} = \underline{N}^{(e)}\ p^{(e)} \tag{3.6}$$

Substituting Eq. 3.6 into Eq. 3.5 and using the pressure interpolation function $\underline{N}$ also as the Galerkin weighting functions leads to the finite element equivalent of Eq. 3.3, after integrating by parts and applying the boundary conditions of Eq. 3.4. When expressions of this type for all elements are assembled, the final results may be written

$$\underline{g}\ \underline{P} = \rho \underline{h}_s\ \ddot{\underline{U}}_s^t \tag{3.7}$$

where $\underline{P}$ = vector of nodal pressures and $\ddot{\underline{U}}_s^t$ = vector of total nodal accelerations in Cartesian coordinates at the dam-reservoir interface. The global matrices $\underline{g}$ and $\underline{h}_s$ are assembled from the corresponding element expressions; note that $\underline{h}_s$ is defined only for elements at the dam-reservoir interface.

Because the RHS of Eq. 3.7 is defined only for nodes at the dam-reservoir interface, the pressures on the LHS can be partitioned correspondingly, and static condensation can be applied to reduce Eq. 3.7 to a form involving only the interface nodes

$$\underline{g}_s\ \underline{P}_s = \rho \underline{h}_s\ \ddot{\underline{U}}_s^t \tag{3.8}$$

This can be solved for the interface pressures

$$\underline{P}_s = \rho \underline{g}_s^{-1}\ \underline{h}_s\ \ddot{\underline{U}}_s^t \tag{3.9}$$

Equation 3.9 expresses the hydrodynamic pressures at the interface in terms of the nodal accelerations at the interface. Applying the principle of virtual displacements, it can be shown that the Cartesian coordinate components of the corresponding nodal forces are given by

$$\underline{f}_s = \underline{m}_a \ \ddot{\underline{U}}^t_s \tag{3.10}$$

where

$$\underline{m}_a = \rho \underline{h}_s^T \underline{g}_s^{-1} \underline{h}_s \tag{3.11}$$

is the added mass of the reservoir resisting the nodal accelerations at the interface. The final analytical step involves combining this added mass matrix with the mass matrix of the dam. It should be noted that this added mass matrix is a full matrix in general, but involves only the interface nodes of the dam; by noting the appropriate nodal locations in the dam mass matrix, $\underline{m}$. They may be combined by standard "direct stiffness assembly" procedures, which may be represented symbolically as

$$\underline{M} = \underline{m} + \underline{m}_a \tag{3.12}$$

3.3.4 Vibration Mode Shapes and Frequencies

The vibration mode shapes and frequencies of the dam-reservoir system are calculated by solving the undamped eigenproblem of the equations of motion (Eq. 3.2) which may be expressed as

$$[\underline{K} - \omega_n^2 \underline{M}]\underline{\phi}_n = \underline{0} \tag{3.13}$$

in which $\underline{\phi}_n$ is the mode shape vector for mode "n" (i.e., it represents the relative values of the nodal displacements $\underline{U}$ in this mode) and ω_n is the circular frequency of vibration in this mode. In ADAP this eigenproblem is solved by subspace iteration[8] for any specified number "p" of the lowest mode shapes and frequencies.

3.3.5 Mode Superposition Procedure

The basic step in the mode superposition analysis procedure is transforming the equations of motion (Eq. 3.2) to the uncoupled modal coordinate form. For this purpose, it is assumed that the displacements

can be expressed in terms of a selected number (M) of the modal coordinates, i.e.,

$$\underline{U}(t) = \sum_{n=1}^{M} \underline{\phi}_n Y_n(t) = \underline{\Phi}\, \underline{Y}(t) \tag{3.14}$$

where the columns of $\underline{\Phi}$ are the first M mode shape vectors $\underline{\phi}_n$ and $\underline{Y}(t)$ is a vector of the corresponding modal displacements. Substituting Eq. 3.14 into Eq. 3.2 and taking advantage of the modal orthogonality properties leads to a set of M independent equations of motion of the form

$$\ddot{Y}_n + 2\xi_n \dot{Y}_n + \omega_n^2 Y_n = \frac{P_n(t)}{M_n} \tag{3.15}$$

in which $M_n = \underline{\phi}_n^T \underline{M}\, \underline{\phi}_n$ is the modal mass, ξ_n is the modal damping ratio, and $P_n(t) = \underline{\phi}_n^T \underline{R}(t)$ is the modal load. The modal response $Y_n(t)$ is obtained by solving Eq. 3.15 by any appropriate method, as will be described later; the total response is then given by Eq. 3.14.

3.3.6 Earthquake Response Analysis

In the case of earthquake excitation of the dam-reservoir-foundation system, no external load $\underline{R}(t)$ is applied directly to the system; however, an effective earthquake force $\underline{R}_{eff}(t)$ is induced by the seismic acceleration of the dam support points $\ddot{\underline{U}}_g(t)$. In this case the displacement vector $\underline{U}(t)$ represents motions of the dam relative to the support points (outer boundary of the foundation element model) and the effective force is given by

$$\underline{R}_{eff}(t) = - \underline{M}\, \underline{r}\, \ddot{\underline{U}}_g(t) \tag{3.16}$$

where $\underline{r}$ is an influence coefficient matrix, each column of which expresses the total displacements of the dam resulting from a unit value of a boundary displacement.

In ADAP, the seismic input can be defined separately for the three global axes, i.e.,

$$\ddot{\underline{U}}_g(t) = < \ddot{U}_{gx}(t) \quad \ddot{U}_{gy}(t) \quad \ddot{U}_{gz}(t) >^T \tag{3.17}$$

so $\underline{r}$ has three columns to correspond, i.e.,

$$\underline{r} = [\underline{r}_x \; \underline{r}_y \; \underline{r}_z] \tag{3.18}$$

The effective modal earthquake force then is given by

$$p_n(t) = \underline{\phi}_n^T \underline{R}_{eff}(t) = -\underline{\mathcal{L}}_n \ddot{\underline{U}}_g(t) \tag{3.19}$$

where the modal earthquake excitation coefficient $\underline{\mathcal{L}}_n$ is defined as

$$-\underline{\mathcal{L}}_n = + \underline{\phi}_n^T \underline{M} \underline{r} \tag{3.20}$$

Time History Analysis: ADAP provides two different procedures for evaluating the earthquake response: the time history method and the response spectrum method. For the time history method, the seismic input $\ddot{\underline{U}}_g(t)$ is specified directly, usually as a seismograph record obtained during an earthquake. From this, the effective modal earthquake force $\underline{P}_n(t)$ is obtained using Eq. 3.19, and then the modal response $Y_n(t)$ is obtained by solving Eq. 3.15. In ADAP, the modal response is calculated by the linear acceleration step-by-step method[8] and then the total response is obtained by superposing the modal responses for each instant of time (Eq. 3.14).

Response Spectrum Analysis: In the response spectrum method, the earthquake input is specified in terms of the response of a single degree of freedom system to the earthquake acceleration history such as is represented by the modal response equation (Eq. 3.15). Using Eq. 3.19 to express the modal force resulting from a single component of earthquake acceleration, $\ddot{U}_g(t)$, the response can be expressed as follows:

$$Y_n(t) = \frac{-\mathscr{L}_n}{M_n \omega_n} \quad V(t) \tag{3.21}$$

where the earthquake response function V(t) can be expressed by the Duhamel integral:

$$V_n(t) = \int_0^t \ddot{U}_g(t) e^{-\xi\omega_n(t-\tau)} \sin \omega_n(t-\tau) d\tau \tag{3.22}$$

The earthquake pseudo-velocity response spectrum, S_{V_n}, is then defined as the maximum value of the response function developed at any time during the earthquake history, i.e., $S_{V_n} = V_n(\max)$; so by Eq. 3.21 the maximum response in mode "n" is given by

$$Y_n(\max) = \frac{\mathscr{L}_n}{M_n \omega_n} \quad S_{V_n} \tag{3.23}$$

in which it will be noted that the negative sign has been dropped because it has little significance in earthquake response analysis.

The maximum system displacements in mode "n" may now be obtained by use of the mode shape vector, thus

$$\underline{U}_n^{(\max)} = \underline{\phi}_n \underline{Y}_n^{(\max)} \tag{3.24}$$

However, because the maximum response in the various modes do not occur at the same time, it is not possible to obtain the total maximum response by simple mode superposition (Eq. 3.14); instead probability considerations must be employed in combining the maximum values determined in the individual modes. The most reliable and convenient procedure for combining the modal maxima is the Complete Quadratic Combination method (designated CQC)[9]. Any desired modal response quantity can be combined in this way; for example, the maximum nodal displacements (given by Eq. 3.24 for a single mode) may be expressed:

$$\underline{U}^{(max)} \doteq \sqrt{\sum_{i=1}^{M} \sum_{j=1}^{M} \underline{U}_i^{(max)} Q_{ij} \underline{U}_j^{(max)}} \tag{3.25}$$

in which the cross-modal coefficient Q_{ij} may be expressed

$$Q_{ij} = \frac{8\xi^2 (1+s)S^{3/2}}{(1-s^2) + 4\xi^2(1+S)^2 S} \tag{3.26}$$

and the subscripts i and j represent the range of mode numbers included in the analysis. Here ξ is the modal damping ratio (assumed to be the same in all modes) and $S = \omega_j/\omega_i$ (i.e., the frequency ratio for modes i and j).

Of course other response quantities can be derived from the system displacements, but it is important to note that the modal maxima of the specific response quantity must be derived first, and then these maxima combined by the CQC procedure--it is not correct to use the combined displacement maxima (e.g., Eq. 3.25) to obtain the maximum derived response quantity. For example, the system stresses $\underline{\sigma}(t)$ can be derived from the nodal displacements at any time by means of the stress transformation matrix E, i.e.,

$$\sigma(t) = \underline{E}\ \underline{U}(t) \tag{3.27}$$

Accordingly the modal maximum stress is obtained similarly from the modal maximum displacements:

$$\underline{\sigma}_n^{(max)} = \underline{E}\ \underline{U}_n^{(max)} \tag{3.28}$$

Then the CQC procedures can be used to approximate the combined effect of all modal maxima, by parallel with Eq. 3.25

$$\underline{\sigma}_n^{(max)} = \sqrt{\sum_{i} \sum_{j} \underline{\sigma}_i^{(max)} Q_{ij} \underline{\sigma}_j^{(max)}} \ .$$

The foregoing response spectrum combination analysis has considered only a single component of seismic input, whereas the arch dam systems will be subjected to independent excitation in the three global coordinate axes. The recommended procedure for dealing with multiple component excitation in a response spectrum analysis is to calculate the maximum due to each component of input by a separate CQC analysis equivalent to Eq. 3.25, and then to combine these maxima by the square root of the sum of the squares (SRSS) method. For example if the maximum response due to the x, y, and z components of input are designated $\underline{U}_x^{(max)}$, $\underline{U}_y^{(max)}$, and $\underline{U}_z^{(max)}$, respectively, then the maximum result due to the combined input may be approximated by

$$\underline{U}^{(max)} = \sqrt{\left(\underline{U}_x^{(max)}\right)^2 + \left(\underline{U}_y^{(max)}\right)^2 + \left(\underline{U}_z^{(max)}\right)^2} \qquad (3.29)$$

3.3.7 Forced Vibration Response

For the purpose of this investigation, it was necessary to extend ADAP so that the forced vibration test procedure could be simulated analytically. Thus, the dynamic input forces, $\underline{R}(t)$, in the equation of motion (Eq. 3.2) were specified to be harmonically varying quantities of arbitrary amplitude acting at the finite element nodal points

$$\underline{R}(t) = \underline{F} \sin \bar{\omega} t \qquad (3.30)$$

where $\underline{F}$ is a vector describing the distribution of the harmonic load and $\bar{\omega}$ is the excitation frequency. Two special subroutines were developed to evaluate the harmonic displacement response and the harmonic hydrodynamic pressure response, respectively, obtained during the forced vibration test procedure, as described in the following sections.

Displacement Amplitude: The basic harmonic excitation subroutine is a post processor called "FORCEVB". It is written specifically to evaluate response to harmonic forces applied at the dam crest, where the forces result from counter-rotating eccentric masses as is the case with the testing machines. In this case, each machine produces a force

$$R(t) = M_e \, r \, \bar{\omega}^2 \sin \bar{\omega} t \tag{3.31}$$

where M_e is the total eccentric mass, r is the radial distance to its center of gravity and $\bar{\omega}$ is the angular velocity of the test machine. In the test of XHD dam, four equal exciting forces were applied, located at the dam crest as shown in Fig. 2.11 and oriented to apply the forces in the radial direction at each point. Thus, the input force can be expressed in terms of the global x and y components of the four equal crest loads,

$$\underline{R}(t) = < f_{1x} \; f_{1y} \; f_{2x} \; f_{2y} \; f_{3x} \; f_{3y} \; f_{4x} \; f_{4y} >^T \; M_e \, r \, \bar{\omega}^2 \sin \bar{\omega} t \tag{3.32}$$

in which f_{px} and f_{py} are the x and y components of a unit radial load applied at shaker position "p".

Because the analysis was performed in modal coordinates, it was necessary to evaluate the modal forces associated with Eq. 3.32 using the standard modal load expression; $P_n(t) = \underline{\phi}_n^T \, \underline{R}(t)$. In the present case this may be written as follows:

$$P_n(t) = P_{n0} \sin \bar{\omega} \, t \tag{3.33}$$

where

$$P_{n0} = \sum_{p=1}^{4} [\phi_{npx} \, f_{px} + \phi_{npy} \, f_{py}] \, M_e \, r \, \bar{\omega}^2 \tag{3.34}$$

in which ϕ_{npx} and ϕ_{npy} are x and y mode shape components at point p in mode n. In general, the shaker locations do not coincide with the finite element nodal points, so these mode shape values at the shaker locations are approximated by assuming cubic interpolation functions along the crest.

The modal response to this harmonic excitation is given by the solution of the modal equation of motion (Eq. 3.15) which may be expressed as[10]

$$Y_n(t) = \frac{P_{n0}}{M_n\ \omega_n^2}\left[\frac{(1-\beta_n^2)\ \sin\ \bar{\omega}\ t\ -\ 2\xi_n\beta_n\ \cos\ \bar{\omega}\ t}{(1-\beta_n^2)^2\ +\ (2\xi_n\beta_n)^2}\right] \tag{3.35}$$

in which $\beta_n = \bar{\omega}/\omega_n$ is the ratio of the exciting frequency to the modal frequency and ξ_n is the modal damping ratio. From this, the amplitude of the response in mode "n", Y_{n0}, could be obtained easily by merely taking the square root of the sum of the squares of the sine and cosine terms, and then the amplitude of motion at the system nodal points due to this mode only would be given by

$$\underline{V}_{n0} = \underline{\phi}_n\ Y_{n0} \tag{3.36}$$

In general, however the vibration exciters operating at any frequency, $\bar{\omega}$, induce some response in all modes. Thus, even though the response in mode "n" tends to dominate the response when the shakers are set to operate in resonance with that mode frequency (i.e., setting $\bar{\omega} = \omega_n$), there can be a significant displacement contribution from the adjacent modes ("n-1" and "n+1"). The analytical procedure employed in FORCEVB has been developed to take account of these two modes adjacent to mode "n"; accordingly Eq. 3.35 is written for three modes:

$$Y_i(t) = \frac{P_{i0}}{M_i\ \omega_i^2}\left[\frac{(1-\beta_i^2)\ \sin\ \bar{\omega}\ T\ -\ 2\xi_i\beta_i\ \cos\ \bar{\omega}\ t}{(1-\beta_i^2)^2\ +\ (2\xi_i\beta_i)^2}\right] \tag{3.37}$$

$$= A_i\ \sin\ \bar{\omega}\ t\ +\ B_i\ \cos\ \bar{\omega}\ t$$

where i = n-1, n, n+1 and $\beta_i = \bar{\omega}/\omega_i$. The amplitude of response obtained with the exciting frequency set to the frequency of mode "n" (i.e., $\bar{\omega} \doteq \omega_n$) then is given by the superposition of the contributions from these three adjacent modes, taking the square root of the sum of the squares of the

sine and cosine terms, i.e.,

$$\underline{U}_{n0} = \sqrt{\left[\sum_{i=n-1}^{n+1} \underline{\phi}_i \, A_i\right]^2 + \left[\sum_{i=n-1}^{n+1} \underline{\phi}_i \, B_i\right]^2} \qquad (3.38)$$

Pressure Amplitude: The forced vibration displacement response analysis procedure described above also was extended to evaluate the pressures developed at the face of the dam by reservoir interaction during the forced vibration test. This extension was relatively simple because the subroutine RSVOIR makes use of the local pressures expressed in terms of the local accelerations in order to establish the added mass matrix. In the present project a post-processor program, called FVHYDRO, was written to evaluate the forced vibration pressures, starting with the hydrodynamic pressure coefficient matrix (pressures due to unit accelerations of the dam face nodes) that was calculated and stored on tape by the basic subroutine RSVOIR. Then FVHYDRO calculates the acceleration of each face node from the forced vibration displacements (described above) by multiplying each displacement by the square of the forced vibration frequency. The final pressure results then are obtained as the product of the local accelerations and the hydrodynamic pressure coefficient matrix.

It is of interest to note that a similar post-processor program, called EQHYDRO, was written to evaluate the hydrodynamic pressures developed at the face of the dam during earthquake response. In this case the local accelerations are obtained by the mode superposition procedure from the modal accelerations calculated in the step-by-step analysis of the modal response. Of course, the hydrodynamic pressure coefficient matrix determined by RSVOIR also is used in this case to obtain the pressures from the local accelerations.

3.4 RESULTS OF PRELIMINARY ANALYSES

3.4.1 General Comments

The first objective in the analytical studies was to establish the extent of the finite element mesh systems required to effectively model the interaction of the foundation rock and the reservoir. For this purpose a series of analyses were carried out to determine how the frequencies of vibration varied with changes of foundation rock and reservoir boundaries, it being assumed that the frequencies would converge to the true values as the extent of the finite element models became sufficiently large. Results of these studies of the effects of various parametric changes on the vibration frequencies are presented in the following sections.

3.4.2 Basic Effects of Reservoir and Foundation Interaction

Before the influence of the extent of foundation and reservoir could be studied, it was necessary to establish the basic effects of their interaction mechanisms on the dynamic behavior of the dam. This was accomplished by first evaluating the vibration frequencies of the concrete dam alone, without foundation or reservoir interaction, and then successively adding a reasonable foundation rock system followed by a reasonably sized reservoir system. The frequencies of vibration for the first 12 modes in each of these cases are listed in Table 3.1. Also shown for comparison are the corresponding results measured experimentally.

The dam idealization considered in this study is that shown in Figs. 3.1 and 3.2; the Young's modulus of the concrete was 4.0×10^6 T/m^2, as mentioned above, and for Case A in Table 3.1 the foundation rock was assumed to be infinitely rigid so that no interaction took place. In Case B, the same dam was considered but the Type-1 foundation mesh was added

(Figs. 3.3 and 3.4); in this case the Young's modulus of the rock was set at 2.6×10^6 T/m^2 (i.e., 65% of that of the concrete). It is evident from these tabulated results that the added flexibility provided by the foundation rock had a somewhat variable effect in reducing the frequencies of the different vibration modes, but it was reasonably consistent and caused an average reduction of about 7 percent. In Case C the reservoir was added to the model, considering it full to 71 m depth and 300 m in length. This caused a similar reduction in vibration frequencies, due to increased effective mass in this case rather than to reduced stiffness. Again the reduction was somewhat variable from mode to mode, as would be expected; the average reduction was about 5 percent. Comparison of Case C with the experimental results demonstrates that the basic reservoir and foundation interaction models are at least qualitatively valid; more refined correlation and adjustment of the models will be discussed later.

3.4.3 Influence of Extent of Foundation

The extent of the foundation model used in the basic studies discussed above (Mesh Generator-Type 1) is based on a general rule developed in static analyses of arch dams--that the foundation block should extend a distance equal to the dam height in all directions from the dam contact surface at the canyon walls and base. Because the foundation rock is assumed to be massless (so that only its flexibility is considered), this criterion should be equally valid for the dynamic analysis. However, the more refined and extensive foundation block models provided by the ADAP foundation mesh generator program (Types 2 and 3) were also considered, to determine if the basic foundation model was significantly too stiff.

Vibration frequencies obtained in this parametric study are listed in Table 3.2, again for the first 12 modes. For reference purposes, a rigid foundation case is listed as Case 1; it should be noted that this is

different from Case A of Table 2.1 because the 71 m deep reservoir is included in all cases in Table 3.2. Thus, Case 2 of Table 3.2 which includes the Type-1 foundation block is identical with Case C of Table 3.1. Comparison of Cases 3 and 4 with Case 2 show that the more refined and extensive foundation blocks of Types 2 and 3 have very little influence on the vibration frequencies. As expected, they do provide a slight reduction in frequency, in general, but these minor changes do not justify the use of the significantly more expensive foundation meshes. Consequently, it was concluded that mesh Type-1 is suitable for the analysis of XHD dam.

3.4.4 Influence of Reservoir Length

The reservoir considered in the basic case of Table 3.1 and in all cases of Table 3.2 had a length of 300 m. This choice was based on independent studies which indicated that a length about three times the height of the dam should be sufficient to avoid significant interference from the assumed upstream face of the reservoir. However, it was decided to verify the chosen length in this investigation by evaluating the vibration frequencies obtained with six different reservoir lengths. The results of this study are listed in Table 3.3, which shows the frequencies calculated for the first six modes for each of the specified lengths. The reservoir is assumed to be full to the crest of the dam in all cases; the position of the end section of the dam for each case is shown on the map of the reservoir, Fig. 3.5. It must be noted that this parametric study was done after the final adjustment of the dam material properties (described later), so the frequencies shown in Table 3.3 for the 300 m length are not consistent with the values listed in Table 3.1 and 3.2 for the corresponding reservoir and foundation model.

As expected, the effective added mass of the reservoir is seen in Table 3.3 to be greatest for the short reservoir because of the constraint provided by the rigid upstream boundary. The frequencies increase with increasing length of reservoir because this constraint becomes less significant as it is moved farther from the dam. Study of the table shows that a length of 130 m provides very little constraint at the upstream end and could be used satisfactorily for most practical work. However, in this study the more refined result obtained with the 300 m length was considered desirable; on the other hand, the table clearly shows that there is no need to use more than 300 m length for this particular reservoir.

3.4.5 Influence of Reservoir Depth

As was mentioned earlier, the reservoir level changed significantly during the field investigation, and this resulted in measureable changes of the vibration frequencies. Thus, it was essential to use the appropriate water level in the analysis of the vibration frequencies in order to correlate them with the measured results. For this reason, it was decided to make a parametric study of the influence of reservoir depth on the vibration frequencies, calculating the first twelve frequencies for each of six water levels ranging from empty to completely full.

Results of this investigation are listed in Table 3.4 and also are plotted in Fig. 3.7. Again this parametric study was done after adjustment of the material properties, so the frequencies are not consistent with those in Tables 3.1 and 3.2, but they are consistent with those in Table 3.3. It is apparent in Fig. 3.7 that the added mass of the reservoir has a very minor effect on the vibration frequencies so long as its surface is below mid-height of the dam. However, it begins to have a very significant influence when it reaches about 0.7 of the height, and the

changes of frequency with reservoir level changes cannot be ignored if the reservoir is more than 0.7 full. This same analytical information is plotted in Fig. 3.8 for the first four modes, but only for the range of water levels observed during the field test program; the observed frequency values for the various water depths also are plotted for comparison. Agreement between analysis and experiment is very good considering that the experimental frequency could be measured only to the nearest 0.05 Hz.

3.4.6 Vibration Mode Shapes

From the results of these parametric studies, it was apparent that the basic reservoir and foundation interaction model (Case C of Table 3.1) was satisfactory and could be used in preliminary analyses of the dam-reservoir system. Thus, the vibration frequencies listed for Case C in Table 3.1 were used as preliminary results; the corresponding mode shapes for these 12 modes are plotted in Figs. 3.9 to 3.20. In each figure, the crest displacements (combined x and y components) are depicted, as well as the displacements of the central vertical section (for the symmetric modes) or of the adjacent vertical node lines (for the antisymmetric modes). These figures clearly demonstrates that the structure is not truly symmetric because of the lack of symmetry or antisymmetry in the mode shapes. It is of interest to note that Mode 5 is the first to show a reversal of sign in the displacements on the vertical sections; the difficulty experienced in distinguising this mode from the next one during the field tests may be associated with this factor, as will be discussed later.

To provide a more complete understanding of these mode shapes, they have been plotted in isometric form in Figs. 3.21 to 3.32. A special post-processing subroutine called MESHPLT was written to produce these

plots. It has the capability of constructing isometric views of the displacements of all nodal points, or of any selected set of nodes. In these figures, the displacements of the finite element nodes on the upstream dam face are shown; because of the simple cylindrical form of this face, these displacements are easier to visualize than those of the downstream face. It is important to realize that the amplitudes of displacements shown in these mode shape plots have no significance -- only the shape (i.e., relative values of displacements) has meaning; the displacements have been normalized to give a reasonably clear picture.

It may be noted in the isometric plots that significant motions are evident along the concrete-rock interface. In general this participation of the foundation rock in the vibrations is greater for the higher modes, as may be expected; however, even in Mode 1 the foundation motions are quite large. In order to better understand the foundation interaction mechanism, enlarged displacement plots were made of a selected set of nodes at the base of the dam and in the adjacent rock. Two plots of this type are shown in Figs. 3.33 and 3.34.

Chapter 4

CORRELATION OF ANALYTICAL AND EXPERIMENTAL RESULTS

4.1 OBJECTIVE OF THE CORRELATION STUDY

Although the basic mathematical model adopted in the preceding chapter provided reasonable estimates of the vibration behavior of XHD dam, it was clear from a comparison of the measured frequencies with frequencies calculated for the same level of water in the reservoir that the mathematical model needed further refinement. In particular it was realized that the Young's modulus values used for the concrete and the foundation rock in the preliminary studies could not be considered reliable. In fact, the only way to obtain accurate values for the dynamic elastic moduli of an arch dam-foundation system is by field vibration measurements. Thus, the first objective in the correlation of analytical and experimental results was the determination of these modulus values.

In the present study, it was decided to first establish the relative values of the rock and concrete moduli by consideration of the vibration mode shapes in the interface region and then to determine the modulus of the concrete by correlation of the vibration frequencies. After the mathematical model properties were refined in this way, the correlation of analytical and experimental results served to verify the mathematical procedures used in the dynamic response analysis, and thus to give confidence in the dynamic response behavior predicted by such analyses.

4.2 FOUNDATION ROCK: CONCRETE MODULUS RATIO

In the preliminary studies of the dam-foundation systems, it was assumed that the Young's modulus of the rock was $E_f = 2.6 \times 10^6$ T/m^2 while that of the dam was $E_d = 4.0 \times 10^6$ T/m^2; thus the assumed ratio of rock to concrete stiffness was 0.65. To determine whether this ratio was

appropriate for XHD dam, a parametric study was carried out considering foundation rock that was twice as stiff and half as stiff as the basic model; in other words, additional modulus ratios of 1.30 and 0.325 were used. In this study, the forced vibration response shape at the rock-concrete interface was calculated, including the response of the mode corresponding to the excitation frequency together with the contributions of the two adjacent modes (as described in the preceding chapter). The damping in each mode was adjusted until the response amplitude calculated at the dam crest corresponded with that observed during the corresponding field test. Then shapes of the forced vibration response in the interface region were plotted for the first five modal excitation frequencies for each of the designated ratios of foundation rock to concrete modulus: 1.30, 0.65, and 0.325. It should be noted that the shape is independent of the actual value of the modulus--it depends only on the ratio.

The plots of the calculated horizontal motions at the right abutment interface are shown in Fig. 4.1 for modes 1, 2, and 3 and in Fig. 4.2 for modes 4 and 5. Also shown in each figure are the corresponding motions measured during the forced vibration field tests. The same data are presented in tabular form in Tables 4.1 to 4.6. Study of these plots and tables reveals that the analysis with the modulus ratio of 1.3 generally gives the best agreement with the experimental result; in general, the relatively softer foundation rock allows too much foundation interaction in the vibratory response.

The forced vibration results shown in Figs. 4.1 and 4.2 were obtained using the standard assumption (mentioned earlier) that the foundation rock had no mass. In order to determine whether this parametric foundation rock study was sensitive to the massless rock assumption, the calculations were repeated (for modulus ratios of 1.30 and 0.65) assuming the foundation

rock to have the same unit weight as the concrete. These displacements calculated at the interface nodes when the rock mass was considered also are listed in Tables 4.1 to 4.6. Comparison of the results for the case with mass with those for the massless case demonstrates that the mass is not a significant factor in this correlation study. Thus, summarizing the results of this parameter study of the foundation rock--the modulus ratio should be set at 1.3 and the rock may be assumed massless.

4.3 YOUNG'S MODULUS OF THE CONCRETE

Making use of this revised foundation rock modulus ratio of 1.3 and the actual reservoir level at the time of the field measurement program (126.9m = 0.811H), the vibration frequencies of the dam-reservoir-foundation system were again calculated--still using the originally assumed Young's modulus for the concrete of 4.0×10^6 T/m^2. The first 12 frequencies obtained in this analysis are listed in the first column of Table 4.7. For comparison the forced response peak frequencies are listed in the last column, the designation S or AS indicates whether the shaker force pattern was symmetrical or antisymmetrical.

It is apparent in this comparison that the analytical frequencies are too high, implying that the assumed concrete modulus is too great. Noting that the frequencies vary with the square root of the modulus of elasticity, the modulus value required to give a calculated frequency equal to the experimental frequency was determined for each of the first four modes of vibration. The average of these adjusted moduli was then assumed to be the true value of the Young's modulus for XHD dam. Only the first four modes were used in this adjustment process because they were considered to be the most important in subsequent dynamic response analyses, and also because the experimental values for these modes were considered to be most reliable.

The adjusted Young's modulus obtained by this procedure was E_d = 3.555 x 10^6 T/m^2; the frequencies of vibration calculated using this adjusted modulus are listed in the second column of Table 4.7. The average discrepancy between these calculated frequencies and the measured values for the first four modes averages only 0.9 percent, which is well within the precision of the measurements. Even for the higher modes the agreement is remarkably good, except for modes 5 and 8. To conclude this discussion, Table 4.8 summarizes the frequencies determined by both experimental procedures, ambient and forced vibration, together with the values calculated with the final mathematical model of the dam-reservoir-foundation system.

4.4 VIBRATION MODE SHAPES

The final mathematical model including the adjusted values of rock and concrete moduli was used in all subsequent analyses and the validity of the analyses was demonstrated by correlation of analytical results with the measured values. The first such correlation involved comparing the mode shapes calculated in the vibration analysis of the dam with the mode shapes measured during the forced vibration testing. Figures 4.3 to 4.7 show the radial displacement mode shapes calculated and measured at the dam crest as well as at the upper two walkways on the downstream face of the dam. For the purpose of this presentation, the analytical shapes have been normalized to match the displacement measured at one point on the dam crest. The apparent quality of the correlation could have been improved in some modes if a different normalizing point had been chosen; however, it is evident that the analytical model duplicates the general character of the measured vibration shapes.

The plot of the fifth mode shape shown in Fig. 4.7 includes both the fifth eigenvector (equivalent to the analytical results shown for the

lower modes) and also the forced vibration shape at the dam crest obtained by including contributions from the fourth and sixth modes, as discussed in the preceding chapter. The difference between the two types of analytical results clearly shows that the adjacent modes should make a significant contribution to the forced response test; however, the measured mode shape actually correlates better with the eigenvector shape (a result which is not understood at present).

No experimental result is plotted for the sixth mode in Fig. 4.8 because this mode was not identified experimentally, as was mentioned earlier; instead, the analytical mode 6 shape (eigenvector) is compared with the calculated forced vibration response which includes contributions from modes 5 and 7. One reason why mode 6 was overlooked in the field test is apparent in Fig. 4.8--the crest shape produced by forced excitation at the sixth mode frequency is very similar to the fifth mode shape. In fact, this figure shows that the fifth mode makes a very large contribution to the response at the sixth mode frequency; on the other hand, it is evident that the antisymmetric seventh mode (Fig. 4.9) contributes very little.

4.5 FREQUENCY RESPONSE CURVES

The forced vibration response analysis capability was used to provide another form of correlation between analysis and experiment by simulating the development of the frequency response curves. First, the damping ratio for each mode was determined which made the calculated peak frequency response amplitude match the value measured at an appropriate point on the dam crest. This was done by calculating the peak frequency response at the designated point using the experimentally determined damping ratio, and then multiplying the experimental damping ratio by the analytical response amplitude divided by the experimental amplitude.Using this adjusted

damping ratio, the response at the designated point was calculated for successively changed exciting frequencies. Figure 4.10 shows the experimental and analytical response curves for the first two symmetrically excited modes and Fig. 4.11 for the first two antisymmetrically excited modes. It will be noted that mode 3 was excited by both symmetrical and antisymmetrical input, but that the response to symmetrical forces is much more prominent. As is to be expected, the frequency response curves demonstrate the same frequency discrepancies noted earlier between the analytical and experimental results. The damping ratios obtained by this adjustment procedure in the forced response analyses and by the half-power method from the experimental frequency response curves are listed on each figure; the agreement between these results is considered to be excellent.

As has been mentioned earlier, the sixth vibration mode obtained by analysis was not identified experimentally. In order to understand why the experimental procedure had not been successful with this mode, the forced vibration procedure was simulated analytically in the range of the fifth and sixth mode frequencies. Figure 4.12 shows the analytical and experimental frequency response curves for mode 5, and also the analytical frequency response curve obtained by combining the response from modes 5, 6, and 7 in the vicinity of the mode 6 frequency. It is apparent that the fifth mode dominates the frequency response curve so that no response peak is obtained for mode 6. This fact, combined with the earlier observation that the crest shapes of modes 5 and 6 are very similar (Figs. 4.7 and 4.8), prevented experimental recognition of mode 6.

4.6 HYDRODYNAMIC PRESSURES

The measurement of hydrodynamic pressures at the face of the dam during forced vibration testing, and the availability of the corresponding pressure analysis subroutine FVHYDRO, made it possible to correlate the measured and

calculated hydrodynamic pressure results. So far as is known, this is the first time that any field test verification has been made of an analytical model used to represent the effects of reservoir interaction on the dynamic response of an arch dam.

The distributions of hydrodynamic pressures across the face of the dam calculated at depths of 5 m, 15 m and 25 m below the surface are plotted in Figs. 4.13 through 4.16 for excitation at the frequencies of modes 1 through 4, respectively. Also shown on these plots (by the "o" symbols) are the pressures measured at various stations on the right side of the dam at these same water depths. The agreement between these analytical and experimental results is considered to be remarkable, especially for the first two modes. It is unfortunate that the shortcircuiting problems with the pressure gages made it impossible to make more water pressure measurements at XHD dam; however these results suggest that excellent results should be obtained in the future with the transducers modified to correct the water leakage problem.

Even though only the above limited correlation with experimental data is possible, the complete pressure distributions obtained from forced vibration in modes 1 through 6 in this analytical study are presented in Figs. 4.17 through 4.22, respectively. These results give a good general picture of the reservoir interaction mechanism during forced vibration. In each figure, the distribution of pressure is shown across the face of the dam at 49.55 m above the bottom (i.e., at a depth of 21.45 m below the surface). In addition, the pressure distribution is shown on three vertical lines extending from the water surface to the reservoir bottom at the dam face. Each of these vertical lines is associated with a node line at the face of the dam, as indicated by its position below the horizontal section graph in the figure. It is evident in these figures that the vibration

pressure is directly related to the local amplitude of motion, but that it is also influenced by boundary constraints such as the reservoir bottom, the canyon walls, and the free surface.

Chapter 5

STATIC AND EARTHQUAKE RESPONSE BEHAVIOR

5.1 GENERAL COMMENTS

The principal reason for developing a mathematical model and an analysis procedure as described in the preceding chapters is to determine whether an existing or proposed arch dam is capable of safely resisting the static and dynamic loads to which it may be subjected. Therefore, the final phase of this study of XHD dam was the calculation of the stresses and displacements that would be developed in it by possible static and seismic loading conditions.

Because this analysis has been performed for demonstration purposes only, not to verify the safety of XHD dam, the static load and vibration properties were taken for the 71 m water depth used in the correlation studies -- rather than for the full reservoir as would be done in an actual safety study. In addition, no detailed study was made to establish the maximum expectable earthquake ground motions for this site; instead an arbitrary choice was made of the earthquake input. For these reasons, the analytical results presented here should be considered only as generally representative of the dam behavior but not of maximum possible response values.

5.2 STATIC ANALYSIS

As was mentioned earlier, ADAP has the capability of evaluating stresses and displacements due to any chosen static load condition, so once the dam model had been defined (as described in the preceding chapters) it was necessary only to specify the water depth in order to obtain the static response behavior. As mentioned above, the water depth was taken to be 71 meters. The crest displacements resulting from this

hydrostatic load and from the dead weight of the concrete are depicted in Fig. 5.1,both separately and combined, and Fig. 5.2 shows the displacements in the y-z plane of the crown cantilever, again showing the separate and combined effects of the two types of static load. As expected in a good design, the gravity load effects tend to cancel the hydrostatic load effects. The stresses associated with these static displacements are very small and will be discussed later, together with the dynamic earthquake response results.

5.3 COMBINED STATIC AND EARTHQUAKE RESPONSE

Because no earthquake records have been obtained near XHD dam, the choice of earthquake input to be used in this demonstration analysis was quite arbitrary. The earthquake record obtained from an aftershock at Hsin Feng Jiang dam in Kwangdong Province was considered to be representative of tectonic conditions reasonably similar to those at the XHD dam site, so it was adopted for this study; but because the peak acceleration in this record is only 0.045g the ground motion intensity was increased by a factor of 5. The resulting peak acceleration of 0.225g probably is representative of a typical design earthquake in the XHD region.

Figure 5.3A(a) shows the magnified acceleration history of the Hsin Feng Jiang earthquake, as it was used for this demonstration analysis. A parabolic baseline correction was applied to the acceleration data to obtain reasonable final values of ground velocity and displacements; plots of these quantities (after correction) are presented in Figs. 5.3A(b) and (c). Figure 5.3B shows the response spectrum of this input motion, obtained by integration of the equations of motion; separate curves are presented for damping ratios of 0, 1, 2, 5 and 10 percent.

The step-by-step time history analysis of response to this earthquake record was carried out using six modes of vibration and a time step of 0.01 sec. for each mode. Two percent damping was assumed in each mode; the rather

low value was chosen to correspond with the low amplitude of response generated by the earthquake. The maximum displacements caused by this earthquake acting in the upstream-downstream direction are depicted in Fig. 5.4; both the crest motions and those of the crown cantilever are shown. It should be noted that these are "envelope" results, i.e., they show the maximum displacement of each node at any time during the earthquake. Thus, the displaced shape was never exactly as shown, but in general the maximum concurrent displacements are not greatly different from these envelope values. Comparing Fig. 5.4 with Figs. 5.1 and 5.2, it is apparent that the dynamic response to the Hsin Feng Jiang earthquake (multiplied by 5) is similar in magnitude to the static load effects.

The maximum stresses resulting from the combined action of the earthquake together with the static loads are shown in Figs. 5.5 for the upstream face and in Fig. 5.6 for the downstream face. The stress values are depicted in the form of contour plots, with the interval between the contours representing a stress of 1 kg/cm^2. It will be noted that the stresses are shown separately for the horizontal (arch) direction and vertical (cantilever) direction; also the maximum tensile and compressive stress distributions are shown in separate figures. The dynamic stresses vary between tensile and compressive during the earthquake while the static stresses are constant; thus, the maximum dynamic stress of each sign has been combined separately with the static stress to obtain these results. The same results for two vertical sections of the dam (A & B, shown in Fig. 5.7) are listed in Tables 5.1 through 5.4. In these tables, the separate contributions from the static and earthquake loads are identified, as well as the superposed results.

The nature of the earthquake response history is indicated in Figs. 5.8 and 5.9. The dynamic radial displacement calculated at the center point of the dam crest (Node 201 in Fig. 5.7) is shown in Fig. 5.8. It is evident from this plot that the displacement response is dominated by the first mode

vibratory motions. Figure 5.9(a) depicts the dynamic variation of arch stress at a point on Section A near the dam crest; this is where the maximum calculated arch stresses were located. Figure 5.9(b) similarly shows the variation of cantilever stress on the upstream face at the dam base near Section A; again this is the region of maximum cantilever stress. By comparing these dynamic response plots, it may be seen that the entire dynamic behavior is largely controlled by the first mode response; all plots vary similarly with time and show peak values at the same instant.

As was noted earlier with the displacement results, it is apparent from the stress values listed in Tables 5.1 to 5.4 that the dynamic stress response is similar in magnitude to the static stresses. Of course, in a highly seismic region where a much more intense earthquake than this might occur, the dynamic stresses would dominate the response. Considering the (amplified) Hsin Feng Jiang earthquake as the design requirement, however, it is evident that the XHD dam is not in danger of being damaged.

Chapter 6

SUMMARY AND CONCLUSIONS

6.1 SUMMARY

This study of Xiang Hong Dian Dam is the first phase of the cooperative research project on "Interaction Effects in the Seismic Response of Arch Dams" being carried out under the U.S.-China Protocol for Scientific and Technical Cooperation in Earthquake Studies. The ultimate purpose of the research is to improve procedures for calculating the response of arch dams to earthquake excitation, and the immediate objective is to obtain better understanding of the dynamic interaction of arch dams with their reservoir and foundation rock systems. This investigation has involved measuring the interaction effects during forced vibration tests of XHD dam and correlating these experimental results with the behavior indicated by the mathematical model of the dam-reservoir-foundation system. The refinements of the model made to improve the correlation of analysis with experiment provide the basis for advancing the state of the art of earthquake response analysis of arch dams.

The present report deals only with the study of Xiang Hong Dian Dam, a single curvature arch located in Anhui Province. The second phase of the investigation concerns Quan Shui Dam, a thin-shell double curvature arch located in Kwangdong Province; a separate report will describe the work done on that structure. Then a final report will be prepared summarizing the information obtained about the dynamic interaction of reservoir and foundation rock with arch dams, and conclusions drawn concerning the mathematical modeling of these interaction effects. The next section of this Chapter summarizes conclusions that have been drawn from the study of XHD Dam; these should be regarded as"preliminary", however, until the Quan Shui Dam investigation has been completed, because the interaction effects

may be quite different in these different types of arch dams.

6.2 CONCLUSIONS ON MODELING OF ARCH DAM RESPONSE

1. The finite element model of the concrete dam provided by the thick-shell and 3D-shell elements in the ADAP computer program seems very satisfactory. Relatively few elements are required to obtain a good representation of the vibration behavior in the first 5 or 6 modes, which is sufficient to indicate the essential character of the earthquake response behavior.

2. The foundation rock model provided by the simplest standard foundation mesh in ADAP serves to represent the foundation interaction effectively, if the modulus ratio of rock to concrete is chosen appropriately. In XHD Dam, the rock base appears to be slightly harder than the concrete, with a ratio of $E_f/E_d = 1.3$. The basic dimension of the foundation rock model used in this study is essentially equal to the dam height in all directions from the concrete-rock interface.

3. The finite element reservoir model included in the present version of the ADAP program gives a good representation of the reservoir interaction effects assuming incompressible water. The extent of the model in the upstream direction need be no more than three times the dam height, but it is important to represent the major topographical features of the reservoir bottom within this reach.

4. It is essential to include the interaction effects of reservoir and foundation, modelled as described above, to obtain good correlation between calculated and measured vibration properties. In addition, it was found necessary with XHD Dam to adjust the dynamic modulus of elasticity of the dam concrete from the value obtained by

laboratory studies (4.0×10^6 T/m^2). In this case, the adjusted value was 3.56×10^6 T/m^2; thus, the dynamic modulus measured in the field was found to be about 89 percent of the laboratory value.

5. This field study demonstrated that the foundation rock interaction can be measured effectively during forced vibration testing of arch dams, and that such measurements should be made to evaluate the dynamic interaction mechanism for the purpose of validating the foundation model.

6. The study also demonstrated that the reservoir interaction can be measured directly by using pressure transducers during the forced vibration test. Results from this study tend to indicate the validity of the incompressible liquid model, but these data are too limited to draw a definite conclusion; it is expected that the Quan Shui Dam study will greatly clarify this issue.

7. Although it was not the purpose of this study to evaluate the structural safety of XHD Dam, the results of the static analyses that have been performed indicate that it is well designed to resist the static loads to which it is subjected. In addition, the response analysis due to the amplified Hsin Feng Xiang earthquake shows that the dam is easily able to resist the intensity of earthquakes that may be expected in this region.

REFERENCES

1. Westergaard, H. M., "Water Pressures on Dams during Earthquakes", Trans. ASCE, Vol. 98, 1933.

2. Chakrabarti, P. and Chopra, A. K., "Hydrodynamic Effects in Earthquake Response of Gravity Dams", J. Struct. Div., ASCE, Vol. 100, pp.1211-1224 (1974).

3. Vogt, Frederick, "On the Calculation of Foundation Deformations", (in German), Det Norske Videnskaps Akademi, Oslo, Norway, 1925.

4. Legas, James et al., "Design and Analysis of Auburn Dam - Vol. 4 Dynamic Studies", U.S. Bureau of Reclamation, Denver, Colorado, April 1978.

5. Rouse, G. C. and Bouwkamp, J. G., "Vibration Studies of Monticello Dam", Res. Report No. 9, U.S. Bureau of Reclamation, Denver, Colorado, 1967.

6. Clough, R. W., Raphael, J. M., and Mojtahedi, S., "ADAP-A Computer Program for Static and Dynamic Analysis of Arch Dams", Earthquake Engineering Research Center Report No. UCB/EERC-73/14, University of California, Berkeley, 1973.

7. Kuo, J. S.-H., "Fluid-Structure Interactions: Added Mass Computations for Incompressible Fluid", Earthquake Engineering Research Center Report No. UCB/EERC-82/09, University of California, Berkeley, August, 1982.

8. Bathe, K. J., and Wilson, E. L., Numerical Methods in Finite Element Analysis, Prentice-Hall, Englewood Cliffs, N. J., 1976.

9. Wilson, E. L., Der Kiureghian, A., and Bayo, E. P., "A Replacement for the SRSS Method in Seismic Analysis", Earthquake Engineering and Structural Dynamics, Vol. 9, No. 2, (pp.187-194), 1981.

10. Clough, R. W., and Penzien, J., Dynamics of Structures, McGraw-Hill, New York City, New York, 1975.

Table 2.1 VIBRATION FREQUENCIES DETERMINED EXPERIMENTALLY-HZ

Mode	Forced Vibration		Ambient Vibration
1	*S	4.1	3.94
2	A	4,3	4.25
3	S	5.1	5.05
4	A	6.0	5.95
5	S	7.0	6.87
6	-	--	7.13
7	A	8.2	8.12
8	S	9.5	9.40
9	A	10.8	10.75
10	S	12.5	12.40
11	S	14.1	14.28

*Note: S = Symmetric Excitation, A = Antisymmetric Excitation

TABLE 2.2 RADIAL RESPONSE, RIGHT SIDE AT CREST

FRE-QUENCY (HZ)	MODE OF EXCITA-TION	EXCITING FORCE OF EACH EXCITER (T)	Displacements at Block No. (0.5×10^{-6}m)										
			3	4	5	6	7	8	9	10	11	12	13
4.1	++++	0.53	-0.54	-1.09	-1.30	-0.11	2.17	6.08	9.45	13.25	15.75	17.38	21.72
4.3	++--	0.60	0.22	0.22	8.89	17.77	32.58	39.98	56.27	53.31	46.65	29.62	20.73
5.1	++++	0.85	-2.72	-21.32	-21.32	-33.12	-45.37	-43.10	-40.83	-21.78	-4.54	14.97	25.86
6.0	+-+-	1.18	-16.96	-42.39	-81.96	-91.85	-85.89	-57.93	-11.30	42.39	56.52	46.63	28.26
7.0	-++-	1.62	26.92	61.69	85.24	59.44	42.62	-3.37	-48.23	-53.84	-26.92	16.82	47.11
8.2	+-+-	2.17	6.42	12.29	13.66	8.33	-0.96	-7.65	-8.88	-2.46	4.37	6.01	4.10
9.5	++++	2.95	-22.96	-36.44	-29.52	-6.56	12.76	12.03	-6.92	-25.15	-18.22	4.37	21.14
10.8	++--	1.25	-2.19	-2.19	-1.24	0.64	1.42	-0.38	-1.66	-1.08	0.44	1.02	0.77
12.5	++++	1.70	11.30	10.62	1.24	-7.69	-5.09	2.71	4.30	-4.30	-7.80	1.58	7.80
14.1	-++-	2.18	32.85	21.02	-8.87	-13.47	8.21	17.08	-2.30	-19.39	-5.91	16.09	14.45

TABLE 2.3 RADIAL RESPONSE, RIGHT SIDE ABUTMENT ROCK

Elev. (m)	Dist. From Dam (m)	Displacements ($x10^{-7}$m) at Frequency			
		4.1 HZ.	4.3 HZ.	5.1 HZ.	6.0 HZ.
143.4	0	-0.52	-1.48	-0.84	-1.42
	12.8	0.13	0.49	0.11	0.34
127.0	0	-0.59	-1.12	-0.47	1.53
	---	---	---	---	---
113.0	0	-0.53	1.33	0.85	2.60
	4.0	0.07	0.51	0.20	1.37
100.0	0	0.14	1.41	0.90	2.75
	5.5	0.07	0.70	0.22	1.48
86.5	0	0.12	1.89	0.77	1.54
	9.7	0.06	0.90	0.20	1.18

TABLE 2.4 COMPARISON OF U.S. AND CHINA DISPLACEMENT MEASUREMENTS
(Recorded at Block No. 3)

Frequency Hz.	Direction R = Radial T = Tangential	Displacement Response (m) ($mx10^{-7}$) U.S.	China	Prop. Factor
4.1	R	3.721	3.745	0.99
	T	0.935	0.785	1.19
4.3	R	1.773	1.695	1.04
	T	6.949	7.140	0.97
5.1	R	20.96	20.70	1.01
	T	9.379	8.920	1.05
6.0	R	40.32	48.89	0.82
	T	5.076	8.745	0.58
7.0	R	34.50	107.06	0.32
	T	8.796	15.880	0.55
8.2	R	29.48	32.10	0.92
	T	0.9438	2.140	0.44

TABLE 2.5 NORMALIZED AMBIENT VIBRATION MODE SHAPES
(Radial Direction, at Crest)

Frequency (Hz)	Relative Displacement at Block No.										
	Right Abutment	3	5.5+	8	10.5+	12.5+	14.5+	16	18.5+	20.5+	Left Abutment
4.05	-0.02	-0.14	-0.09	0.19	0.64	0.81	*	1.00	0.05	-0.08	*
4.27	-0.05	0.05	0.20	0.55	1.00	0.63	*	-0.76	-0.45	-0.13	*
5.03	-0.07	-0.09	-0.74	-1.00	-0.27	0.55	*	-0.37	-1.00	-0.12	*
5.88	-0.12	-0.31	-1.00	-0.58	0.57	0.48	*	0.37	0.67	0.24	*
6.88	-0.07	0.18	0.50	-0.27	-0.40	0.36	*	-0.44	-0.23	1.00	*
**7.13	0.13	0.39	0.84	-0.33	-1.00	-0.48	*	-0.54	-0.01	0.14	*

* Seismometer did not work.

** This is the "missing mode" in the forced vibration experiment.

+ Block No. 5.5 (etc.) denotes left edge of Block No. 5.

TABLE 2.6 DAMPING RATIOS FROM EXPERIMENTAL FREQUENCY RESPONSE CURVES

FREQUENCY HZ.	LOCATION OF TRANSDUCER	DAMPING RATIO
4.1	13	0.017
4.3	11	0.014
5.1	13	0.010
6.0	11	0.011
7.0	3	0.011
8.2	3	0.010
9.5	3	0.006
10.8	9	0.009
12.5	13	0.011
14.1	3	0.010

TABLE 2.7 HYDRODYNAMIC PRESSURES MEASURED DURING FORCED VIBRATION

Frequency (Hz)	Location of Pressure Gage		Hydrodynamic Pressure $x10^{-3}$ T/M^2
	Block No.	Water Depth (m)	
4.1	11	5	2.1
	9	5	2.0
	11	15	3.1
	11	25	3.5
	9	25	1.8
4.3	11	5	7.4
	9	5	6.3
	11	15	9.5
	9	15	8.4
	7	15	6.3
	11	25	9.8
	9	25	7.0
5.1	11	5	2.1
	9	5	7.0
	11	15	2.8
	7	15	7.6
	11	25	3.0
	9	25	3.1
6.0	11	5	7.0
	9	5	2.5
	11	15	9.15
	7	15	4.2
	11	25	7.7

TABLE 3.1 FREQUENCIES OF VIBRATION, BASIC FOUNDATION AND RESERVOIR CASES

	Frequency - Hz.			
CASE	A	B	C	Experimental Forced Response Frequency*
Basic Foundation	No	Yes	Yes	
Basic Reservoir	No	No	Yes	
Mode 1	4.80	4.50	4.06	4.1
Mode 2	5.06	4.76	4.46	4.3
Mode 3	5.84	5.55	5.32	5.1
Mode 4	6.67	6.39	6.24	6.0
Mode 5	8.08	7.73	7.69	7.0
Mode 6	9.02	8.68	7.84	--
Mode 7	10.00	8.98	8.72	8.2
Mode 8	11.61	10.12	9.16	9.5
Mode 9	11.81	11.02	10.32	--
Mode 10	12.56	11.25	11.06	10.8
Mode 11	13.14	12.35	12.20	12.5
Mode 12	13.82	12.45	12.32	14.1

*Note: The reservoir was not at the maximum depth during these experiments, as was assumed in these analyses.

TABLE 3.2 INFLUENCE OF FOUNDATION MODEL ON VIBRATION FREQUENCIES

	Frequency - Hz			
Case	1	2	3	4
Foundation Mesh	Rigid	Type 1	Type 2	Type 3
Mode 1	4.41	4.06	4.07	4.02
Mode 2	4.80	4.46	4.46	4.43
Mode 3	5.64	5.32	5.31	5.29
Mode 4	6.54	6.24	6.22	6.20
Mode 5	8.06	7.69	7.65	7.64
Mode 6	8.65	7.84	7.85	7.75
Mode 7	9.09	8.72	8.70	8.67
Mode 8	10.17	9.16	9.15	9.01
Mode 9	11.55	10.32	10.31	9.92
Mode 10	12.21	11.06	11.02	10.94
Mode 11	12.40	11.20	11.18	11.10
Mode 12	13.11	12.32	12.25	11.71

TABLE 3.3 INFLUENCE OF RESERVOIR LENGTH ON VIBRATION FREQUENCIES

Mode No.	Reservoir Length					
	L = 15 m	L = 65 m	L = 130 m	L = 300 m	L = 600 m	L = 700 m
1	2.841	3.233	3.242	3.262	3.262	3.262
2	3.411	3.577	3.596	3.606	3.606	3.606
3	4.178	4.255	4.332	4.342	4.342	4.342
4	5.083	5.122	5.237	5.266	5.266	5.266
5	6.523	6.553	6.632	6.750	6.750	6.750
6	6.525	7.049	7.137	7.156	7.156	7.156

Note: The reservoir is full and boundary is natural topography.

TABLE 3.4 INFLUENCE OF RESERVOIR DEPTH ON VIBRATION FREQUENCIES (HZ)

Mode No.	Depth of Reservoir Water, Z					
	Z = 0 (No Reservoir)	Z = 37.6m (0.43H)	Z = 68.78m (0.786H)	Z = 71.0m (0.811H)	Z = 71.59m (0.818H)	Z = 87.5m (1.0H)
1	4.398	4.349	4.036	3.977	3.957	3.262
2	4.620	4.610	4.396	4.347	4.328	3.606
3	5.379	5.360	5.204	5.156	5.137	4.342
4	6.140	6.130	6.034	5.996	5.986	5.266
5	7.745	7.730	7.530	7.501	7.491	6.750
6	8.556	8.508	7.662	7.623	7.613	7.156
7	8.737	8.477	8.400	8.381	8.380	7.775
8	9.964	9.905	9.150	9.100	9.090	8.812
9	10.850	10.849	10.519	10.509	10.499	9.962
10	11.181	11.039	10.723	10.656	10.637	10.458
11	12.308	12.201	11.006	10.967	10.957	10.585
12	13.117	12.984	12.675	12.665	12.655	12.583

Note: H = maximum height of the dam.
Length of Reservoir is 300 m.

TABLE 4.1

MODE 1 FORCED VIBRATION DISPLACEMENTS AT ROCK-CONCRETE INTERFACE

Node No.	Displacements ($m \times 10^{-8}$)					
	Measured	$E_f/E_d = 1.3$		$E_f/E_d = 0.65$		E_f/E_d =0.325
		Massless	w/Mass	Massless	w/Mass	
422	-5.2	-1.67	-2.20	-3.97	-6.16	-4.32
394	-5.5	-2.79	-3.05	-5.82	-6.60	-5.41
360	-0.5	-0.44	-0.49	-0.28	-0.32	-0.47
320	4.0	1.86	1.94	4.20	4.47	4.67
274	--	6.84	7.2	13.90	14.47	14.23

Note: Analytical $E_d = 4.0 \times 10^6$ T/m^2 (5.68×10^6 psi).

TABLE 4.2

MODE 2 FORCED VIBRATION DISPLACEMENTS AT ROCK-CONCRETE INTERFACE

Node No.	Displacements ($m \times 10^{-8}$)					
	Measured	$E_f/E_d = 1.3$		$E_f/E_d = 0.65$		E_f/E_d =0.325
		Massless	w/Mass	Massless	w/Mass	
422	-14.8	-4.26	-5.48	-9.59	-14.48	-11.60
394	2.5	-0.70	- .73	1.75	2.11	2.92
360	15.5	19.60	20.36	39.97	43.78	40.68
320	26.5	21.42	22.31	42.73	46.96	44.89
274	---	24.96	25.87	47.31	51.67	48.58

Note: Analytical $E_d = 4.0 \times 10^6$ T/m^2 (5.68×10^6 psi).

TABLE 4.3

MODE 3 FORCED VIBRATION DISPLACEMENTS AT ROCK-CONCRETE INTERFACE

Node No.	Displacements (m x 10^{-8})					
	Measured	E_f/E_d = 1.3		E_f/E_d = 0.65		E_f/E_d =0.325
		Massless	w/Mass	Massless	w/Mass	
422	-8.40	-4.24	-5.32	-10.05	-14.50	-12.03
394	6.00	7.13	7.48	17.42	19.01	16.44
360	8.50	21.47	22.47	42.55	45.89	41.02
320	8.00	14.40	15.2	28.62	31.32	30.29
274	---	6.14	6.53	12.07	13.40	14.85

Note: Analytical $E_d = 4.0 \times 10^6$ T/m^2 (5.68×10^6 psi).

TABLE 4.4

MODE 4 FORCED VIBRATION DISPLACEMENTS AT ROCK-CONCRETE INTERFACE

Node No.	Displacements ($m \times 10^{-8}$)					
	Measured	$E_f/E_d = 1.3$		$E_f/E_d = 0.65$		E_f/E_d =0.325
		Massless	w/Mass	Massless	w/Mass	
422	-14.2	-10.20	-10.23	-20.70	-16.79	-31.67
394	24.0	41.96	45.82	87.87	105.7	108.00
360	22.5	51.79	55.87	93.38	108.6	134.60
320	8.0	17.60	19.66	31.87	39.89	63.89
274	--	-5.80	-5.61	-10.61	-9.32	6.68

Note: Analytical $E_d = 4.0 \times 10^6$ T/m^2 (5.68×10^6 psi).

TABLE 4.5

MODE 5 FORCED VIBRATION DISPLACEMENTS AT ROCK-CONCRETE INTERFACE

Node No.	Displacements ($m \times 10^{-8}$)					
	Measured	$E_f/E_d = 1.3$		$E_f/E_d = 0.65$		E_f/E_d =0.325
		Massless	w/Mass	Massless	w/Mass	
422	16.3	12.76	12.58	22.56	9.26	11.11
394	-27.0	-63.95	-70.92	-123.90	-157.7	-23.99
360	-26.0	-34.66	-39.51	-54.80	-72.8	-24.96
320	9.0	-16.15	-15.31	9.99	-16.28	-34.94
274	--	-40.69	-37.85	40.00	-24.88	-80.36

Note: Analytical $E_d = 4.0 \times 10^6$ T/m^2 (5.68×10^6 psi).

TABLE 4.6

MODE 7 FORCED VIBRATION DISPLACEMENTS AT ROCK-CONCRETE INTERFACE

Node No.	Displacements ($m \times 10^{-8}$)					
	Measured	$E_f/E_d = 1.3$		$E_f/E_d = 0.65$		E_f/E_d =0.325
		Massless	w/Mass	Massless	w/Mass	
422	-5.2	-2.68	- 1.02	-3.80	- .22	-6.32
394	18.0	15.94	16.26	23.72	33.13	38.88
360	4.5	5.60	5.86	8.76	14.56	21.92
320	-1.0	-2.36	-2.14	-0.80	4.03	6.53
274	--	-4.91	-5.23	-5.03	4.68	-2.74

Note: Analytical $E_d = 4.0 \times 10^6$ T/m^2 (5.68×10^6 psi).

TABLE 4.7

MODIFICATION OF CALCULATED FREQUENCIES WITH YOUNG'S MODULUS ADJUSTMENT

	Frequencies - HZ		
	Calculated		
Mode No.	$E_d = 4 \times 10^6$ T/m^2	$E_d = 3.555 \times 10^6$ T/m^2	Measured
1	4.23	3.98	4.1 (S)
2	4.62	4.35	4.3 (AS)
3	5.48	5.16	5.1 (S)
4	6.37	6.00	6.0 (AS)
5	7.96	7.50	7.0 (S)
6	8.07	7.62	---
7	8.90	8.38	8.2 (AS)
8	9.58	9.03	9.5 (S)
9	10.60	9.99	---
10	11.27	10.63	10.8 (AS)
11	11.55	10.89	---
12	12.19	11.49	---

Notes: $E_f/E_d = 1.3$.

Water level = 0.811 H (126.9m).

TABLE 4.8

FINAL COMPARISON OF CALCULATED AND MEASURED VIBRATION FREQUENCIES

Mode No.	Vibration Frequencies - HZ		
	Measured		Calculated
	Forced	Ambient	
1	4.1 (S)	3.94	3.99
2	4.3 (A)	4.25	4.36
3	5.1 (S)	5.05	5.17
4	6.0 (A)	5.95	6.01
5	7.0 (S)	6.87	7.50
6	--	7.13	7.61
7	8.2 (A)	8.12	8.39
8	9.5 (S)	9.40	9.03
9	--	--	9.99
10	10.8 (A)	10.75	10.63
11	--	--	10.89
12	--	--	11.49
--	*12.5 (S)	12.40	--
--	*14.1 (S)	14.28	

*Note: These were assumed to be Modes 10 and 11 in early stages of the investigation (see Table 2.1), and later were assumed to be Modes 11 and 12 (see Table 3.1). Only in the final correlation study was it realized that Modes 6, 9, 11, and 12 all were missed experimentally.

Table 5.1 MAXIMUM ARCH STRESSES AT SECTION A-A - kg/cm^2

Elevation (m.)	Upstream Face			Downstream Face		
	Gravity and Hydrostatic	Earthquake	Total	Gravity and Hydrostatic	Earthquake	Total
137.9	-4.43	-7.56	-11.99	-3.46	-6.75	-10.21
122.9	-6.54	-4.64	-11.18	-4.12	-4.32	- 8.44
112.36	-7.05	-2.79	- 9.84	-4.12	-3.02	- 7.14
98.54	-6.23	-1.40	- 7.63	-3.85	-1.58	- 5.43
90.34	-5.28	-0.82	- 6.10	-3.37	-1.03	- 4.40
81.66	-4.12	-0.38	- 4.50	-2.85	-0.58	- 3.43
76.00	-3.48	-0.04	- 3.52	-2.46	-0.27	- 2.73
71.00	-2.23	0.37	1.86	-3.38	-0.20	- 3.58
65.35	-0.12	1.67	1.55	-3.13	0.02	- 3.11

Table 5.2 MAXIMUM CANTILEVER STRESSES AT SECTION A-A - kg/cm^2

Elevation (m.)	Upstream face			Downstream Face		
	Gravity and Hydrostatic	Earthquake	Total	Gravity and Hydrostatic	Earthquake	Total
137.9	-2.38	-0.18	- 2.56	-0.04	-1.20	- 1.24
122.9	-7.76	-1.52	- 9.28	0.36	-4.52	- 4.88
112.36	-9.52	-2.77	-12.29	-0.30	-5.56	- 5.86
98.54	-8.28	-3.62	-11.90	-4.10	-4.70	- 8.80
90.34	-7.10	-3.75	-10.85	-6.63	-3.93	-10.56
81.66	-5.97	-3.71	- 9.68	-9.14	-3.24	-12.38
76.00	-3.44	-3.27	- 6.71	-12.50	-2.43	-14.93
71.00	-3.99	-2.95	- 6.94	-14.10	-2.40	-16.50
65.35	-0.07	-6.47	- 6.54	-15.60	-2.20	-17.80

Table 5.3 MAXIMUM ARCH STRESSES AT SECTION B-B - kg/cm^2

Elevation (m.)	Upstream Face			Downstream Face		
	Gravity and Hydrostatic	Earthquake	Total	Gravity and Hydrostatic	Earthquake	Total
137.9	-4.14	-6.33	-10.47	-3.28	-6.98	-10.26
122.9	-6.07	-4.31	-10.38	-4.10	-4.25	- 8.35
112.36	-6.53	-2.37	- 8.90	-4.10	-3.01	- 7.11
98.54	-5.52	-1.09	- 6.61	-4.11	-1.77	- 5.88
90.34	-4.42	-0.43	- 4.85	-3.90	-1.21	- 5.11
81.66	-3.30	-0.01	- 3.31	-3.48	-0.80	- 4.28
76.00	0.0	0.21	0.21	-0.001	-0.52	- 0.52
71.00	1.73	0.37	2.10	0.16	-0.42	- 0.26
65.35	0.64	1.68	2.32	-2.71	-0.06	- 2.77

Table 5.4 MAXIMUM CANTILEVER STRESSES AT SECTION B-B - kg/cm^2

Elevation (m.)	Upstream Face			Downstream Face		
	Gravity and Hydrostatic	Earthquake	Total	Gravity and Hydrostatic	Earthquake	Total
137.9	-2.36	0.54	- 1.82	-0.05	-0.103	- 0.15
122.9	-7.64	-1.02	- 8.66	0.20	-3.74	- 3.54
112.36	-9.35	-2.18	-11.53	-0.51	-5.01	- 5.51
98.54	-8.10	-3.00	-11.10	-4.50	-4.25	- 8.75
90.34	-6.85	-3.30	-10.15	-7.02	-3.62	-10.64
81.66	-5.73	-3.31	- 9.04	-9.63	-3.02	-12.65
76.00	0.02	-2.65	- 2.63	-0.004	-2.37	- 2.38
71.00	-1.01	-2.70	- 3.71	-0.51	-3.05	- 3.56
65.35	-7.05	-6.70	-13.75	-4.07	-2.30	- 6.37

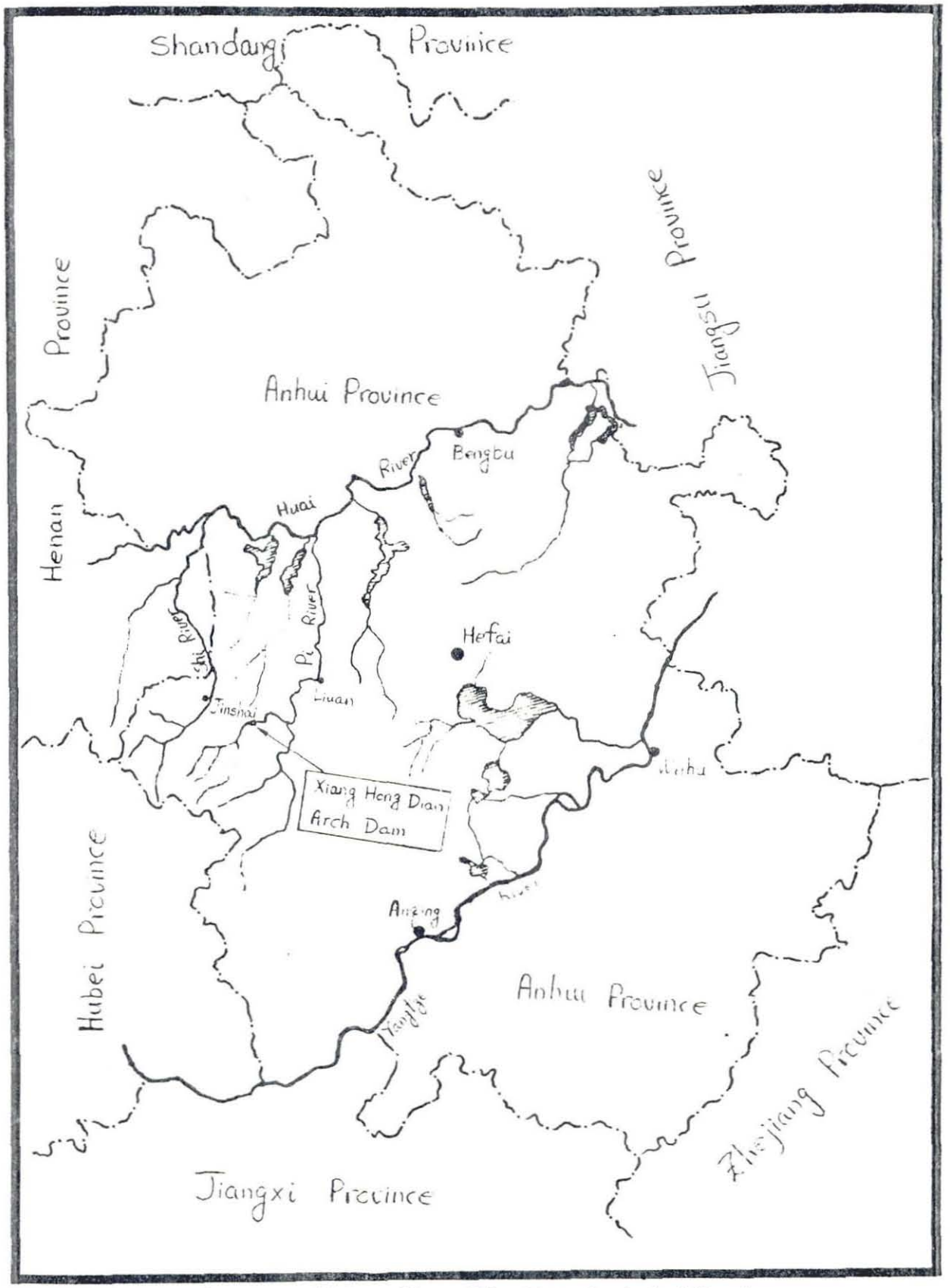

FIG. 2.1 Location of Xiang Hong Dian Dam In Anhui Province

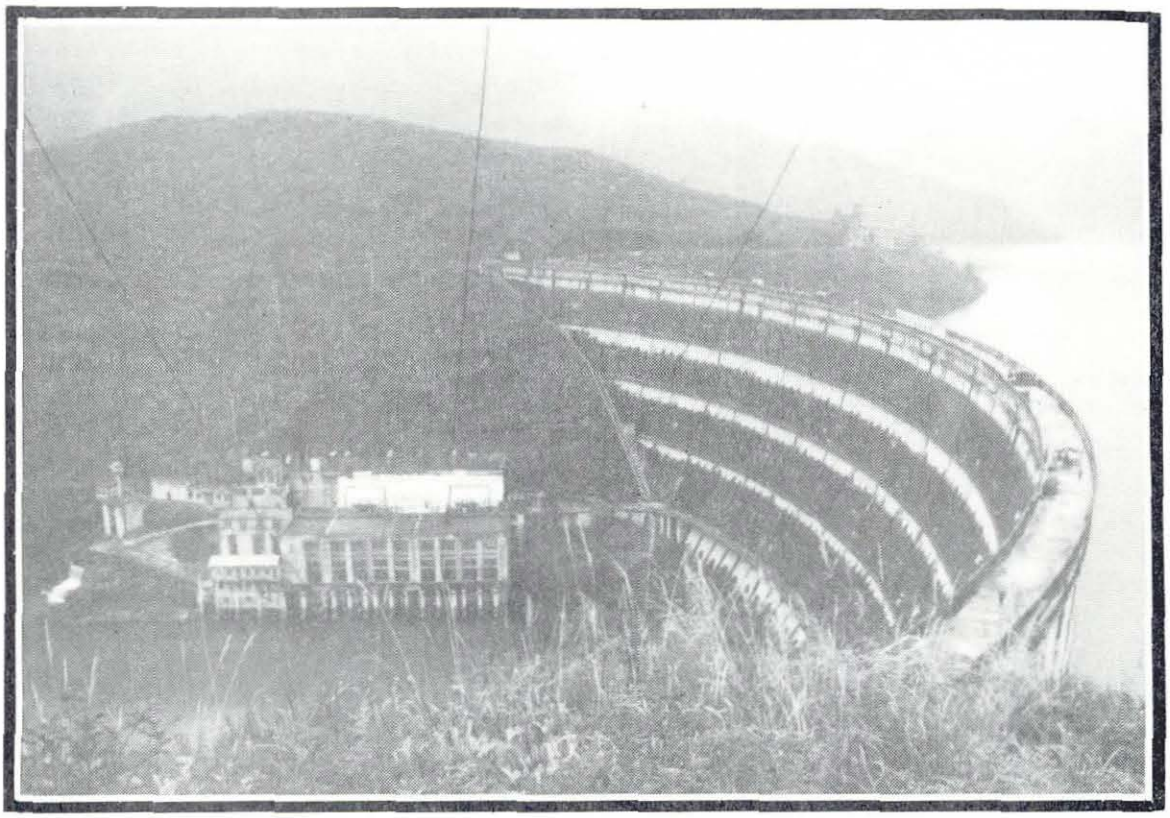

FIG. 2.2 View Of Xiang Hong Dian Dam And Reservoir

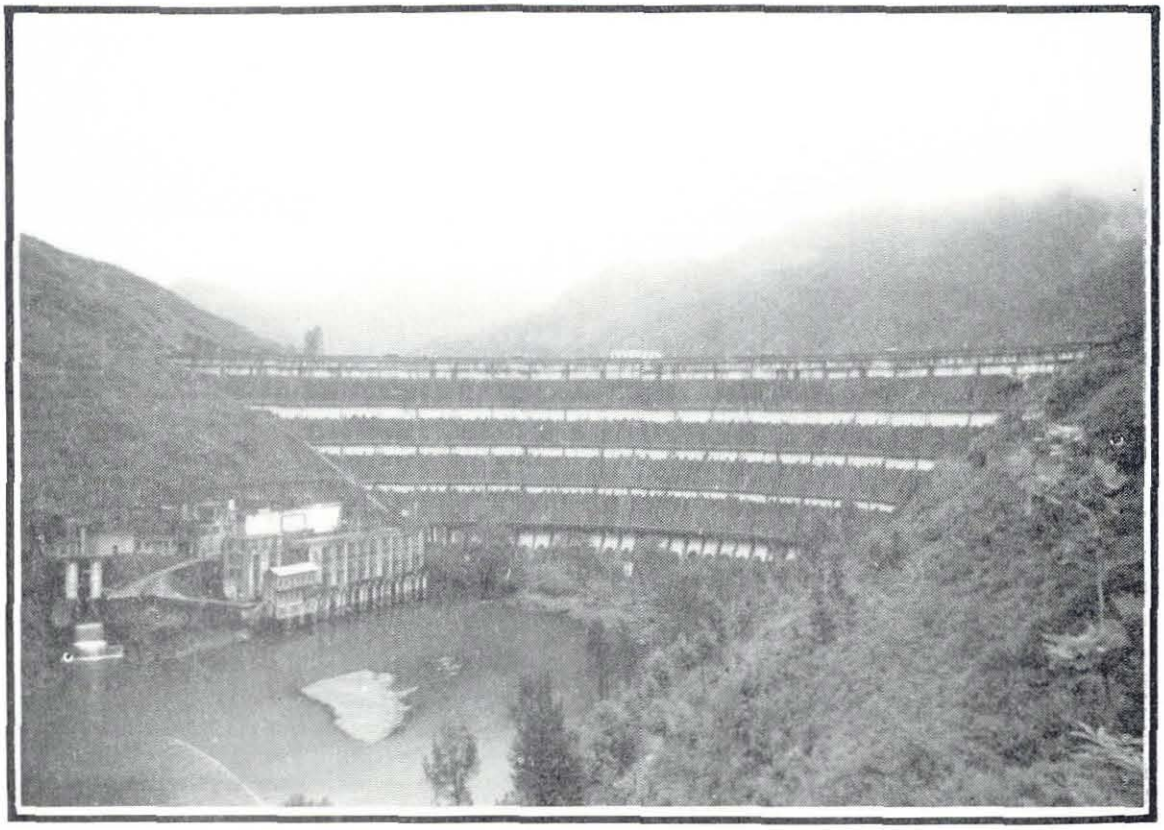

FIG. 2.3 Downstream Face of Xiang Hong Dian Dam

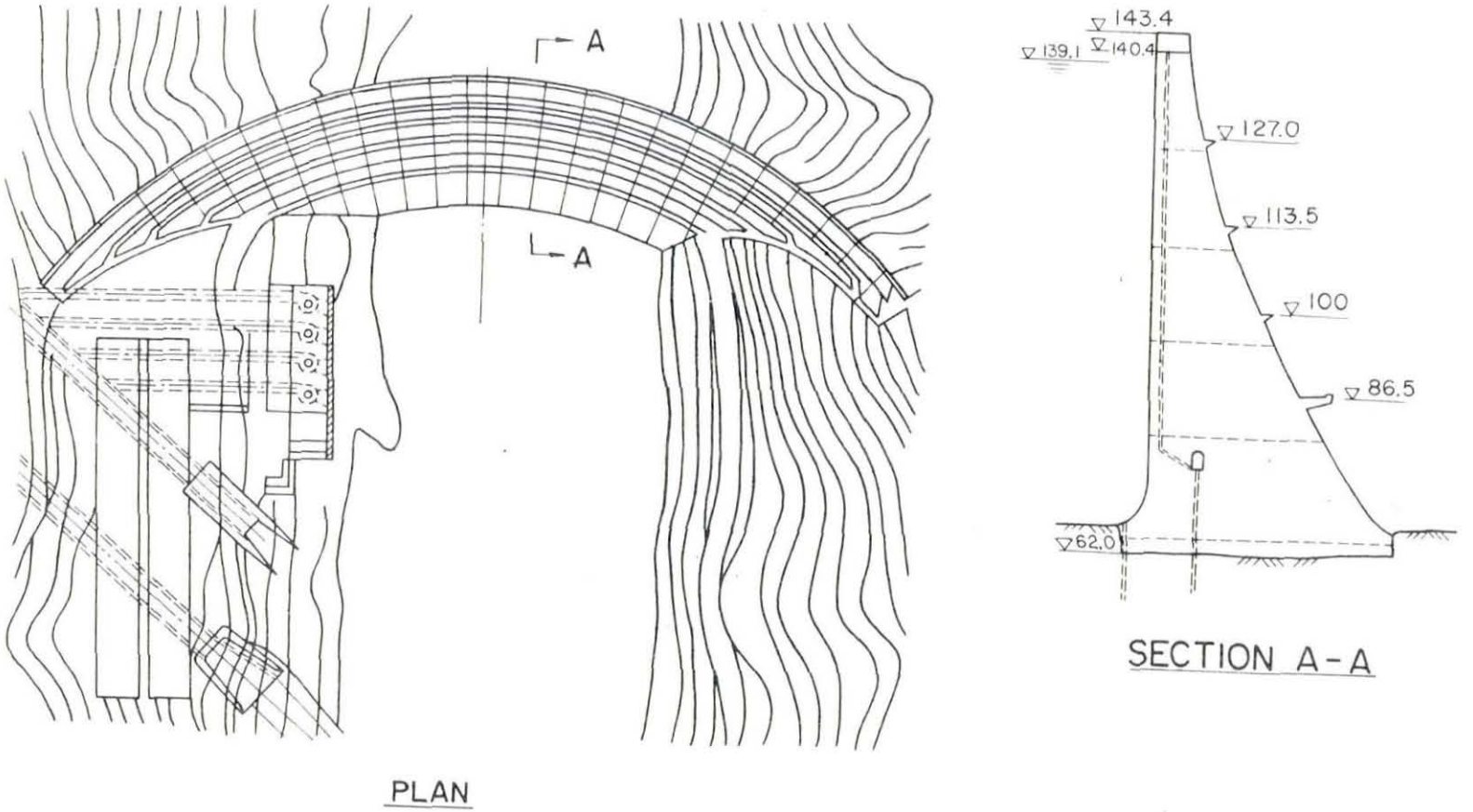

FIG. 2.4 Layout Of Xiang Hong Dian Dam

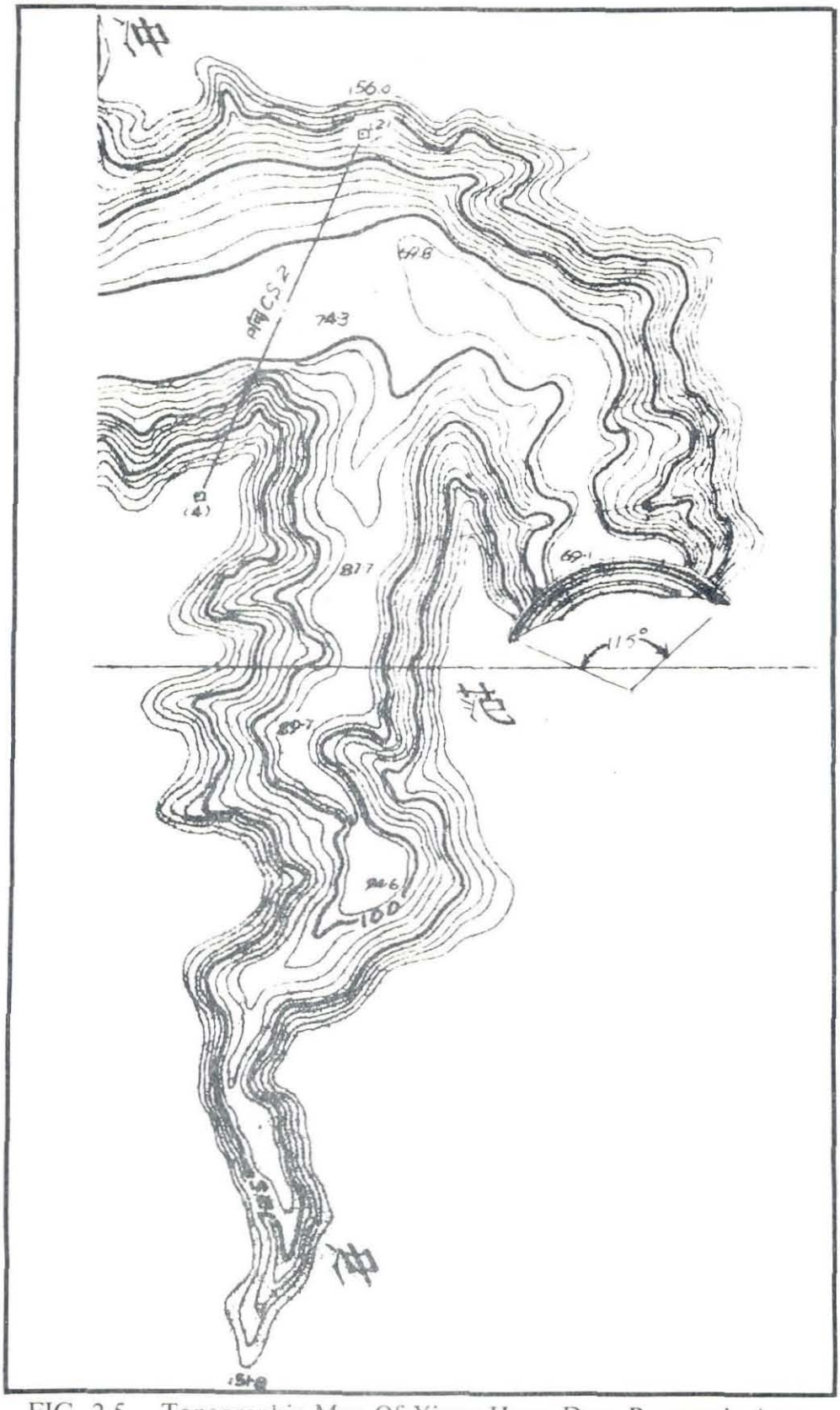

FIG. 2.5 Topographic Map Of Xiang Hong Dam Reservoir Area (Contour Interval = 5m)

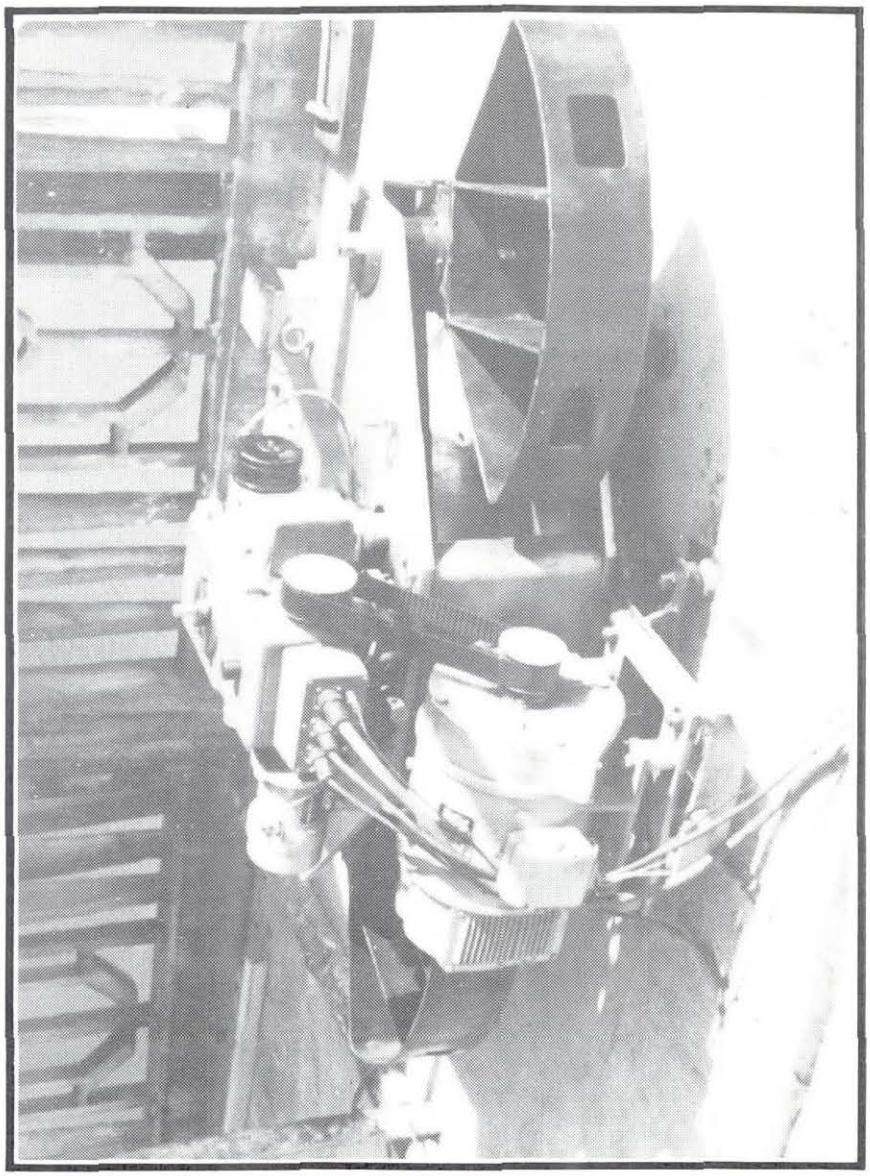

FIG. 2.6 Rotating Mass Shaker Unit

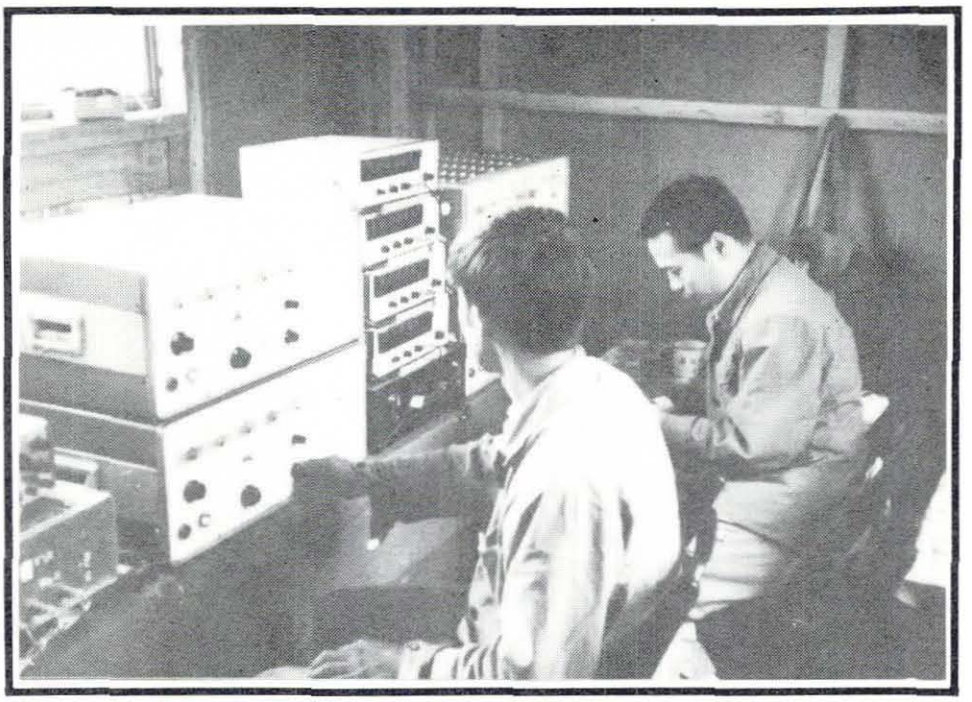

FIG. 2.7 Shaker Control System In Operation

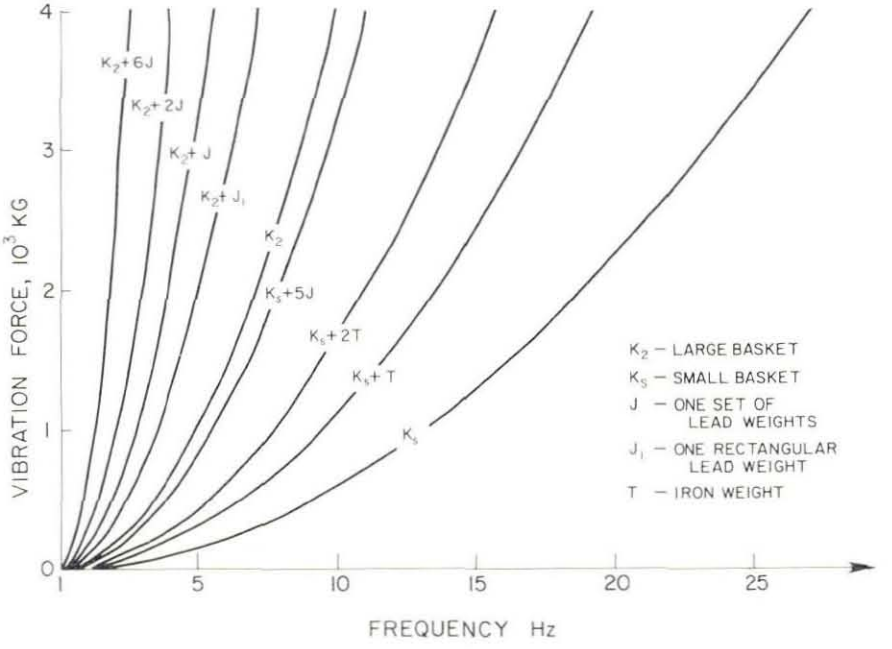

FIG. 2.8 Exciting Force Induced By Single Shaker Unit

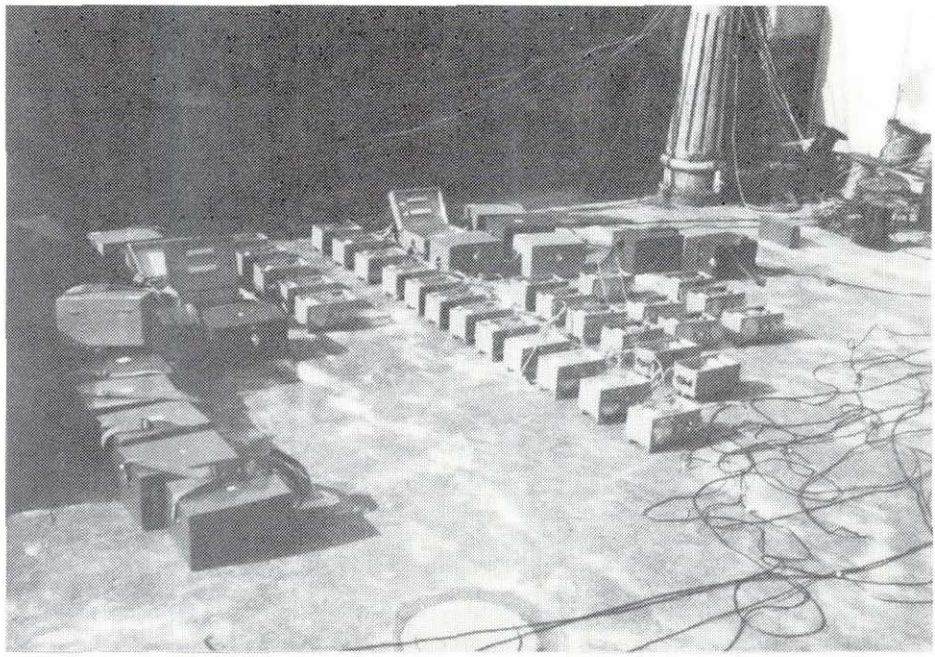

FIG. 2.9 Velocity Meters Ready To Be Positioned On Dam

FIG. 2.10 Ranger Seismometer In Position On The Abutment Rock

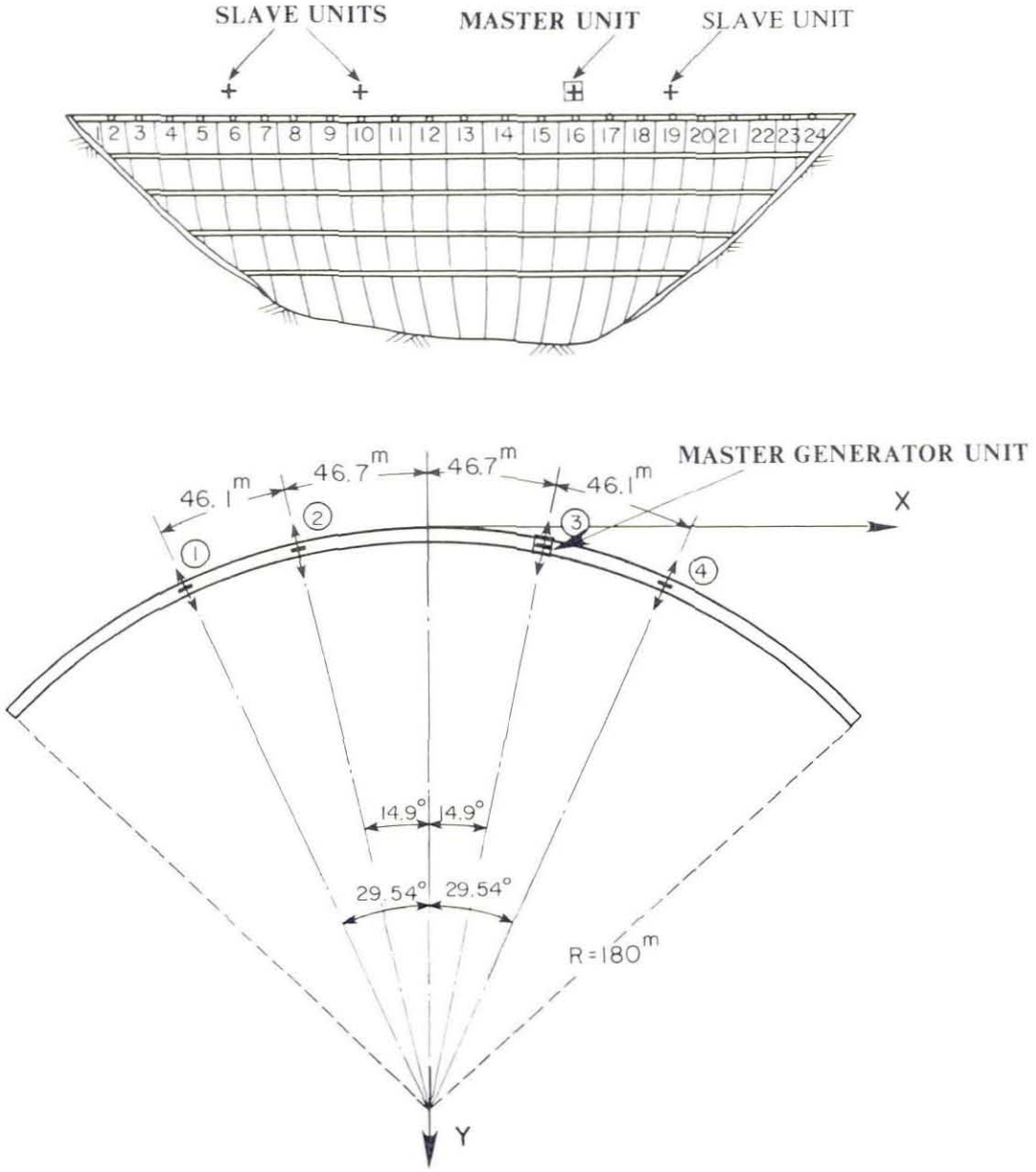

FIG. 2.11 Position Of Vibration Generators On The Dam Crest

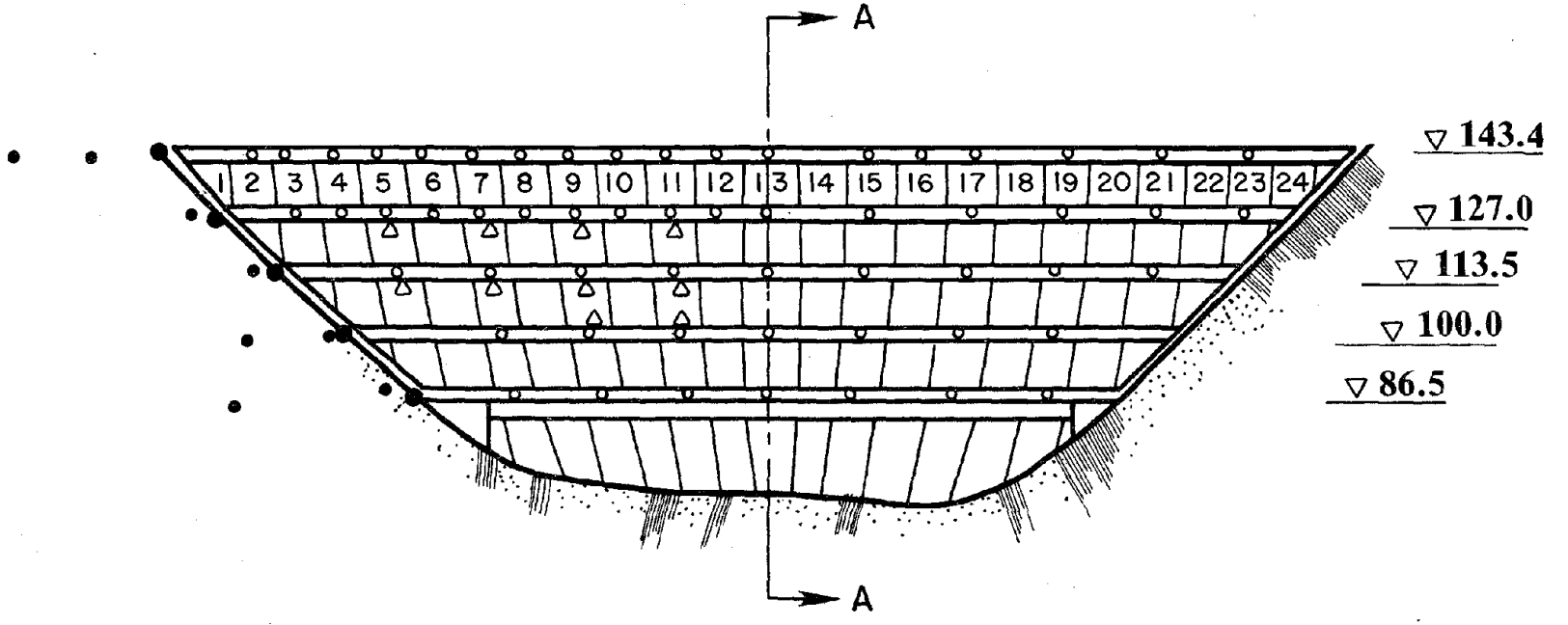

○ SRIWCHP AND SRIWCAP SURVEY STATION
● EERC SURVEY STATION FOR DISPLACEMENT
△ EERC SURVEY STATION FOR HYDRODYNAMIC PRESSURE

FIG. 2.12 Locations Of Transducer Stations On Dam And Abutment Rock

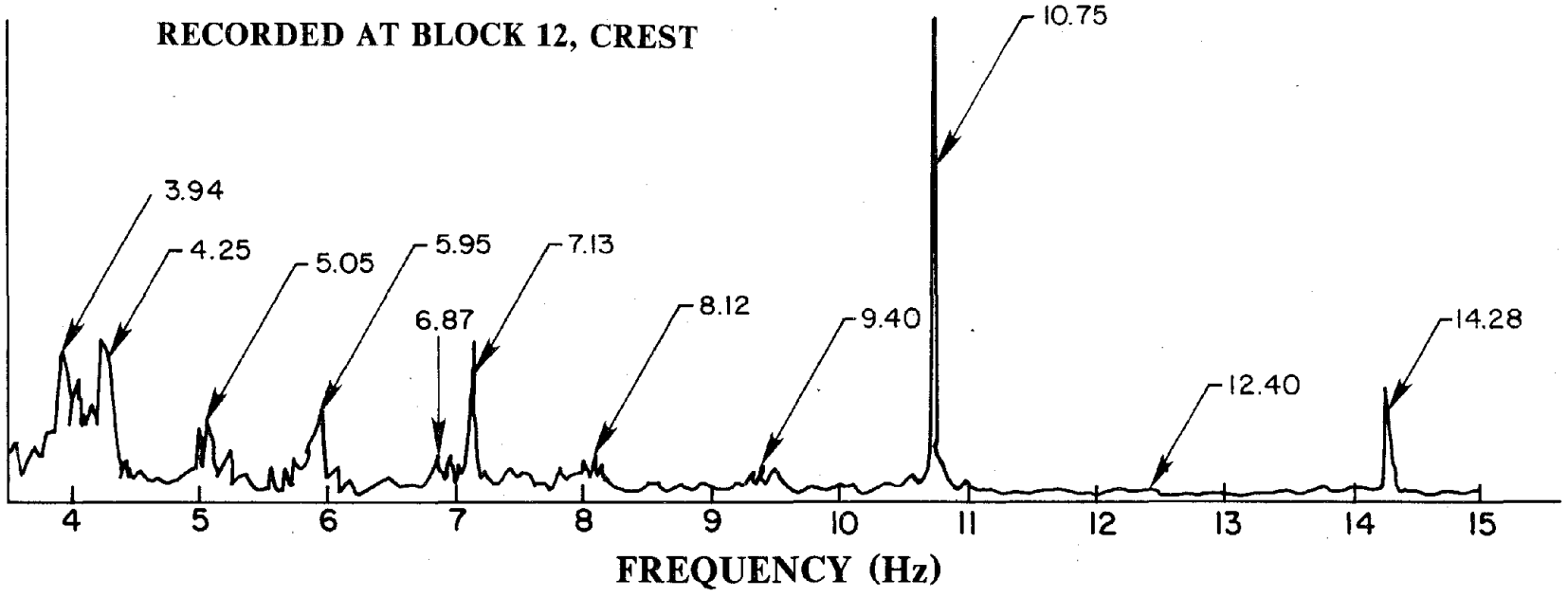

FIG. 2.13 Fourier Amplitude Spectrum From Ambient Vibrations

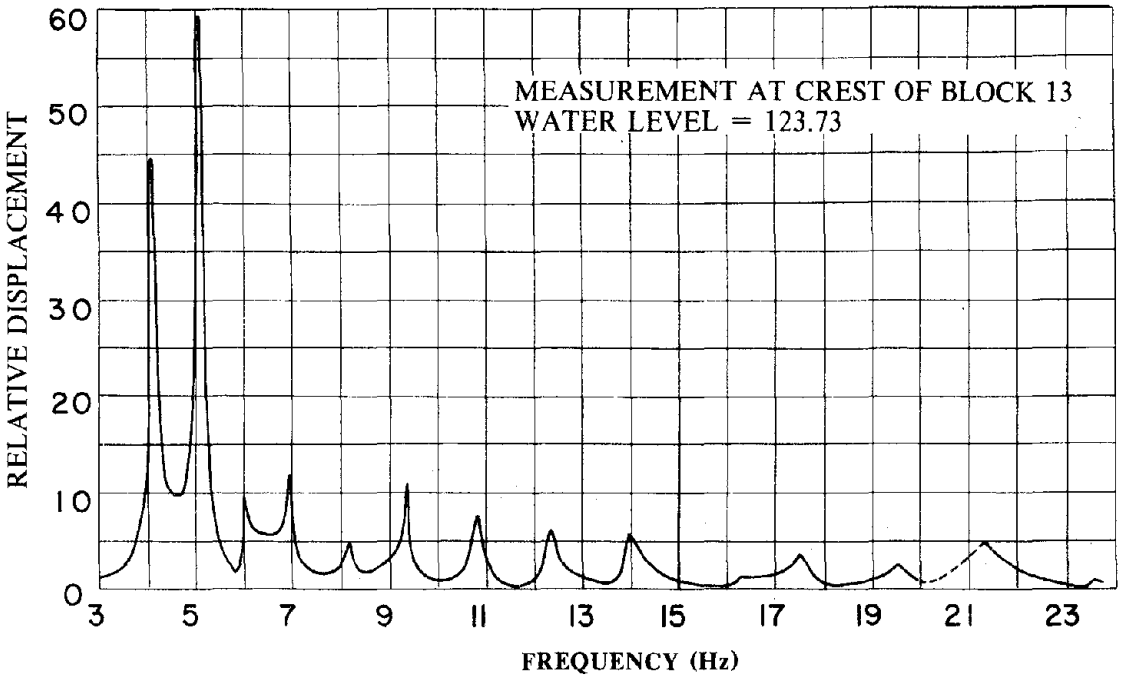

FIG. 2.14 Displacement Frequency Response Curve From Symmetric Excitation

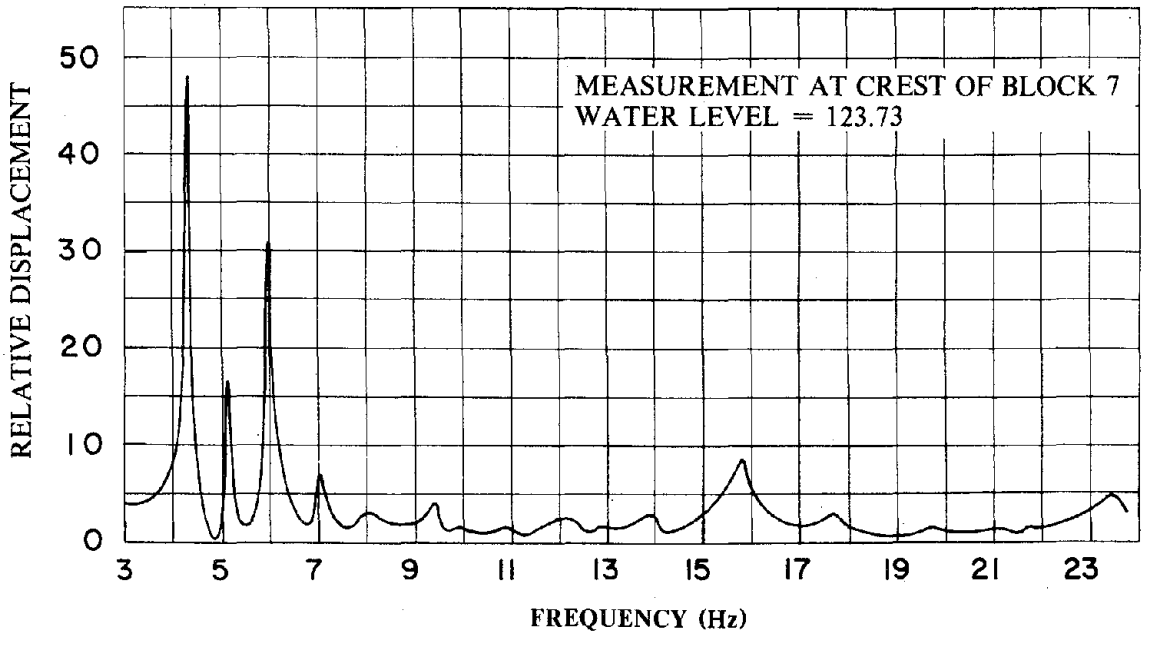

FIG. 2.15 Displacement Frequency Response Curve From Antisymmetric Excitation

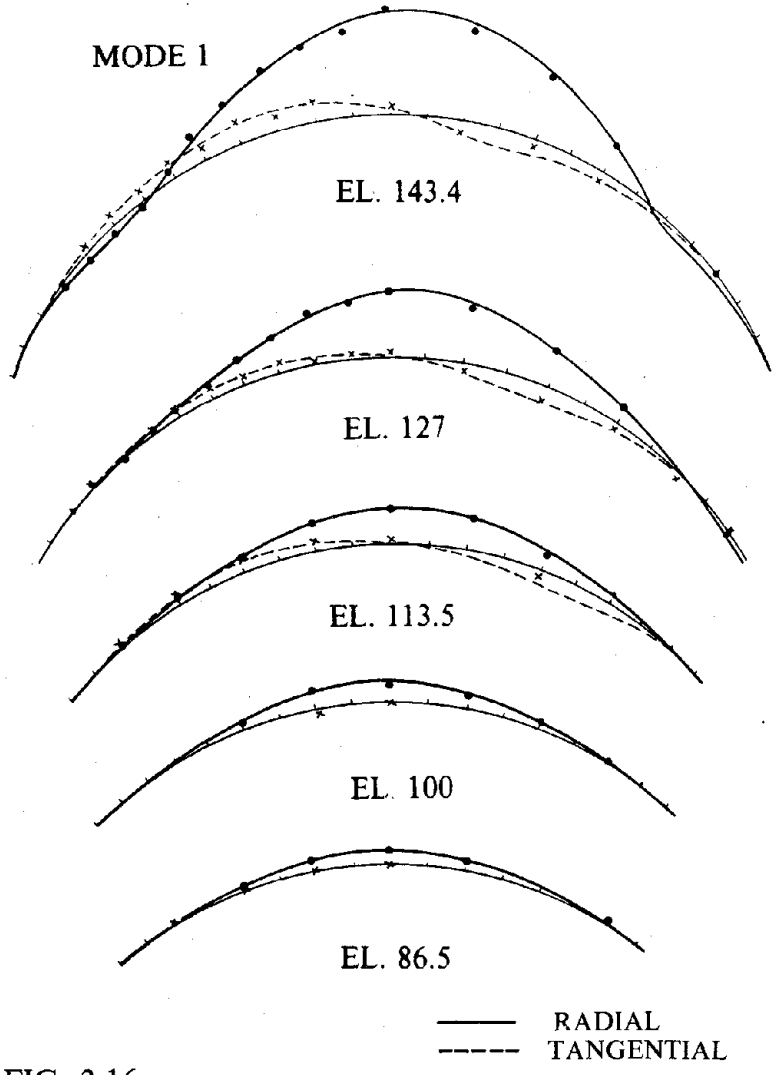

FIG. 2.16
Horizontal Forced Vibration Response: f=4.1 Hz

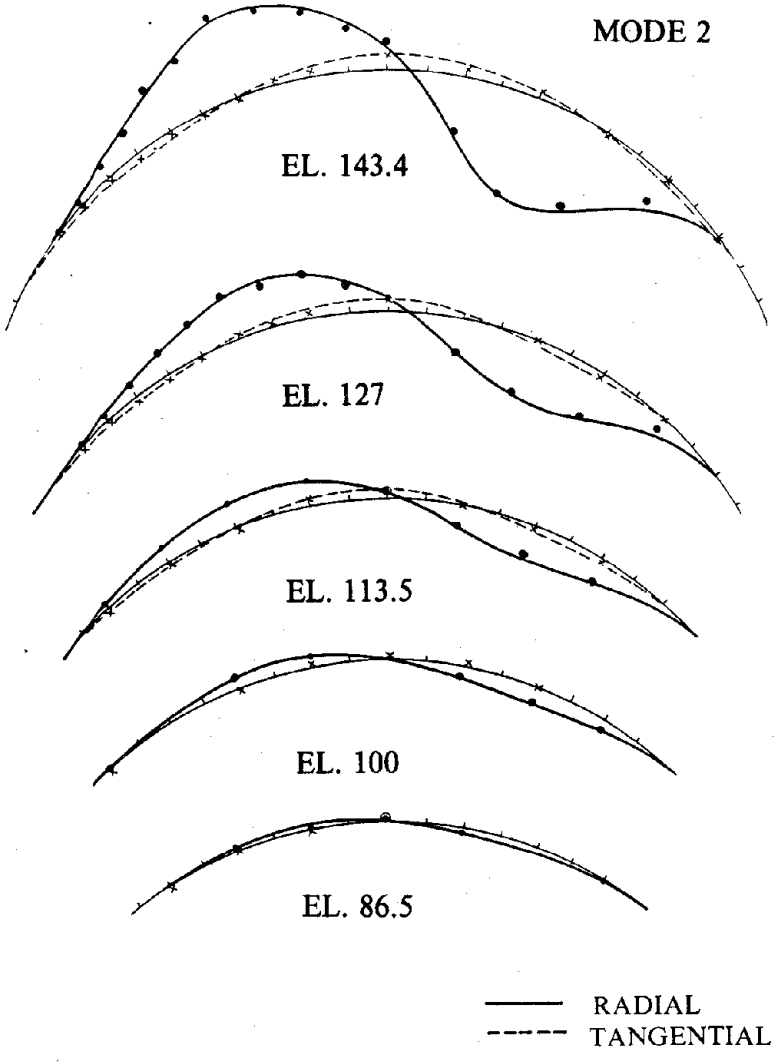

FIG. 2.17
Horizontal Forced Vibration Response: f=4.3 Hz

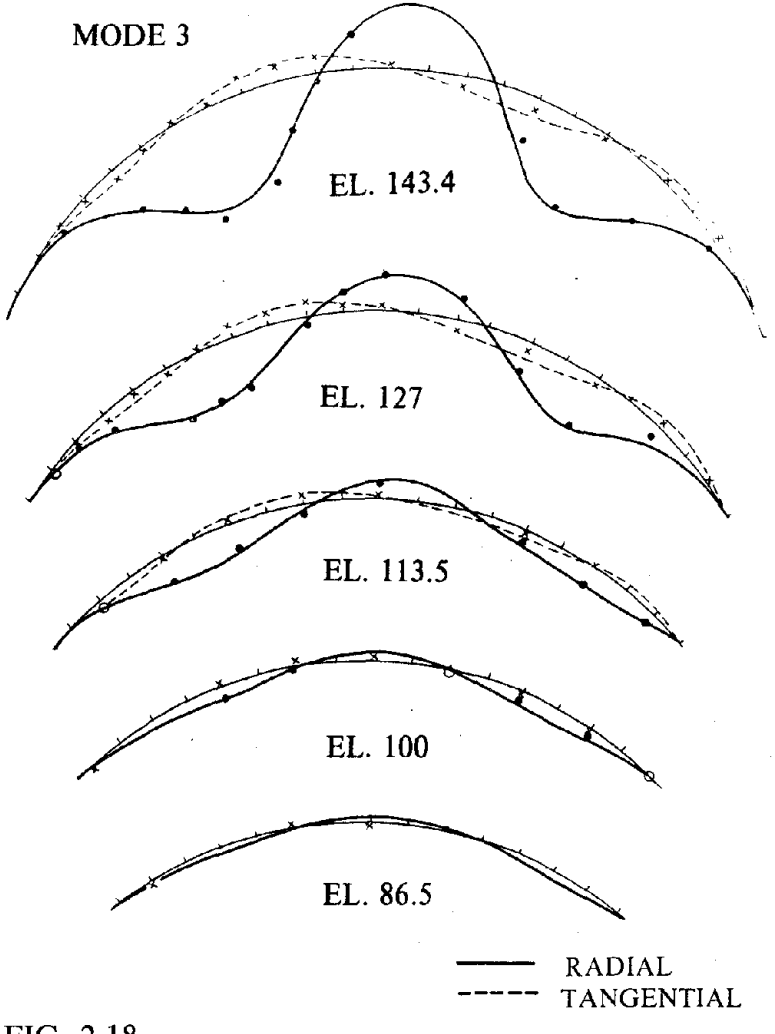

FIG. 2.18
Horizontal Forced Vibration Response: f=5.1 Hz

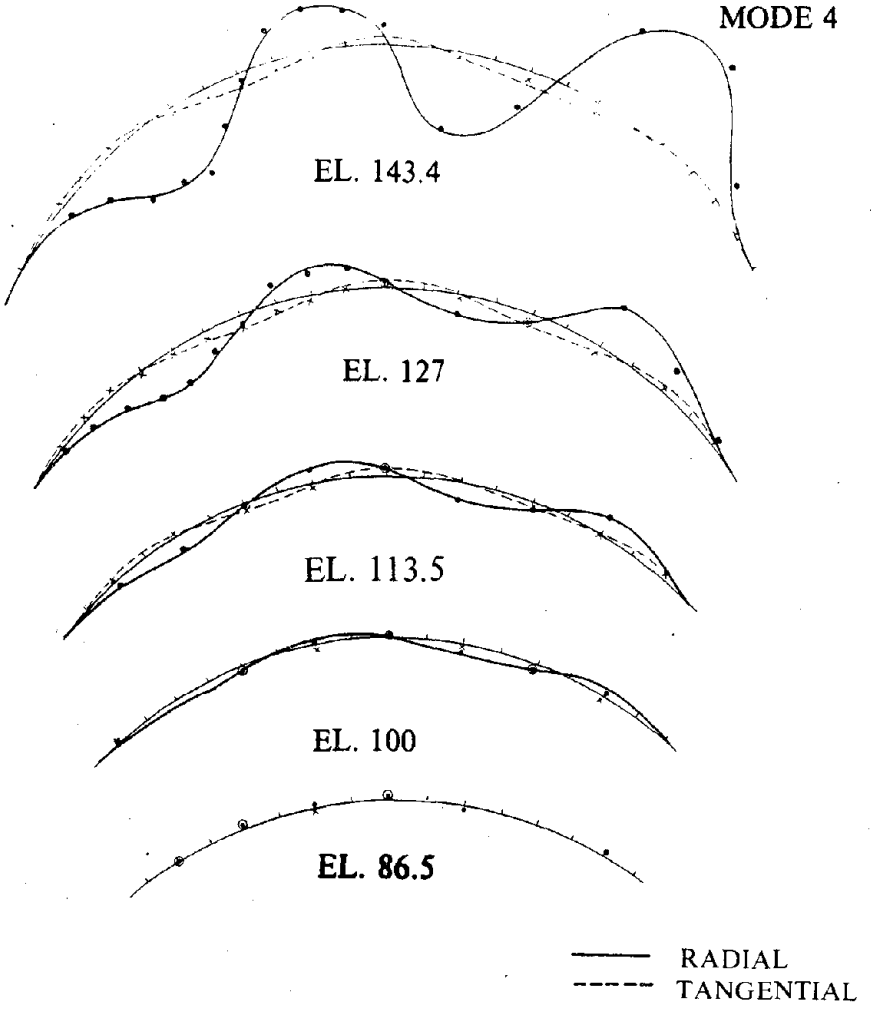

FIG. 2.19
Horizontal Forced Vibration Response: f=6.0 Hz

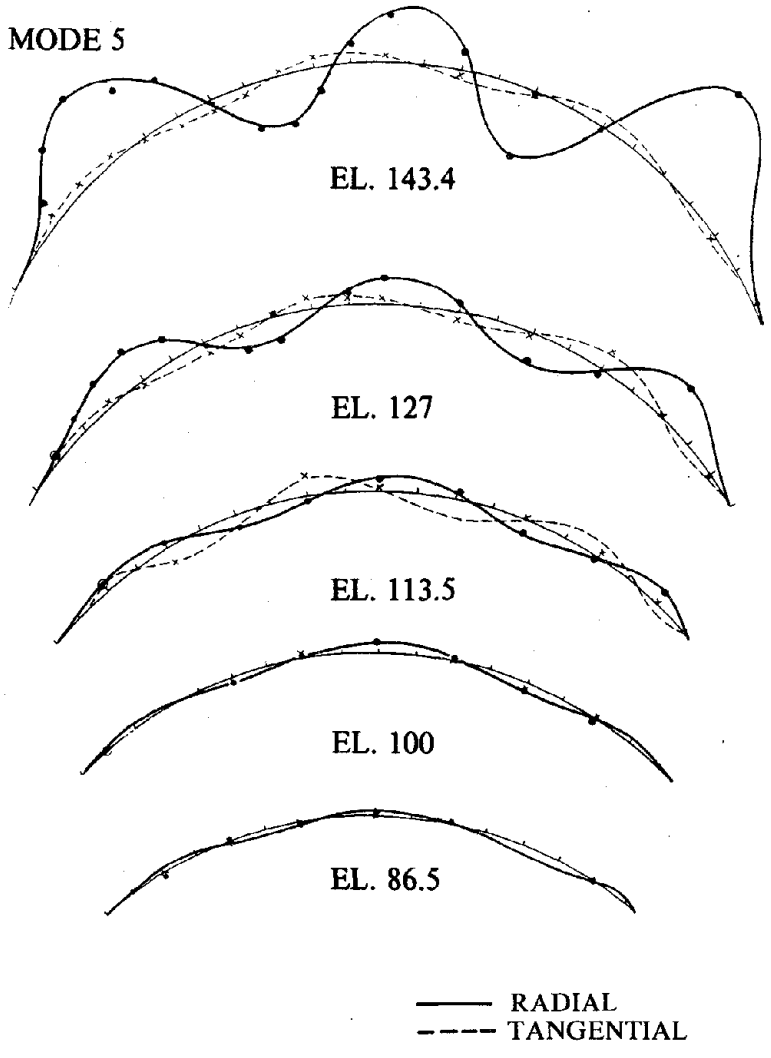

FIG. 2.20
Horizontal Forced Vibration Response: f=7.0 Hz

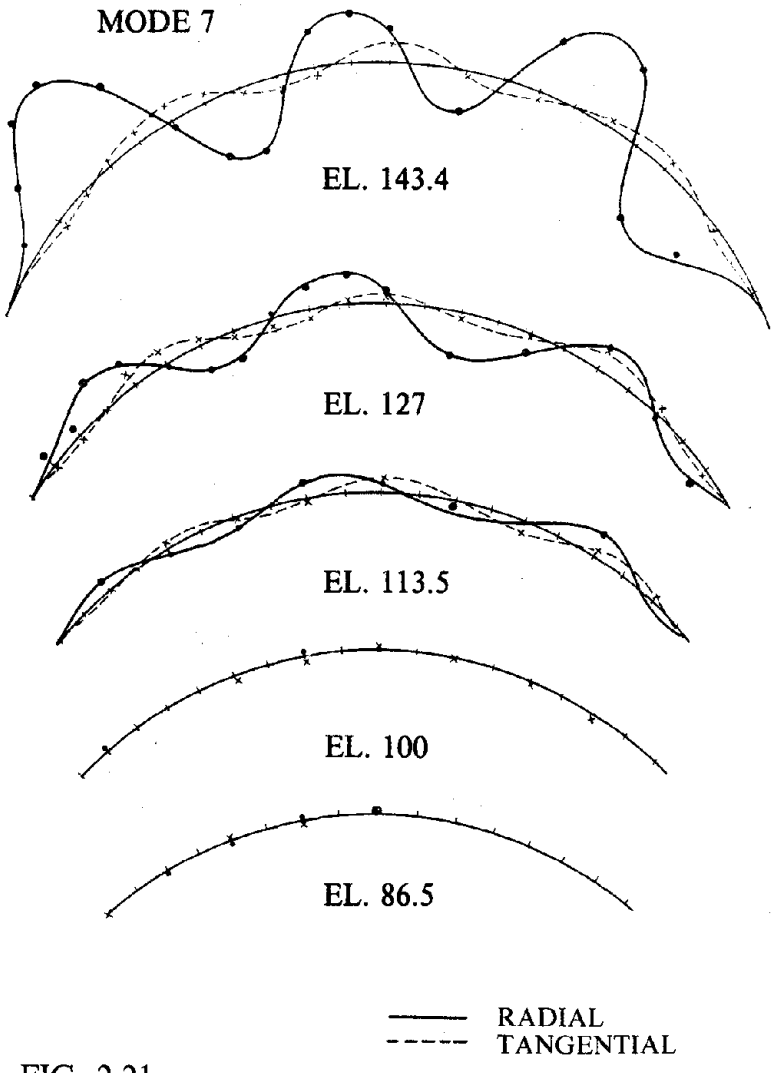

FIG. 2.21
Horizontal Forced Vibration Response: f=8.2 Hz

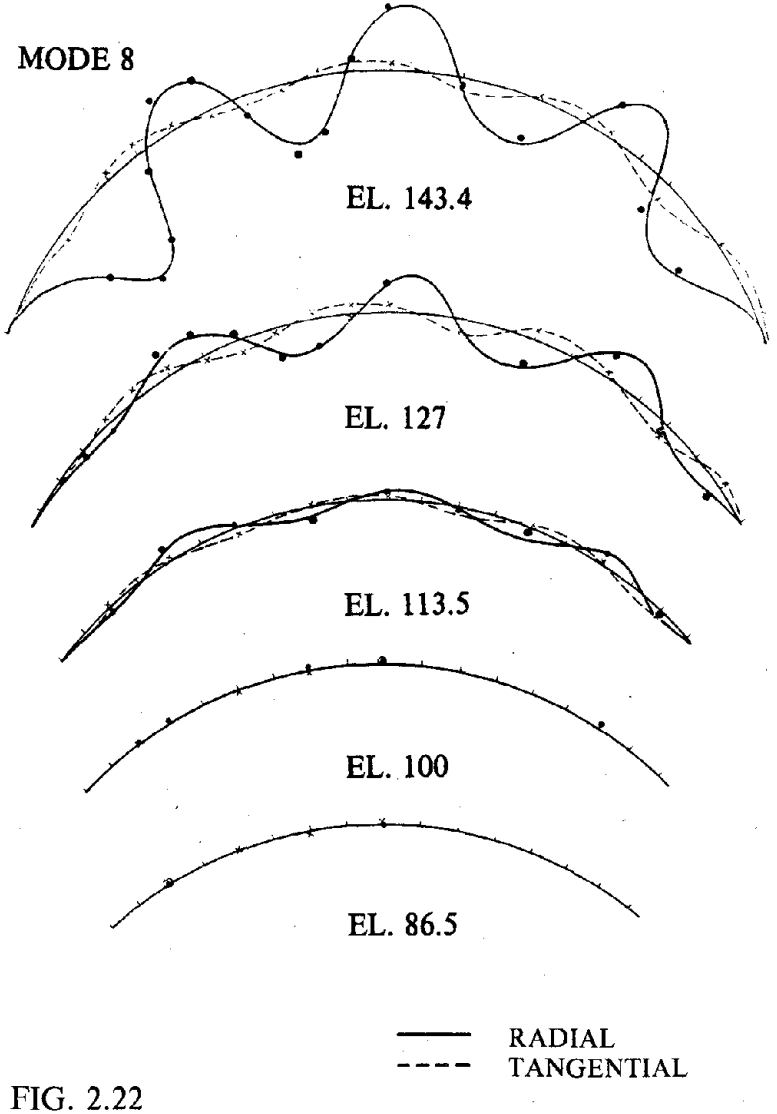

FIG. 2.22
Horizontal Forced Vibration Response: f=9.5 Hz

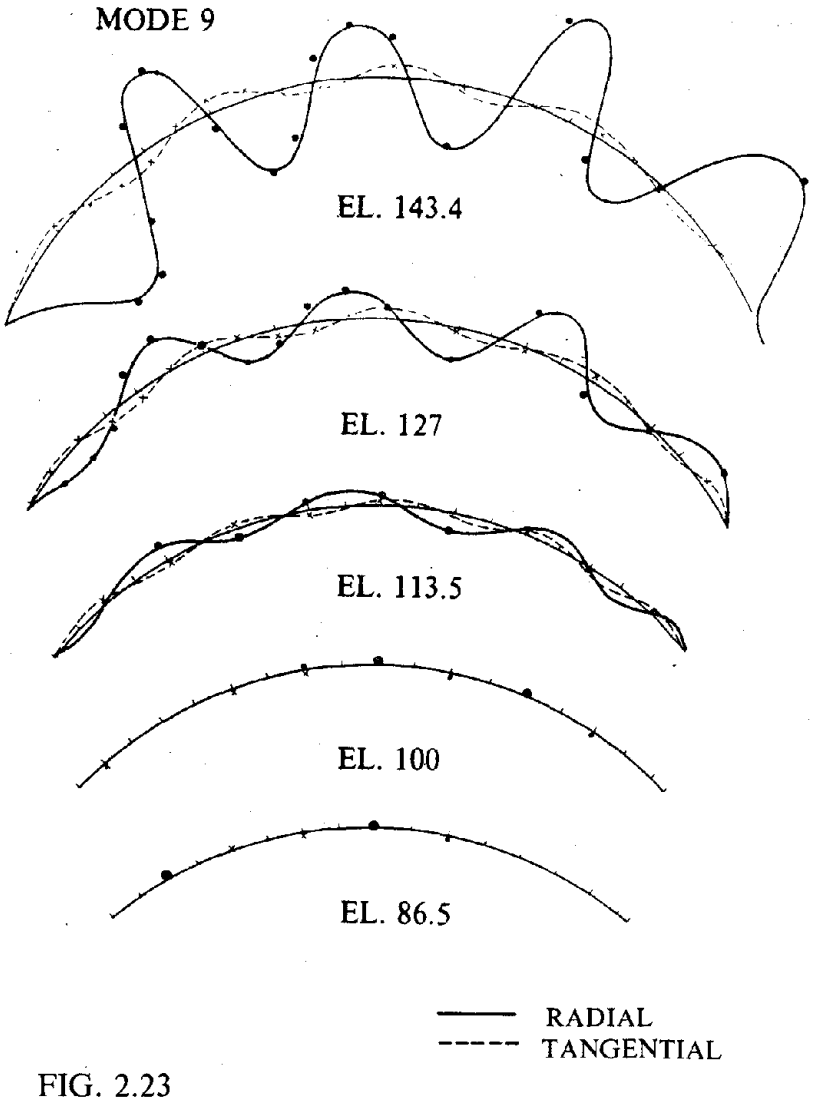

FIG. 2.23
Horizontal Forced Vibration Response: f=10.8 Hz

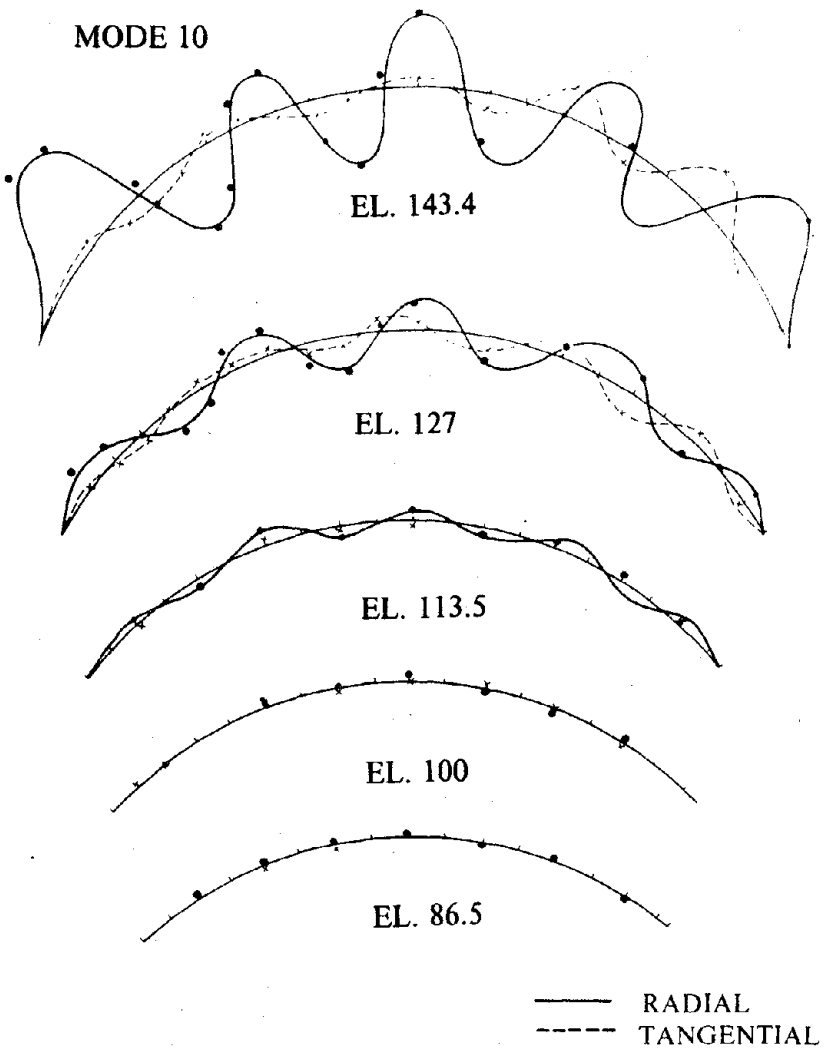

FIG. 2.24
Horizontal Forced Vibration Response: f=12.5 Hz

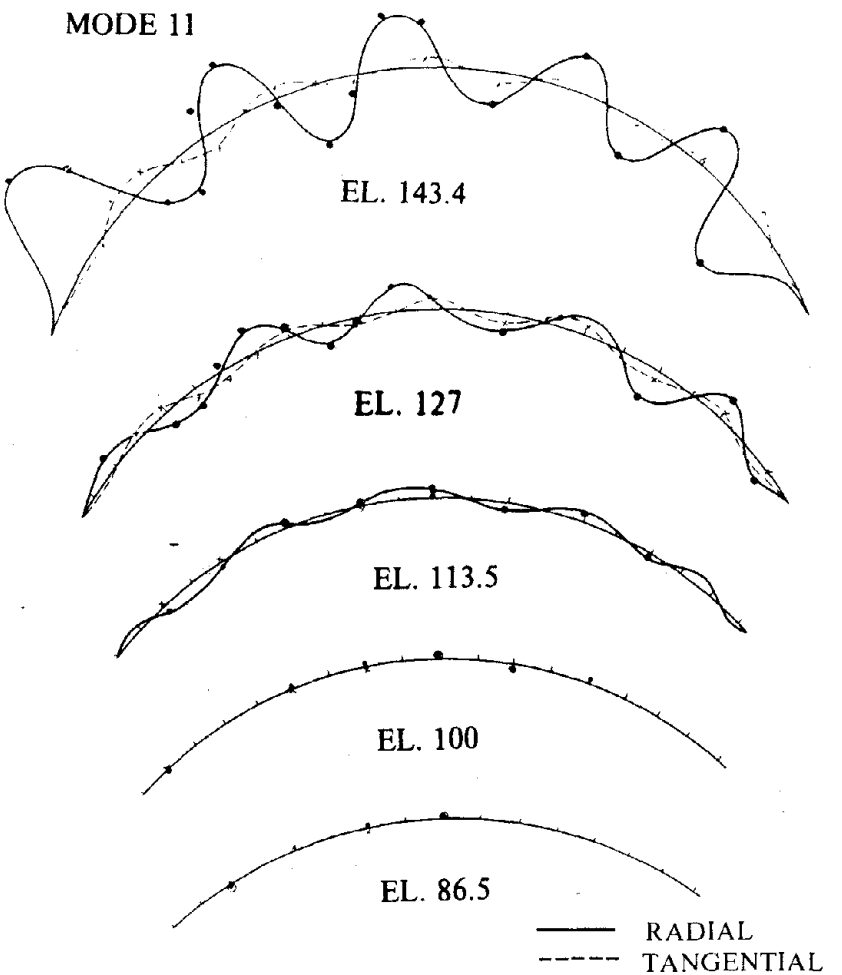

FIG. 2.25
Horizontal Forced Vibration Response: f=14.1 Hz

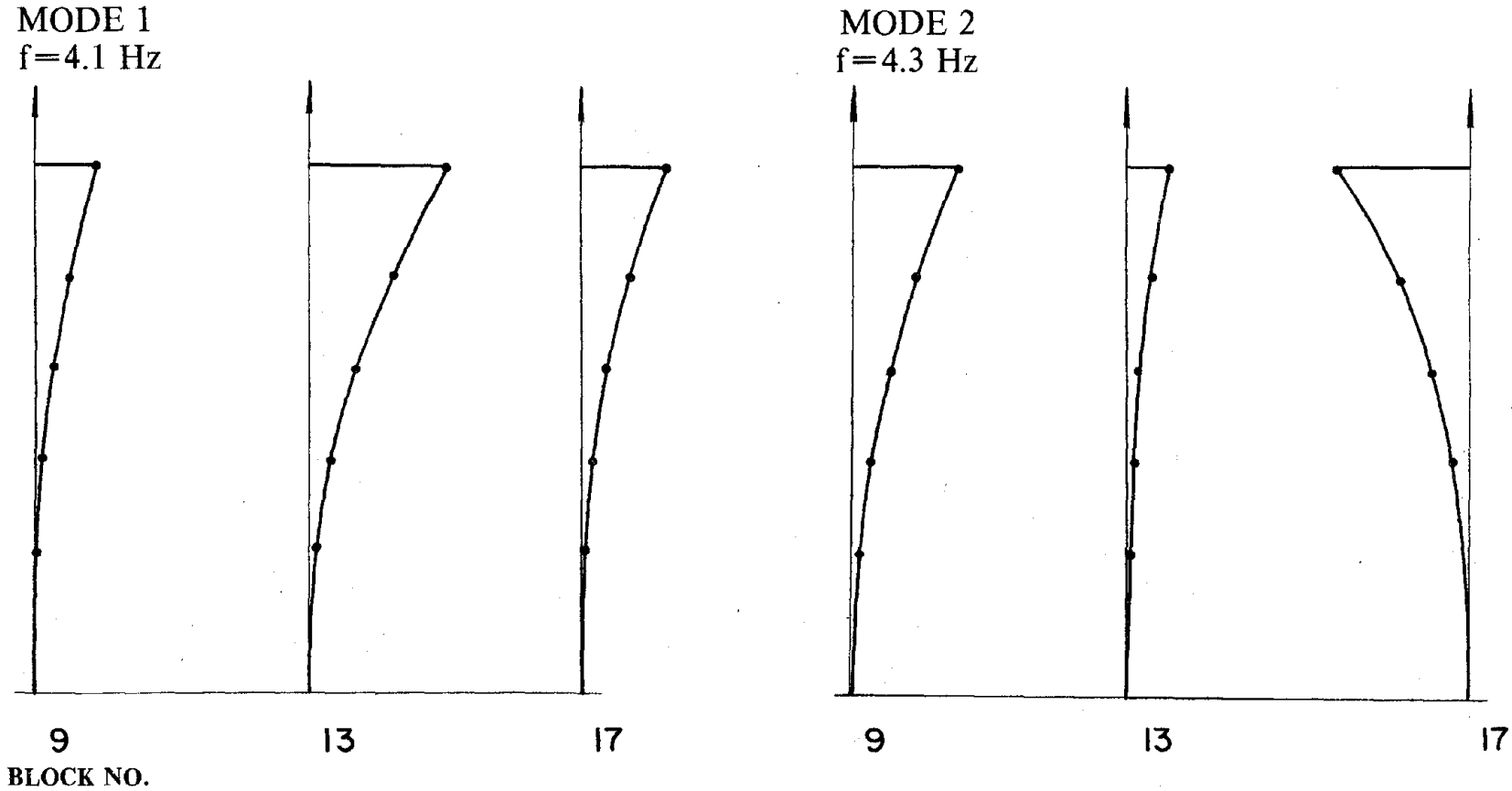

FIG. 2.26 Horizontal Forced Vibration Response To Vertical Systems

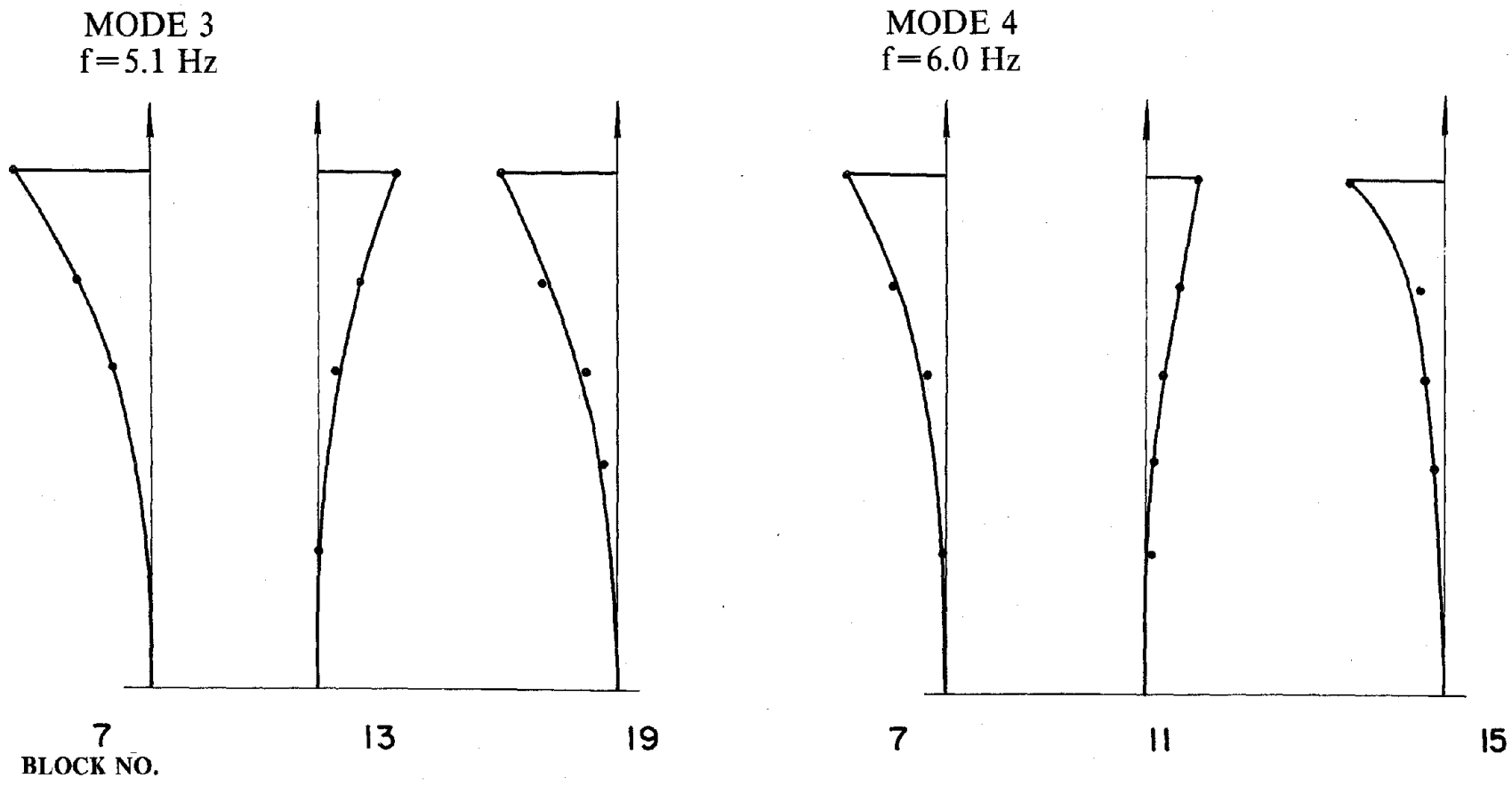

FIG. 2.27 Horizontal Forced Vibration Response To Vertical Systems

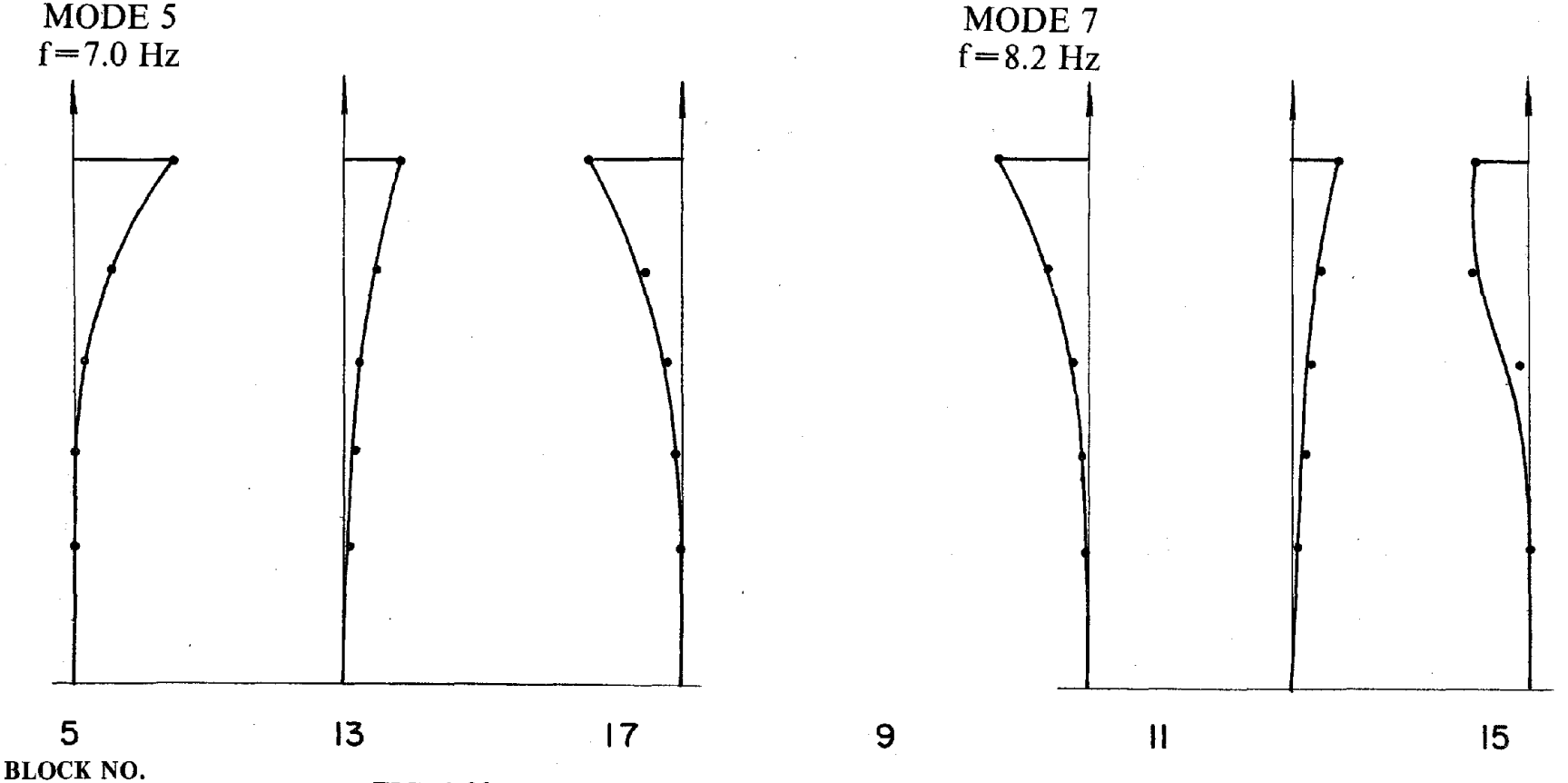

FIG. 2.28 Horizontal Forced Vibration Response To Vertical Systems

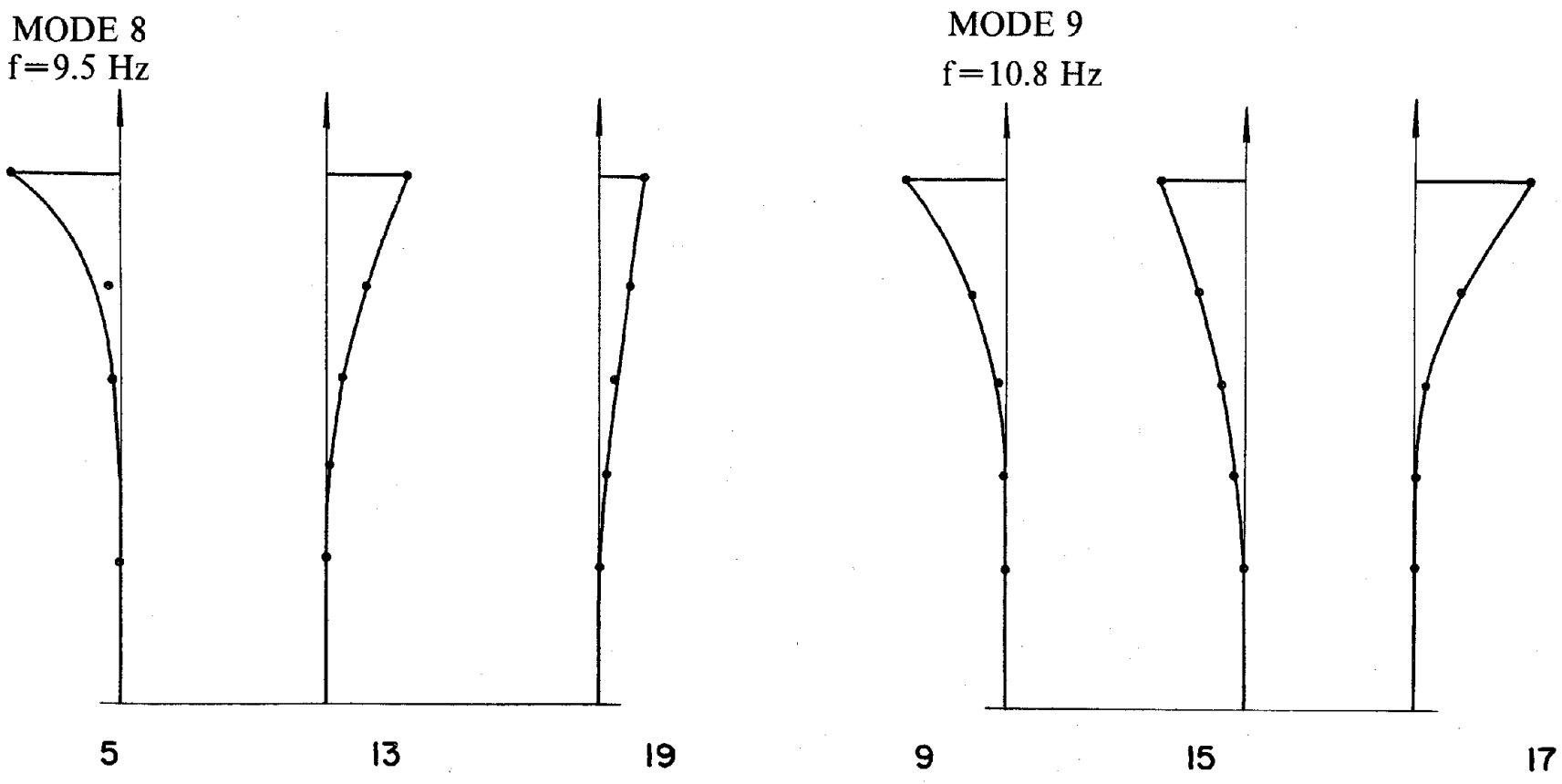

FIG. 2.29 Horizontal Forced Vibration Response To Vertical Systems

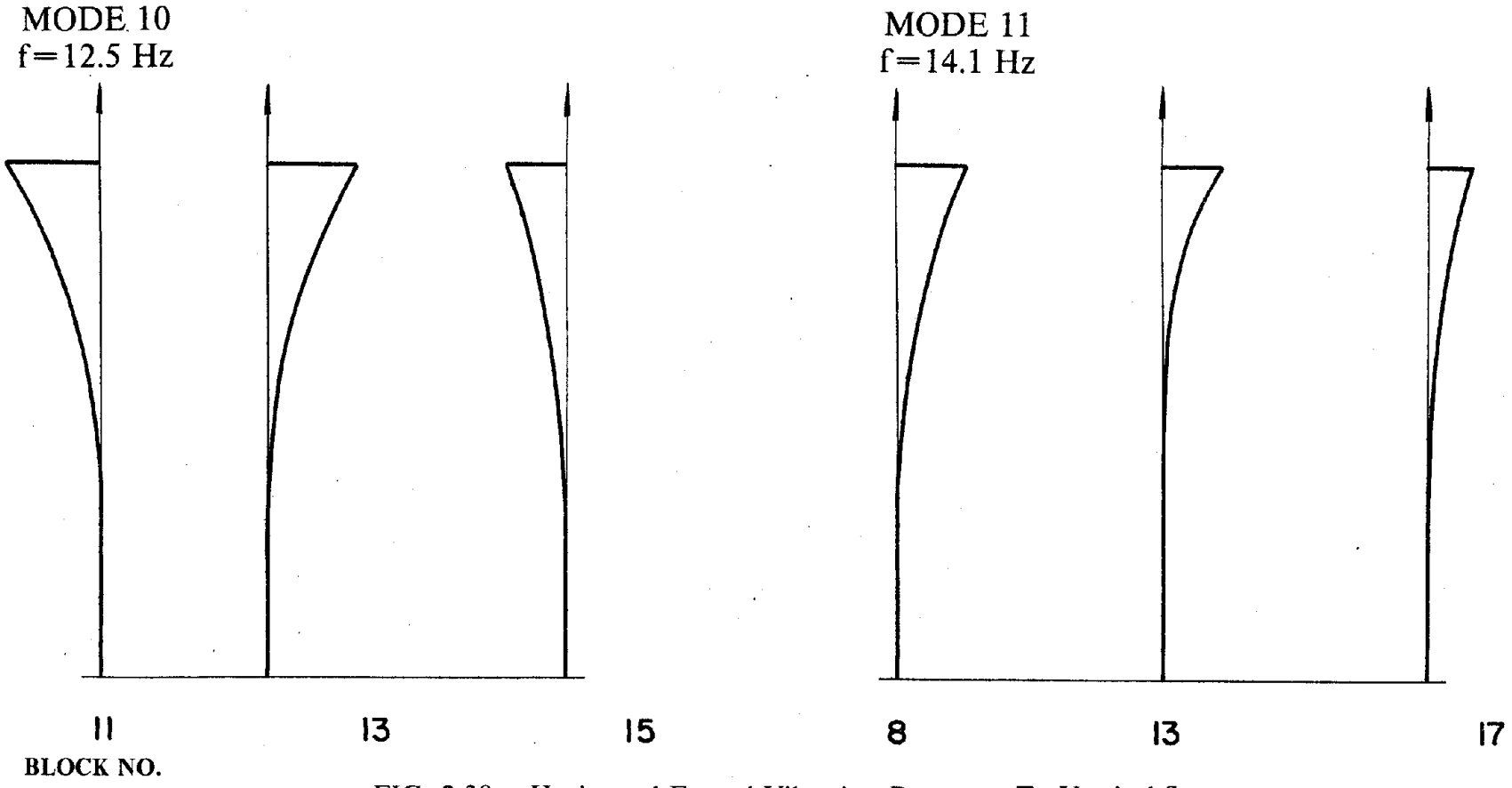

FIG. 2.30 Horizontal Forced Vibration Response To Vertical Systems

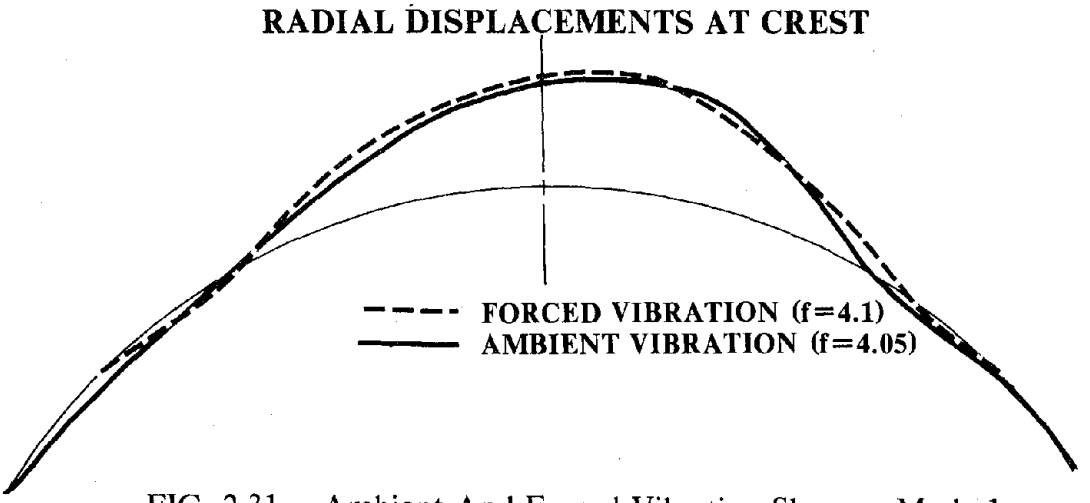

FIG. 2.31 Ambient And Forced Vibration Shapes: Mode 1

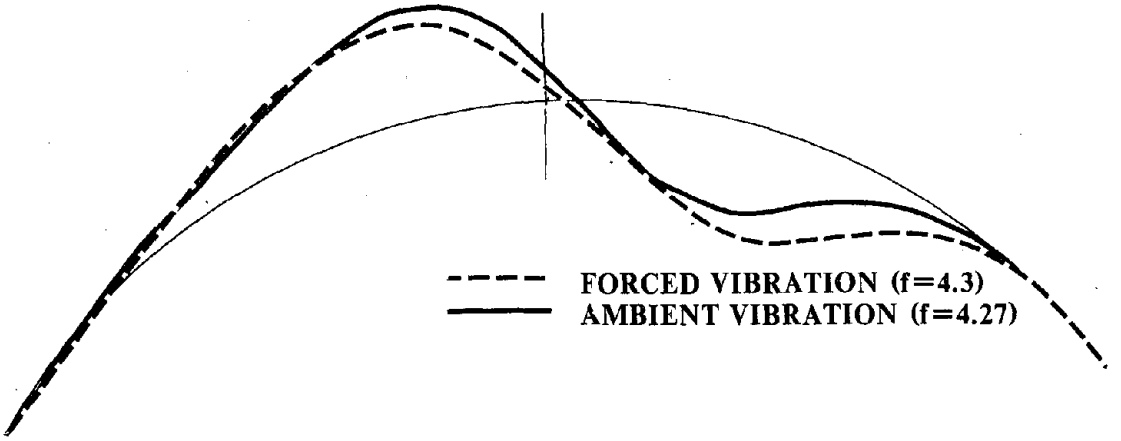

FIG. 2.32 Ambient And Forced Vibration Shapes: Mode 2

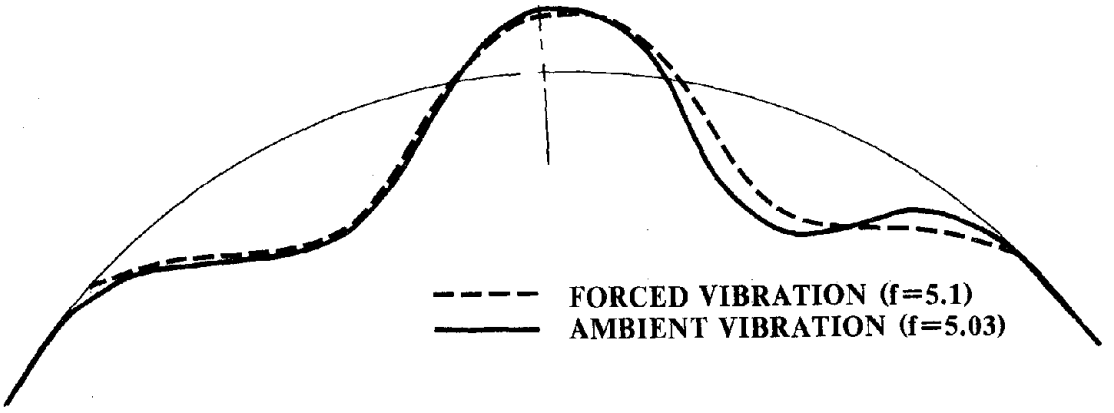

FIG. 2.33 Ambient And Forced Vibration Shapes: Mode 3

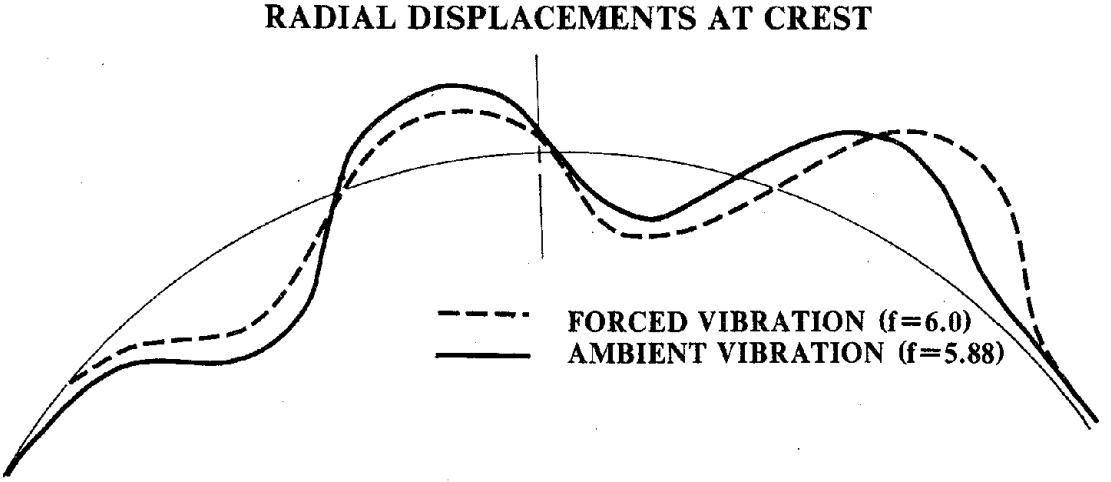

FIG. 2.34 Ambient And Forced Vibration Shapes: Mode 4

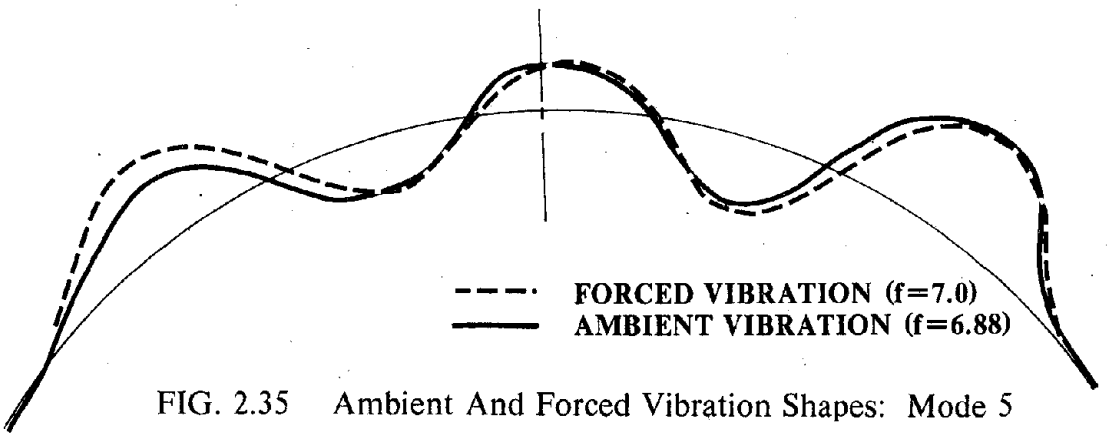

FIG. 2.35 Ambient And Forced Vibration Shapes: Mode 5

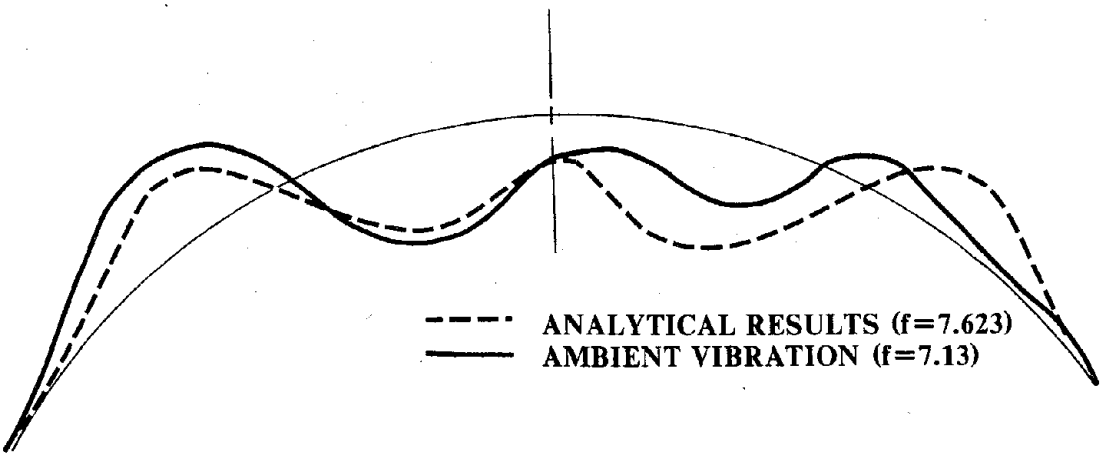

FIG. 2.36 Calculated And Ambient Vibration Shapes: Mode 6
(Missed Mode In Forced Vibration)

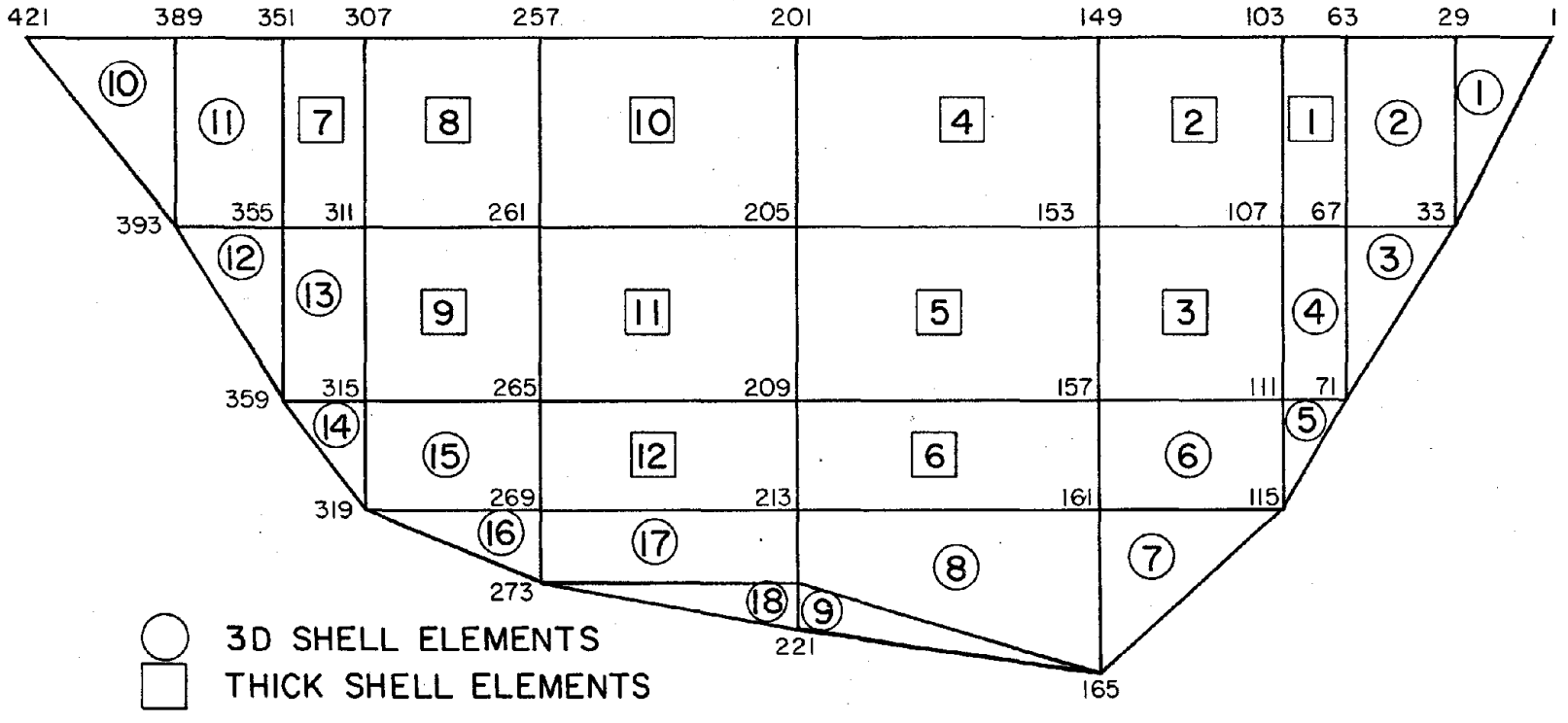

FIG. 3.1 Element Mesh On Upstream Face Projected On X-Z Plane

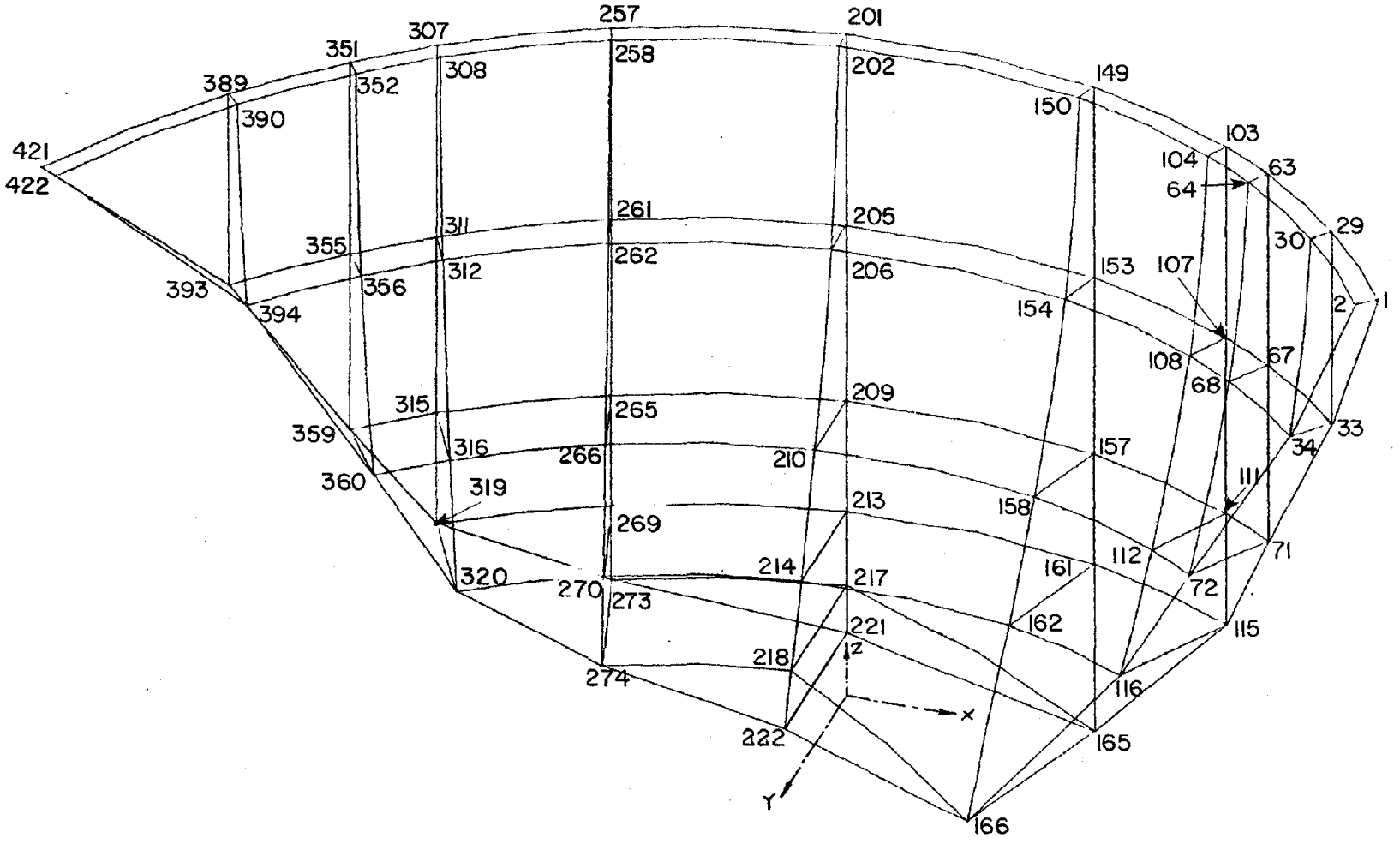

FIG. 3.2 Perspective View Of Xiang Hong Dian Dam Elements

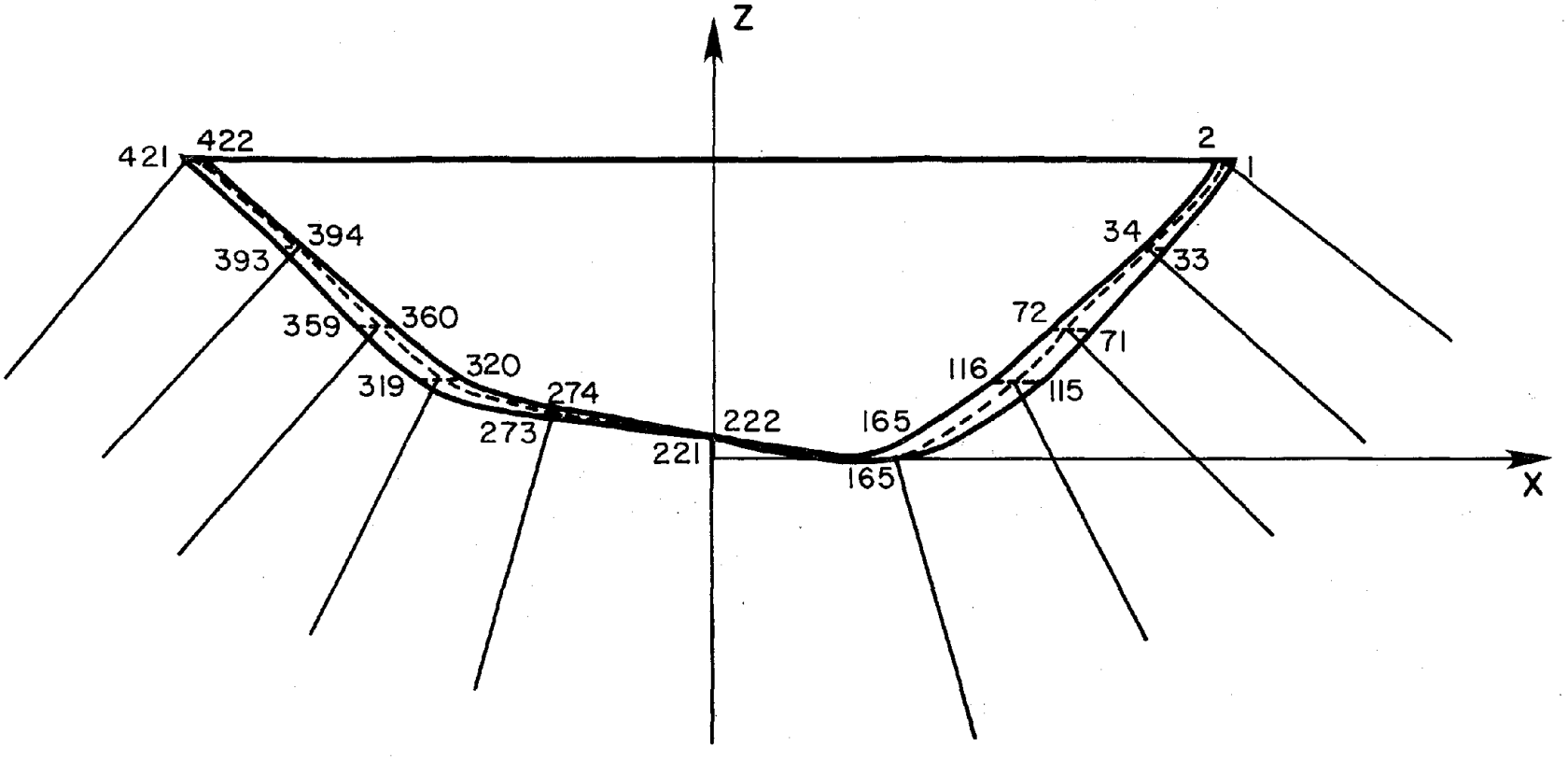

FIG. 3.3 Traces Of Intersections Of Foundation Mesh Planes With X-Z Plane

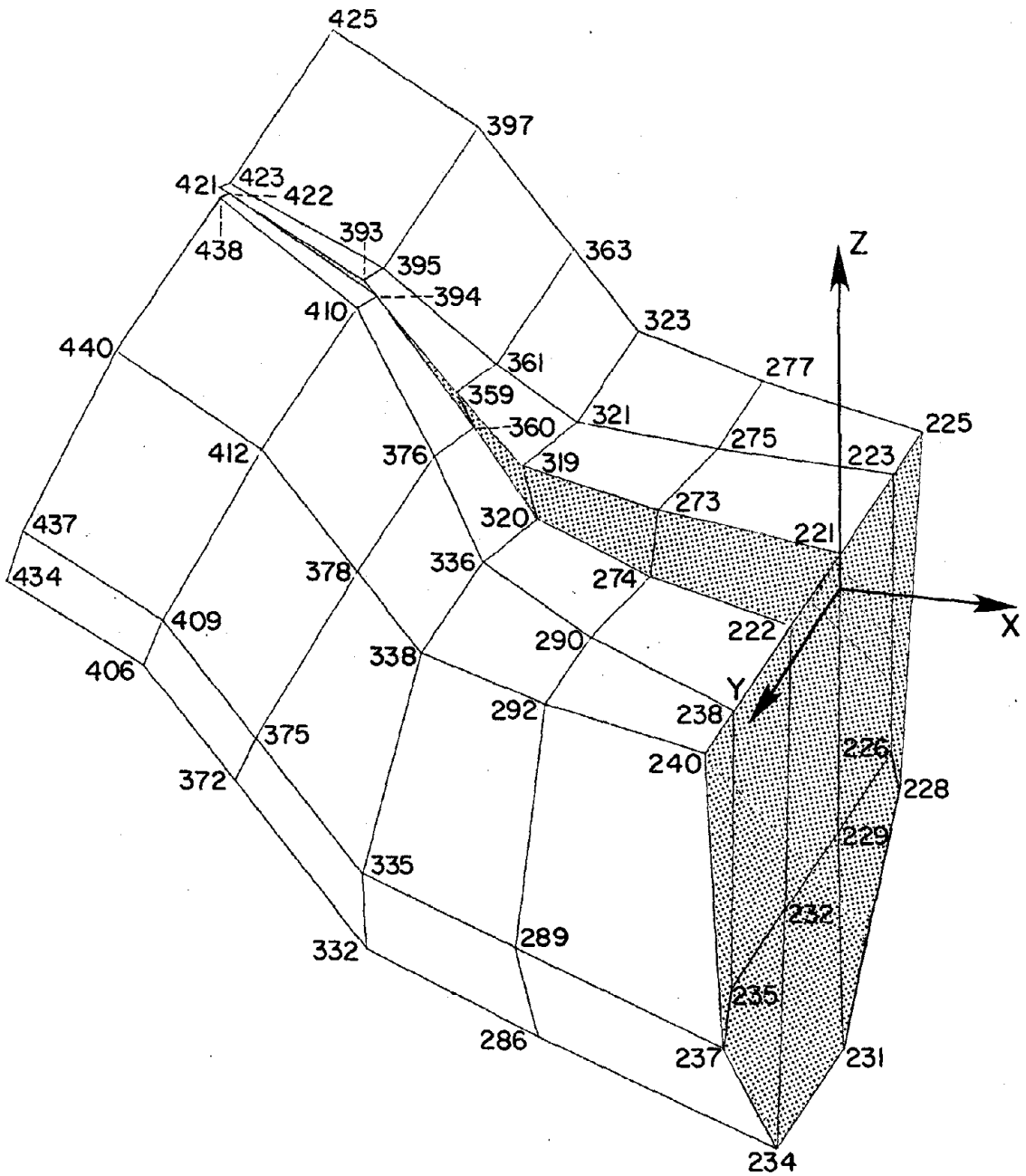

FIG. 3.4 Perspective View Of Foundation Elements, Right Side Of Canyon

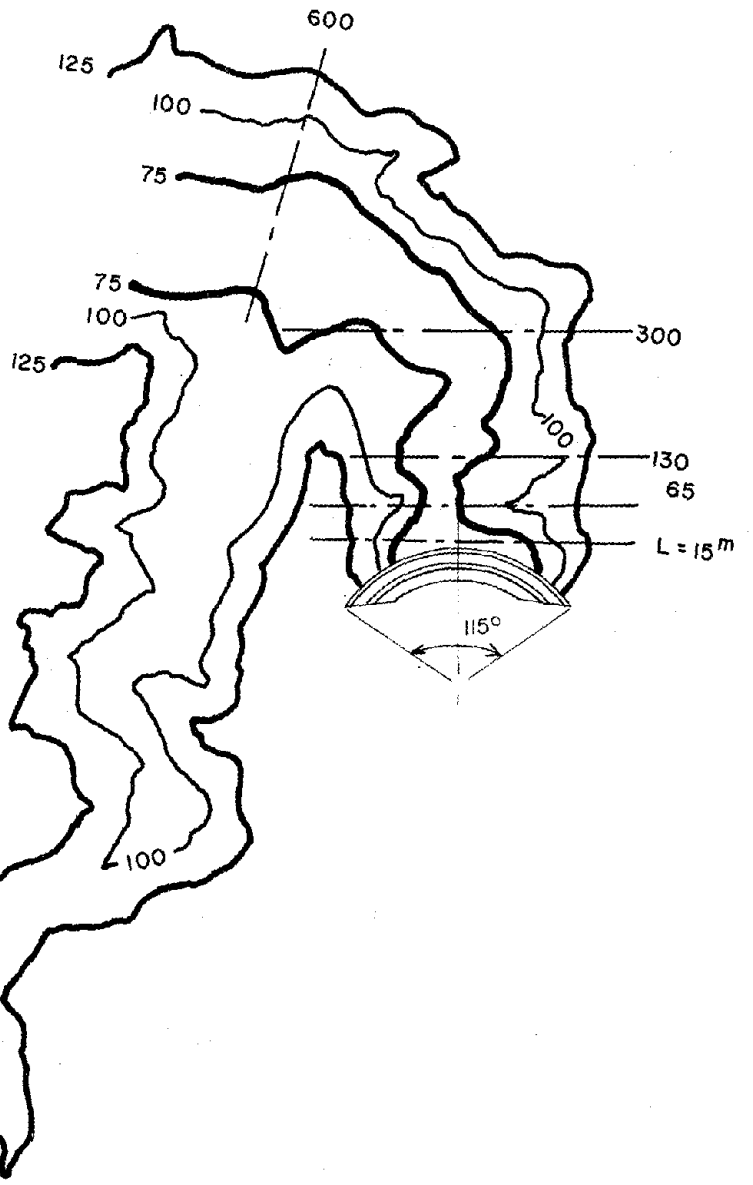

FIG. 3.5 Plan Of Xiang Hong Dian Reservoir (1:10000)

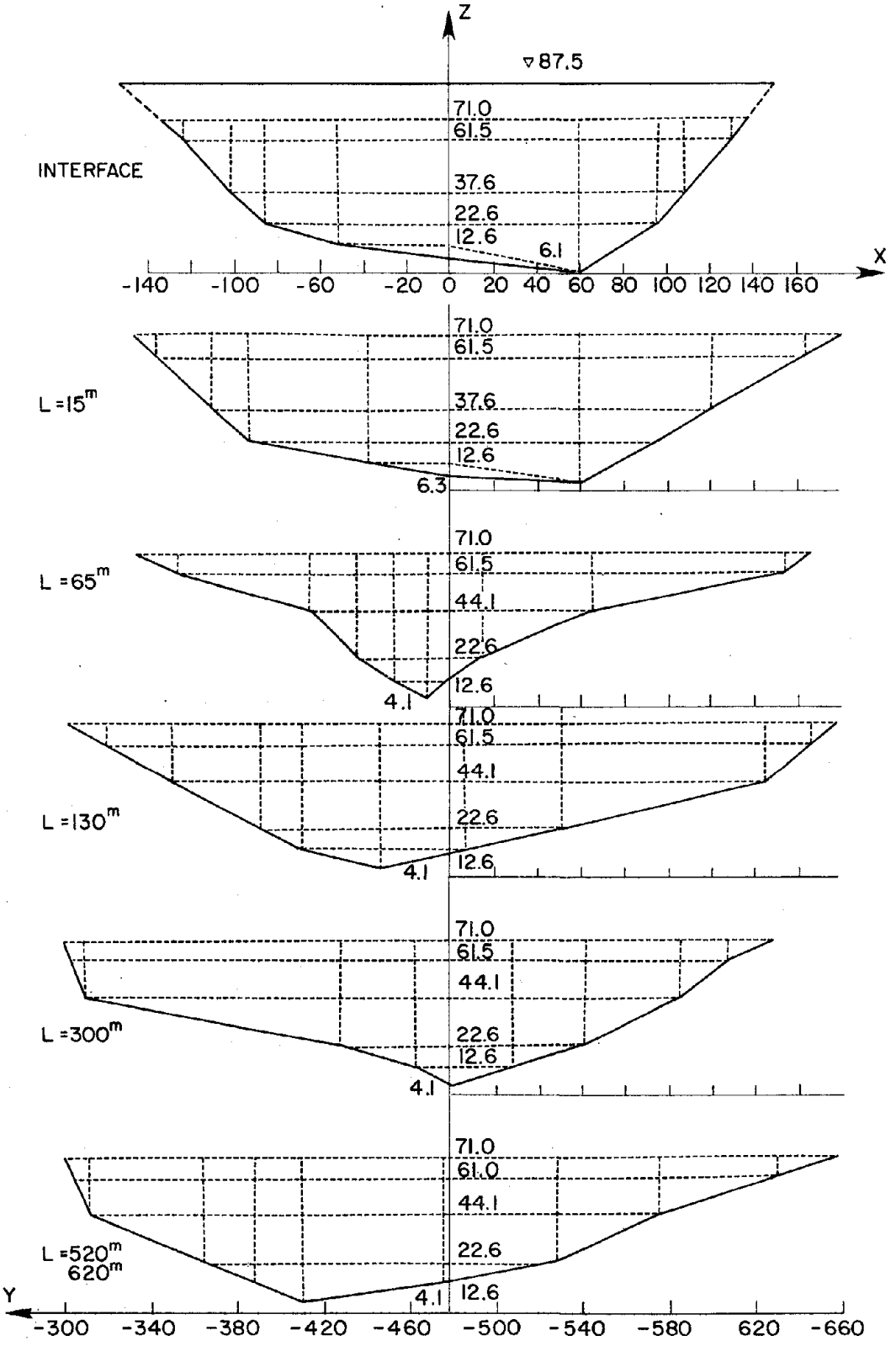

FIG. 3.6 Liquid Element Meshes At Six Sections In Reservoir

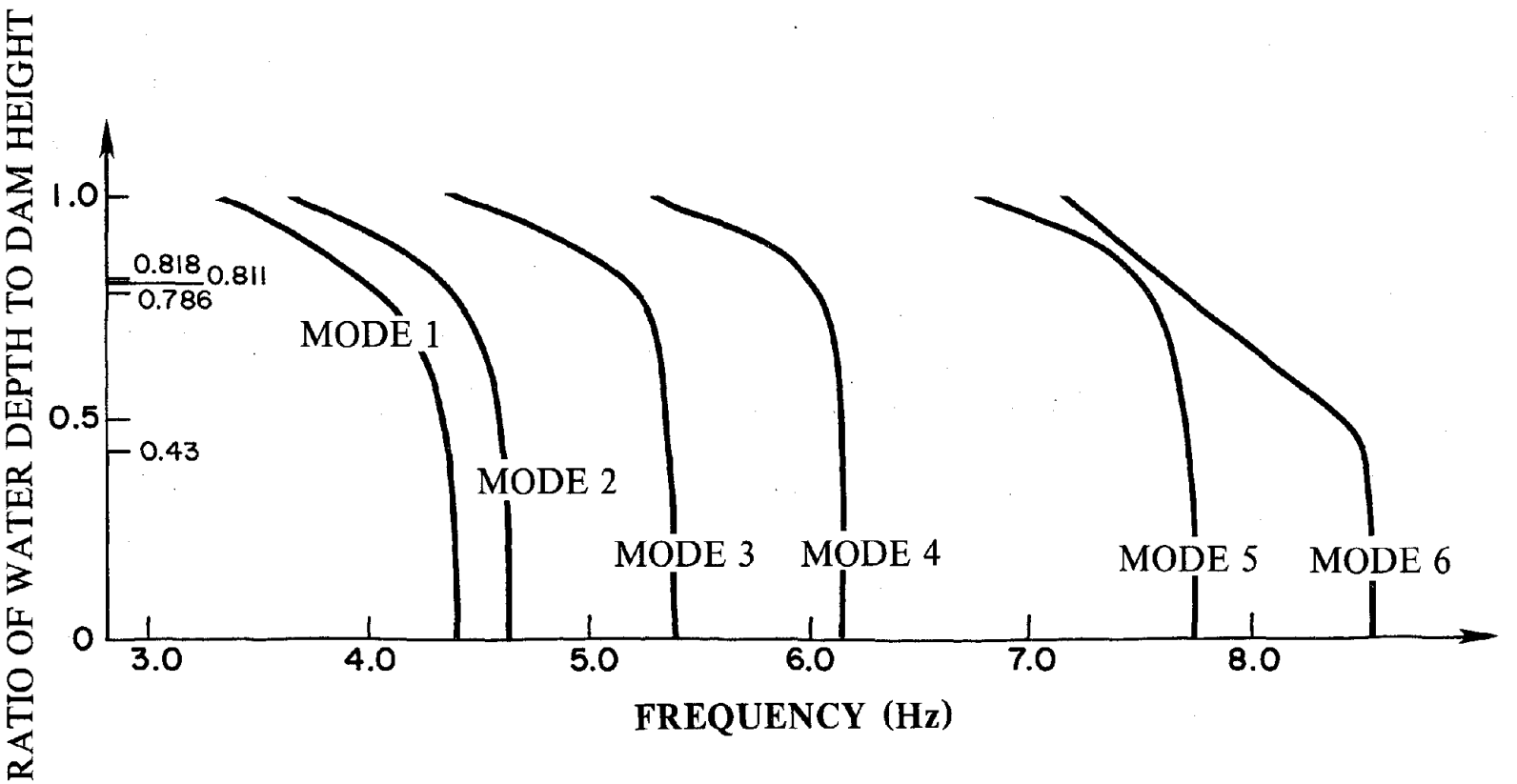

FIG. 3.7 Variation of Vibration Frequencies With Reservoir Depth

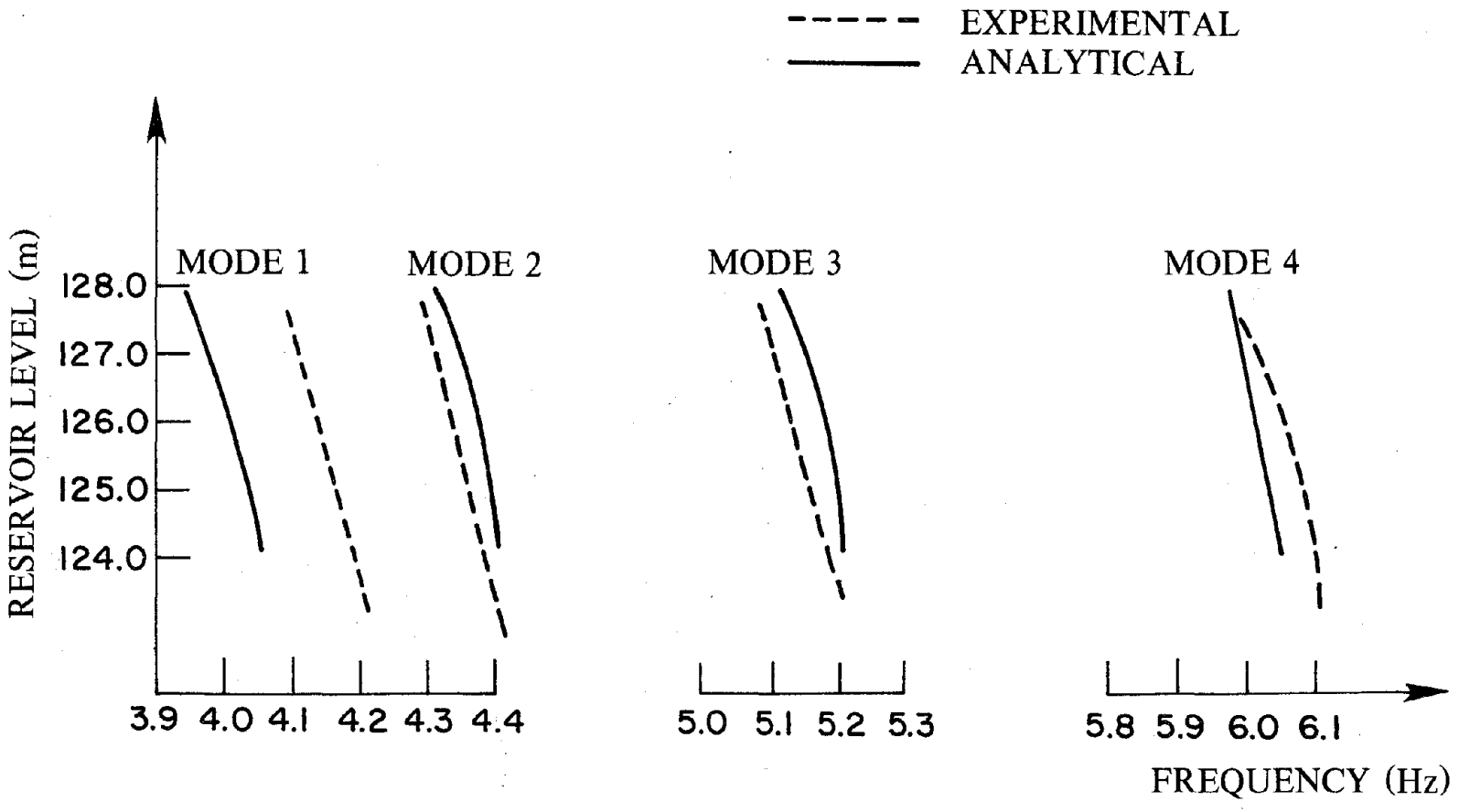

FIG. 3.8 Observed And Calculated Variation Of Frequency With Reservoir Level

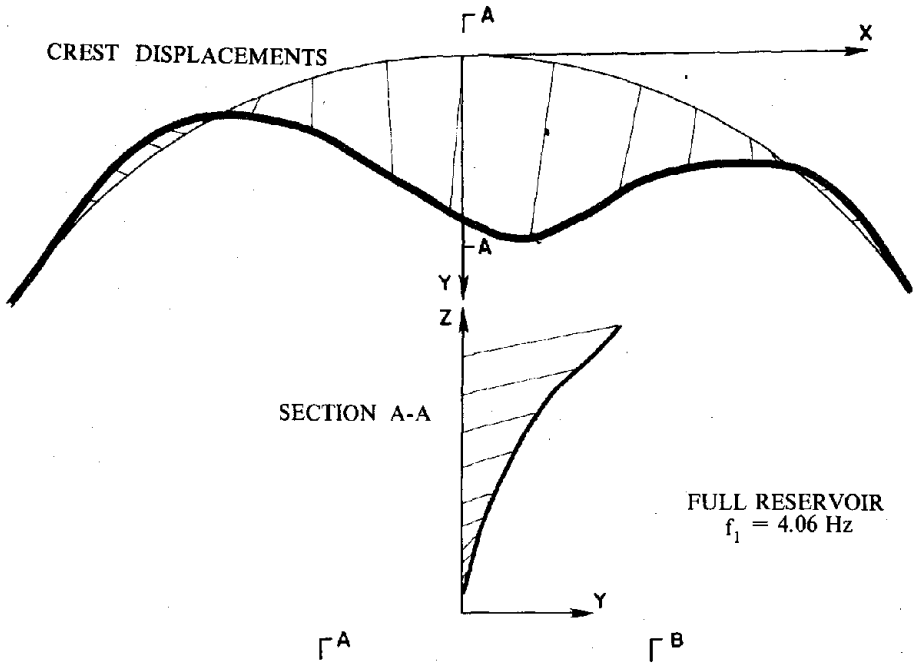

FIG. 3.9 Calculated Shape (Eigenvector): Mode 1

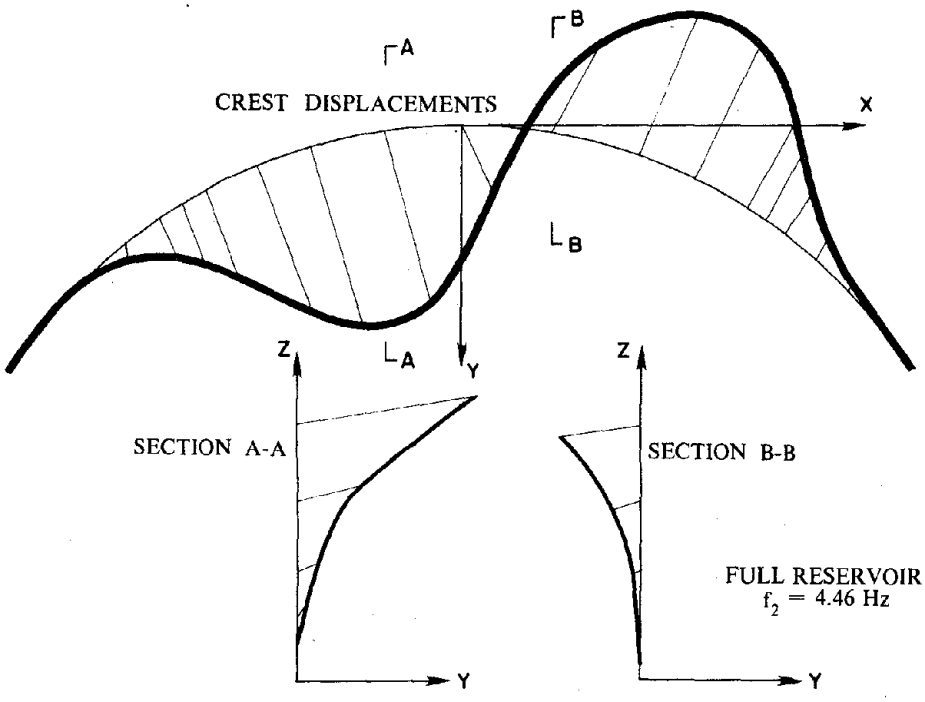

FIG. 3.10 Calculated Shape (Eigenvector): Mode 2

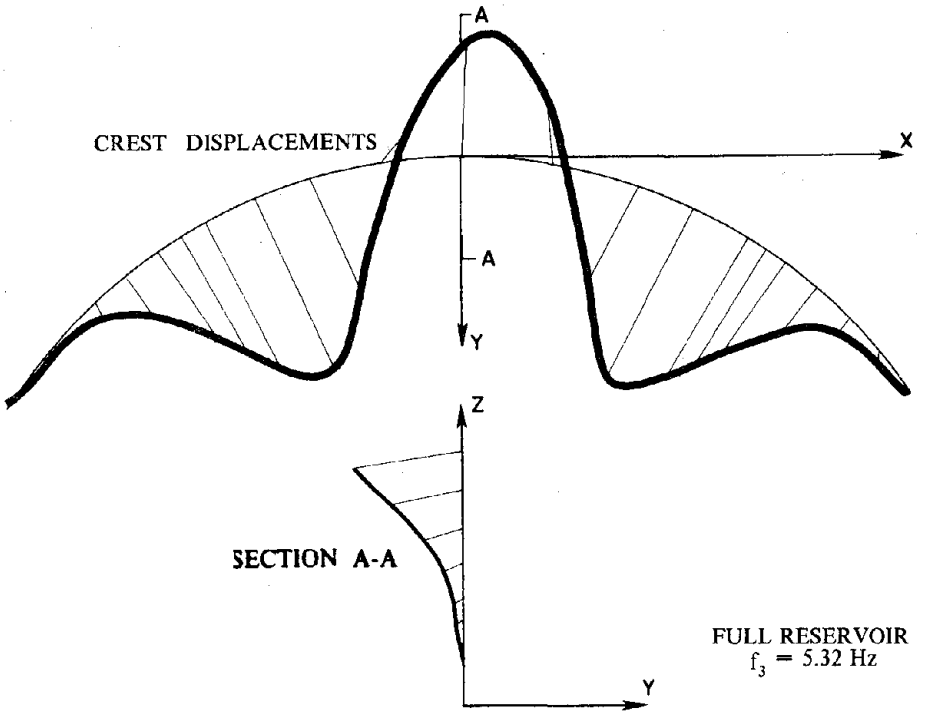

FIG. 3.11 Calculated Shape (Eigenvector): Mode 3

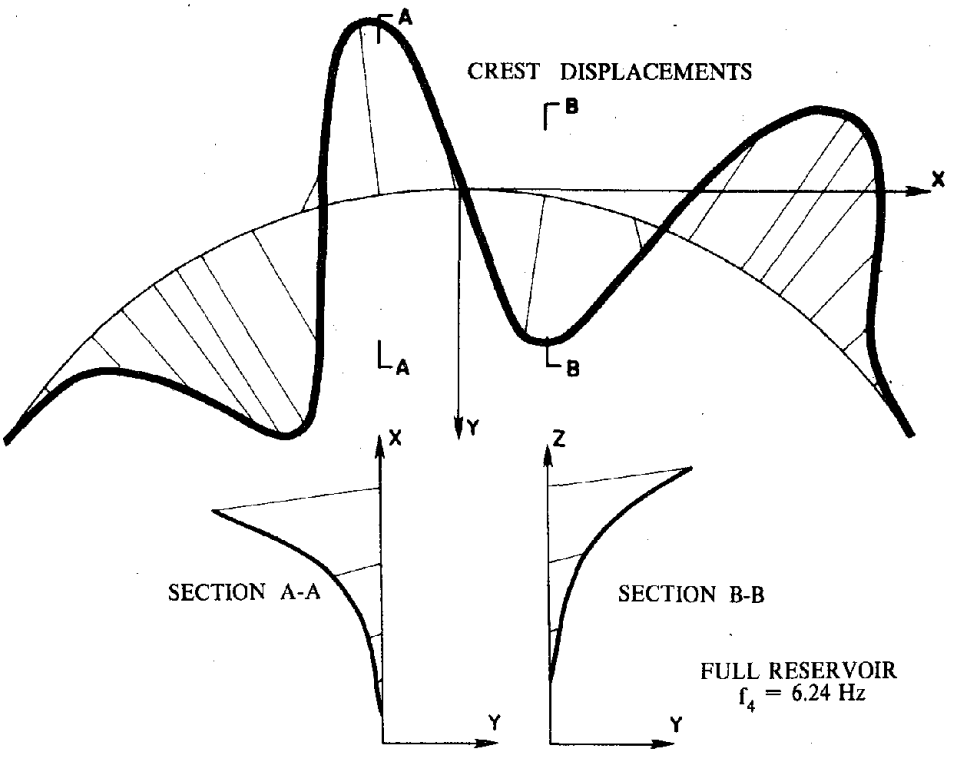

FIG. 3.12 Calculated Shape (Eigenvector): Mode 4

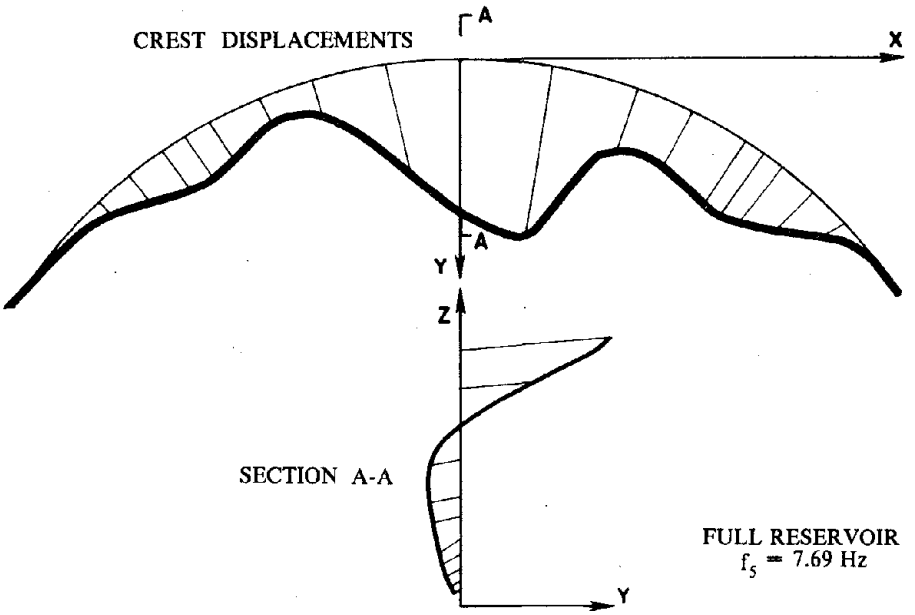

FIG. 3.13 Calculated Shape (Eigenvector): Mode 5

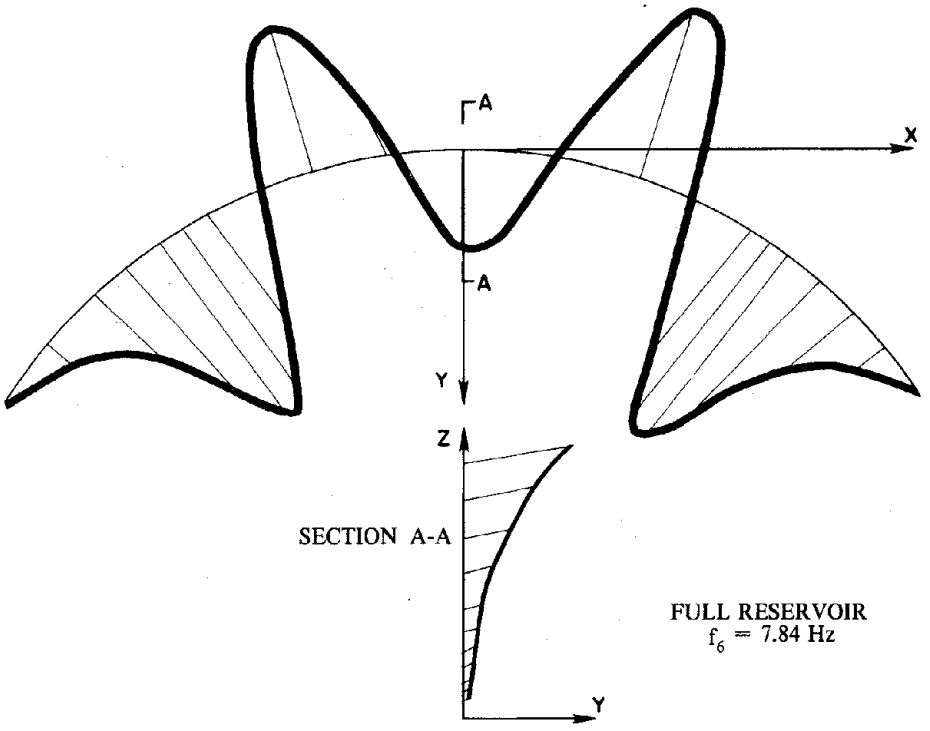

FIG. 3.14 Calculated Shape (Eigenvector): Mode 6

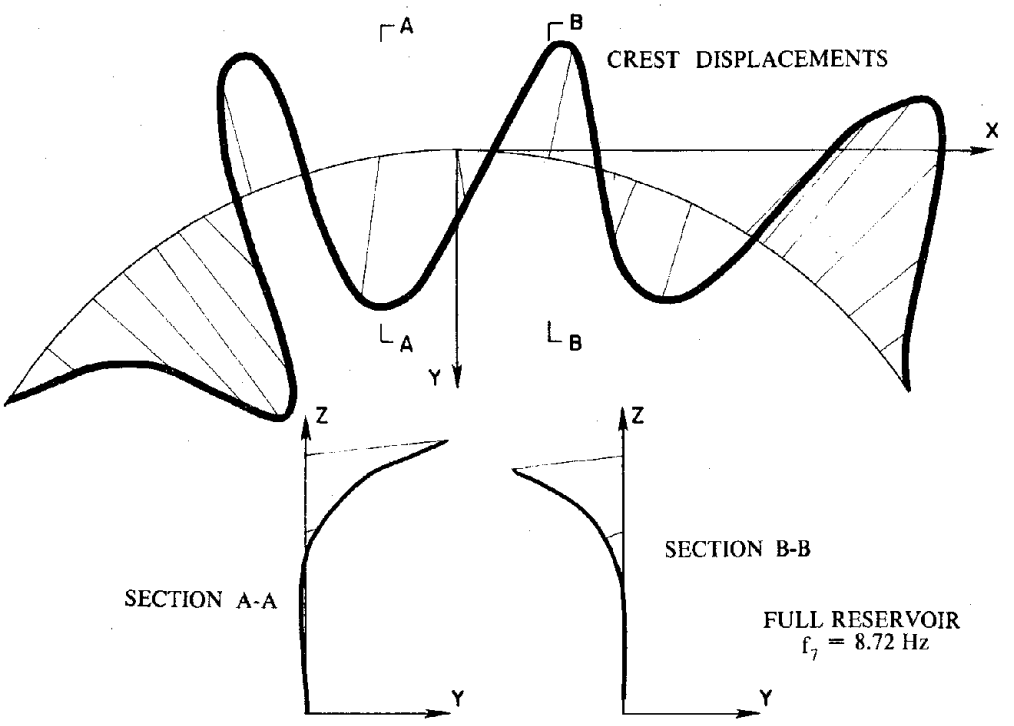

FIG. 3.15 Calculated Shape (Eigenvector): Mode 7

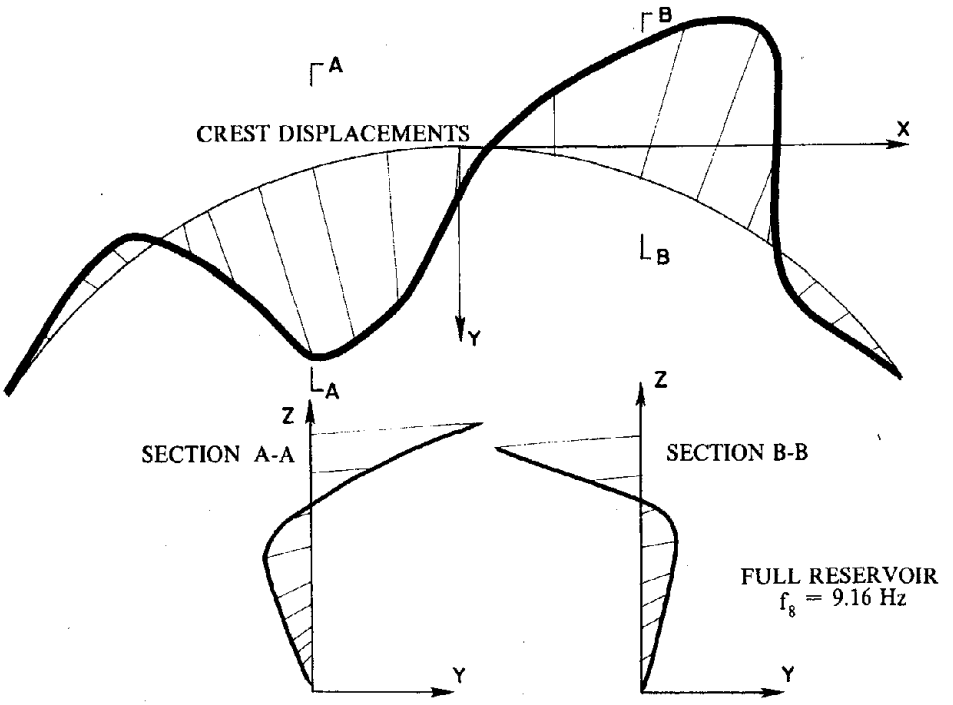

FIG. 3.16 Calculated Shape (Eigenvector): Mode 8

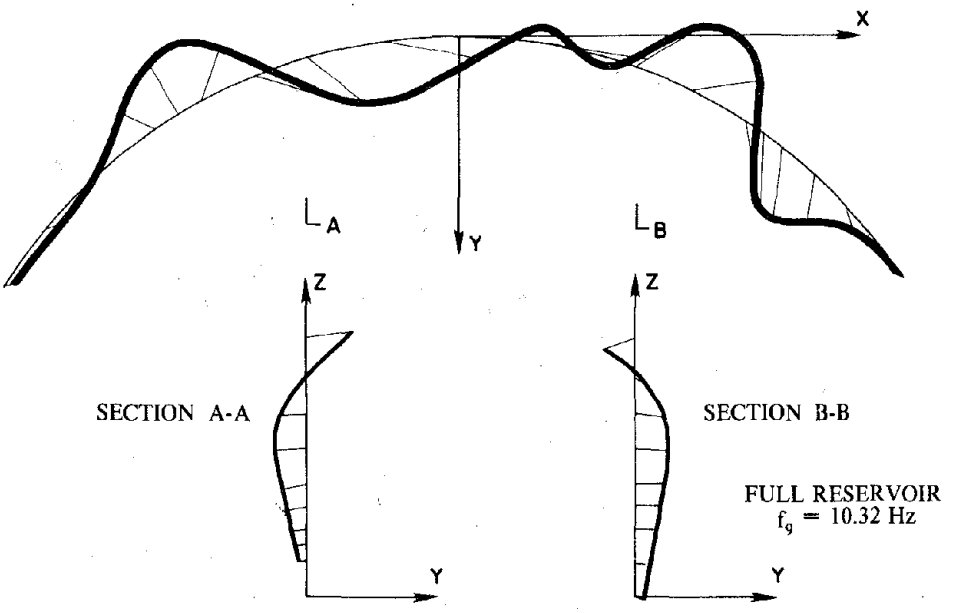

FIG. 3.17 Calculated Shape (Eigenvector): Mode 9

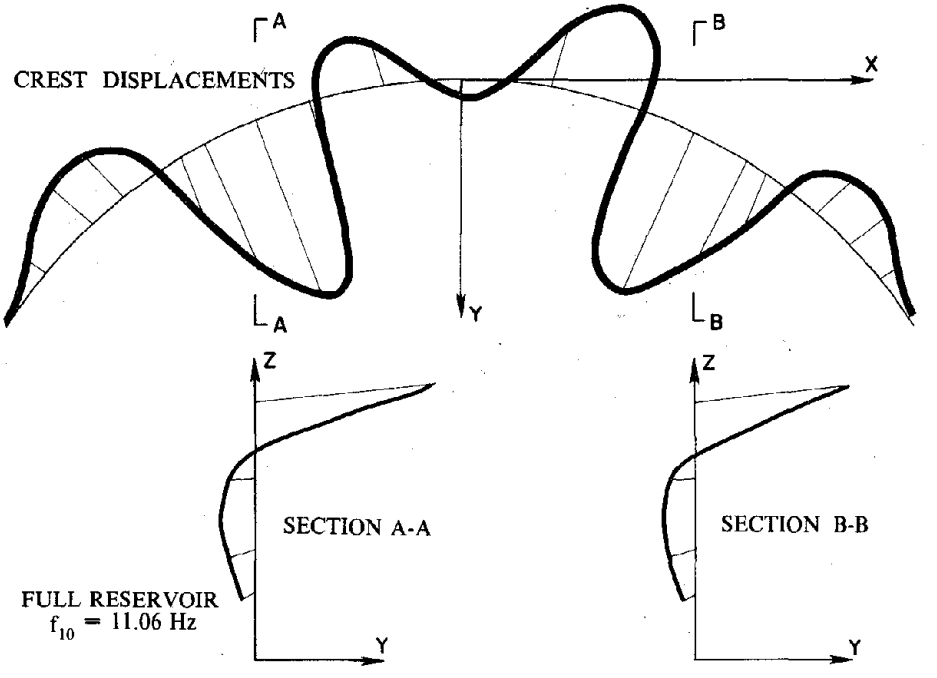

FIG. 3.18 Calculated Shape (Eigenvector): Mode 10

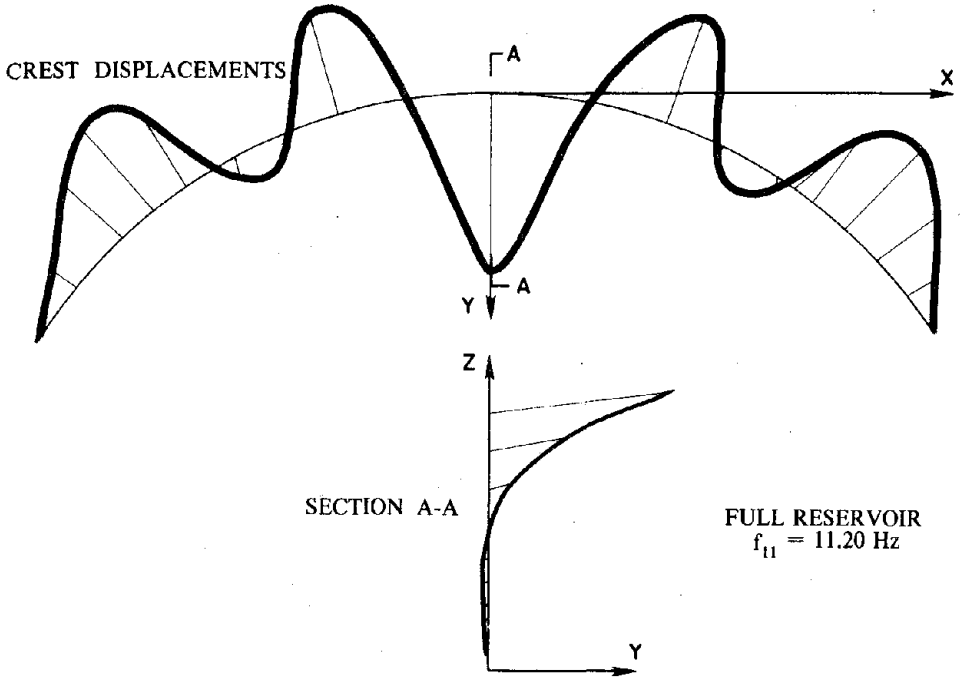

FIG. 3.19 Calculated Shape (Eigenvector): Mode 11

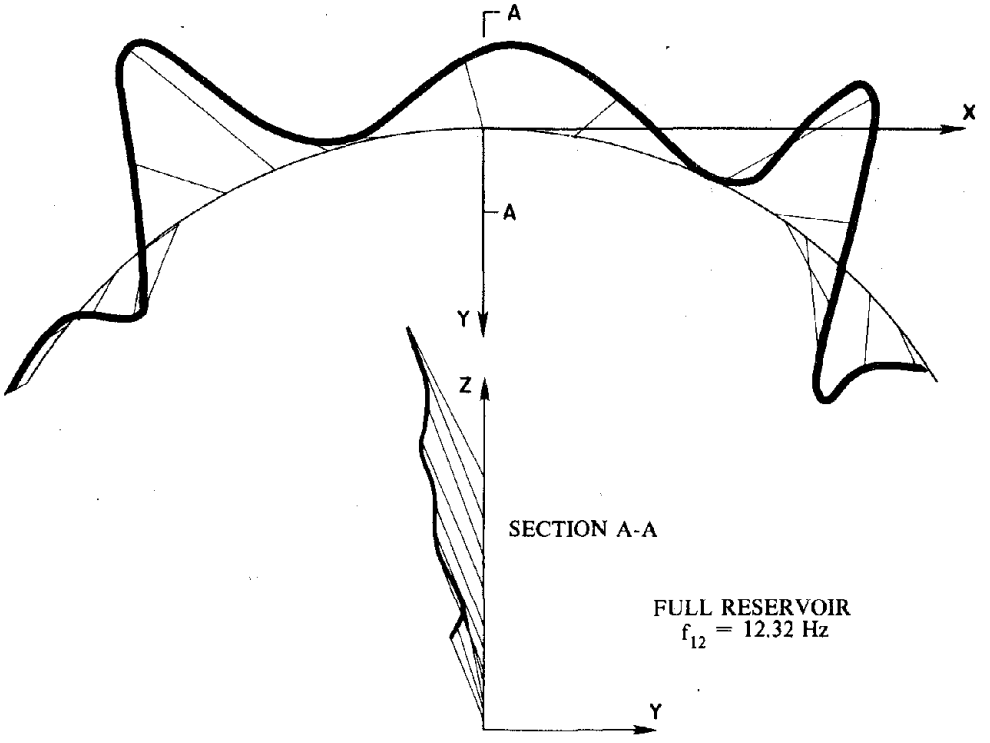

FIG. 3.20 Calculated Shape (Eigenvector): Mode 12

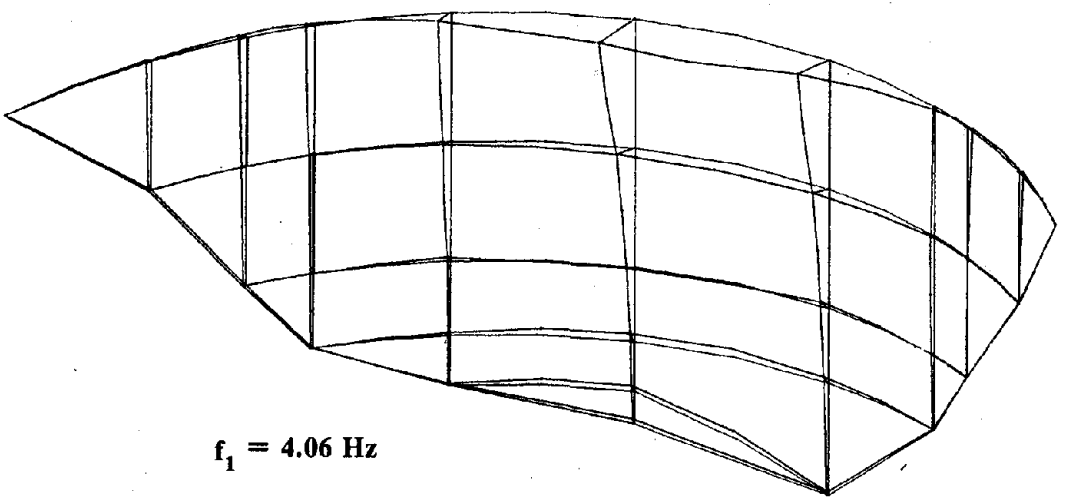

FIG. 3.21 Perspective View Of Upstream Face Displacements: Mode 1

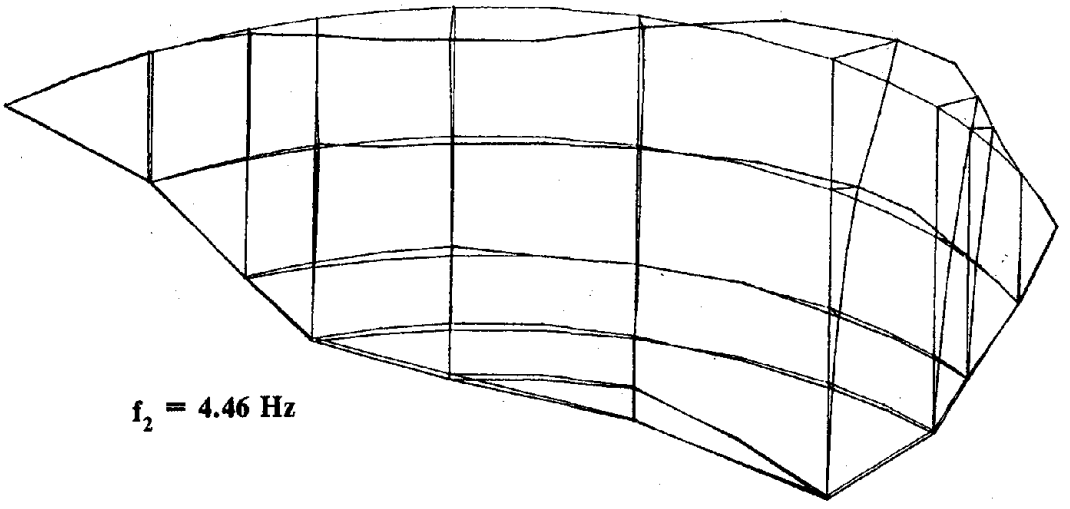

FIG. 3.22 Perspective View Of Upstream Face Displacements: Mode 2

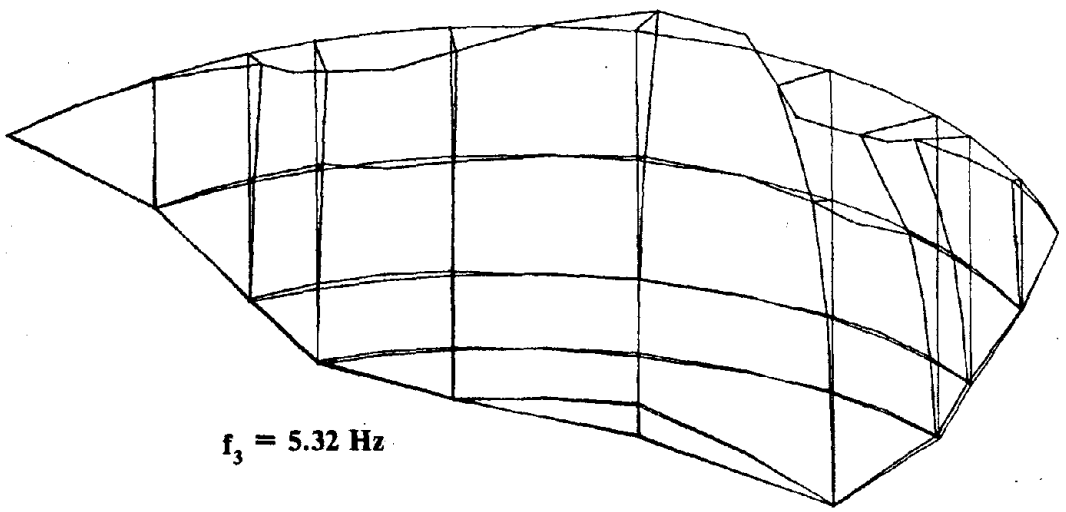

FIG. 3.23 Perspective View Of Upstream Face Displacements: Mode 3

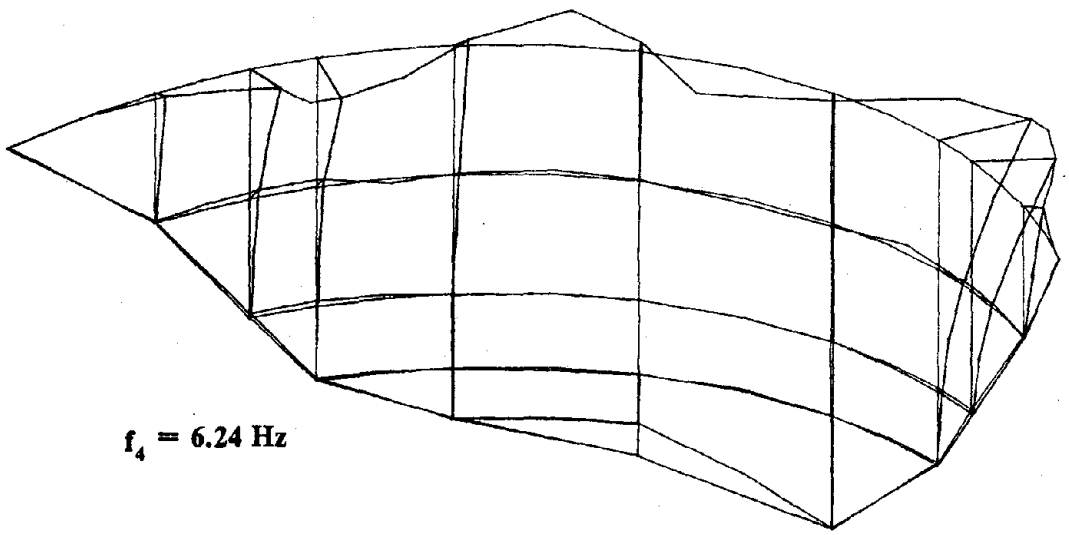

FIG. 3.24 Perspective View Of Upstream Face Displacements: Mode 4

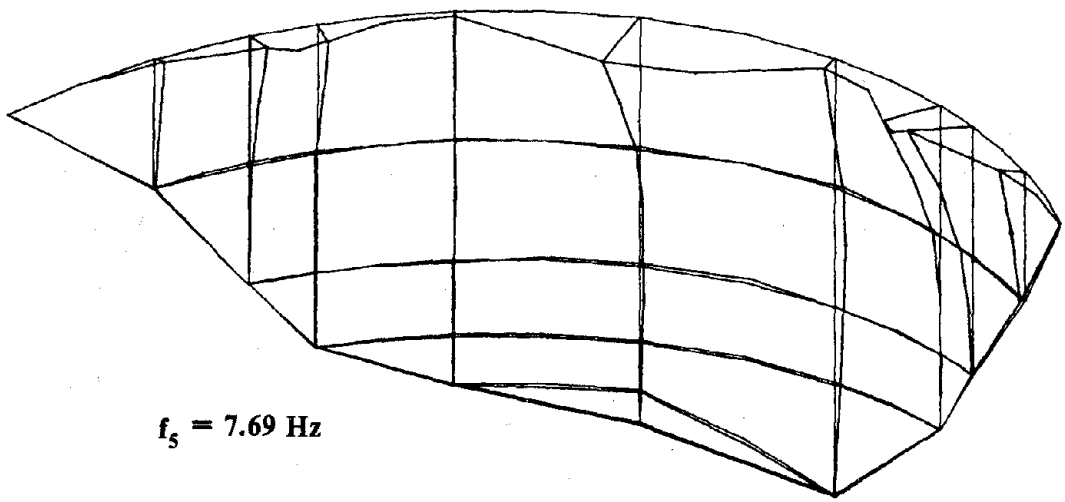

FIG 3.25 Perspective View Of Upstream Face Displacements: Mode 5

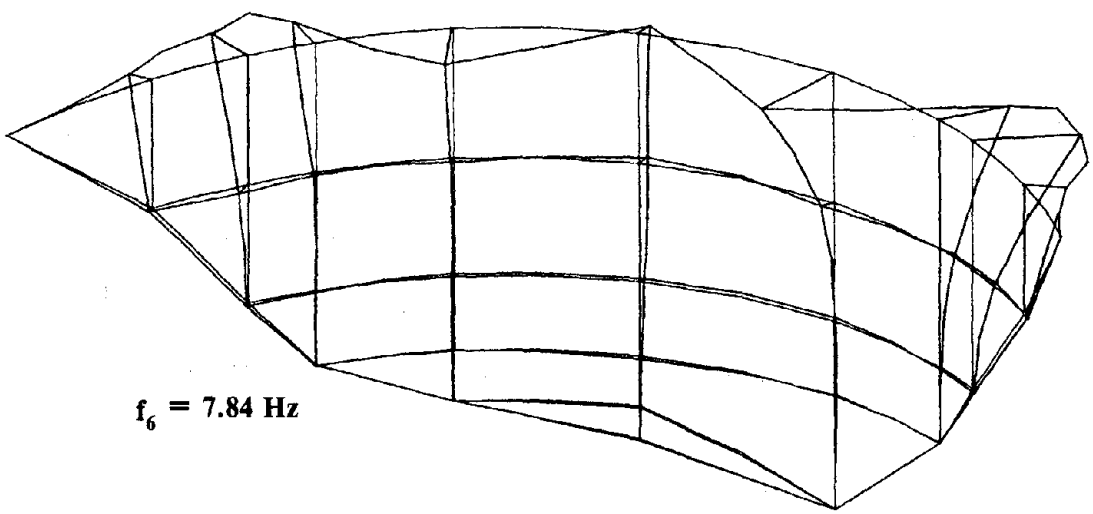

FIG. 3.26 Perspective View Of Upstream Face Displacements: Mode 6

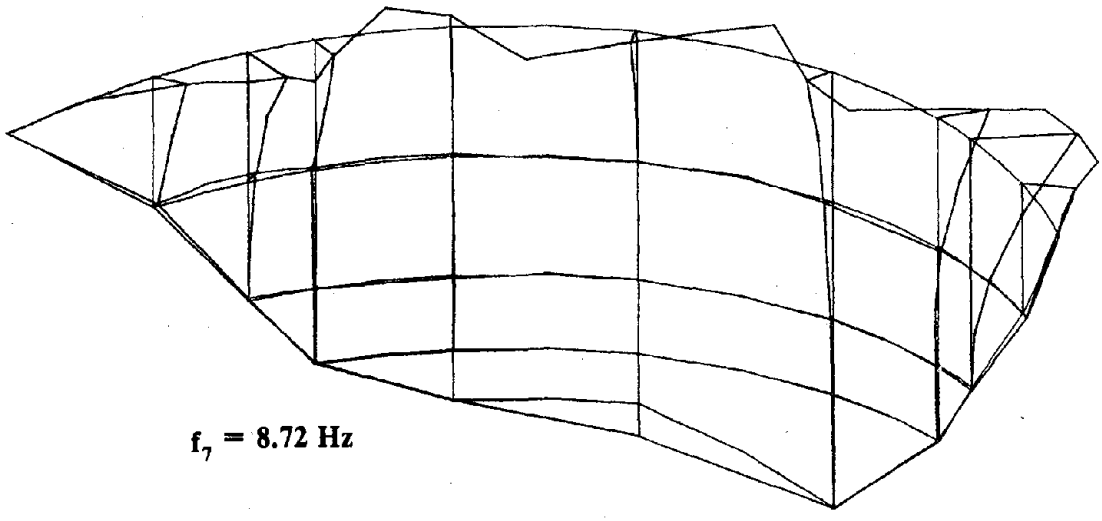

FIG. 3.27 Perspective View Of Upstream Face Displacements: Mode 7

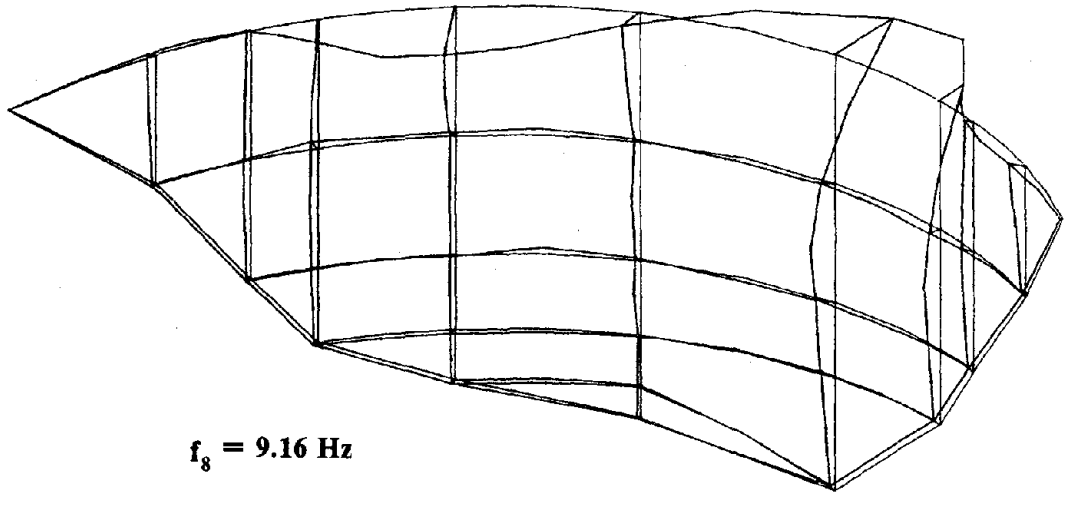

FIG. 3.28 Perspective View Of Upstream Face Displacements: Mode 8

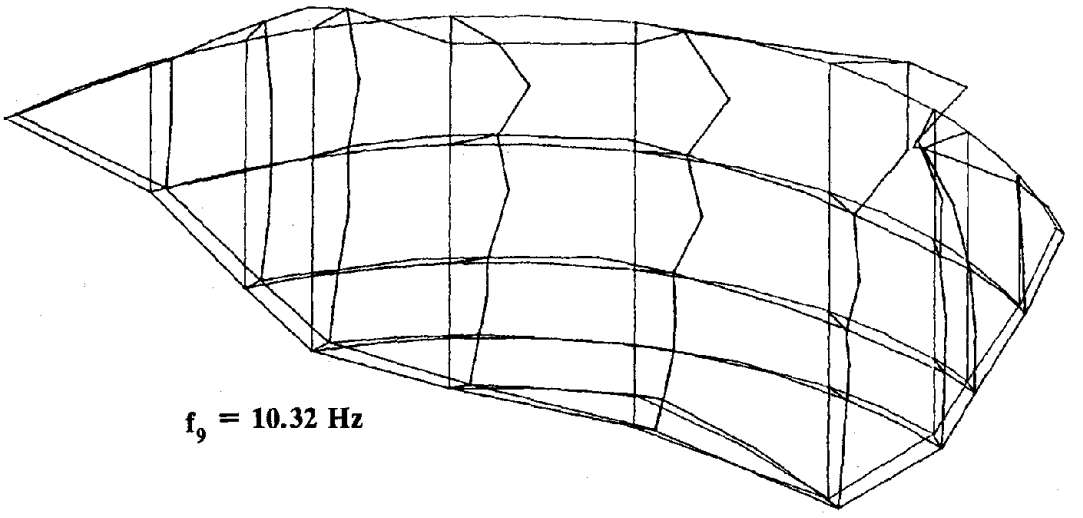

FIG. 3.29 Perspective View Of Upstream Face Displacements: Mode 9

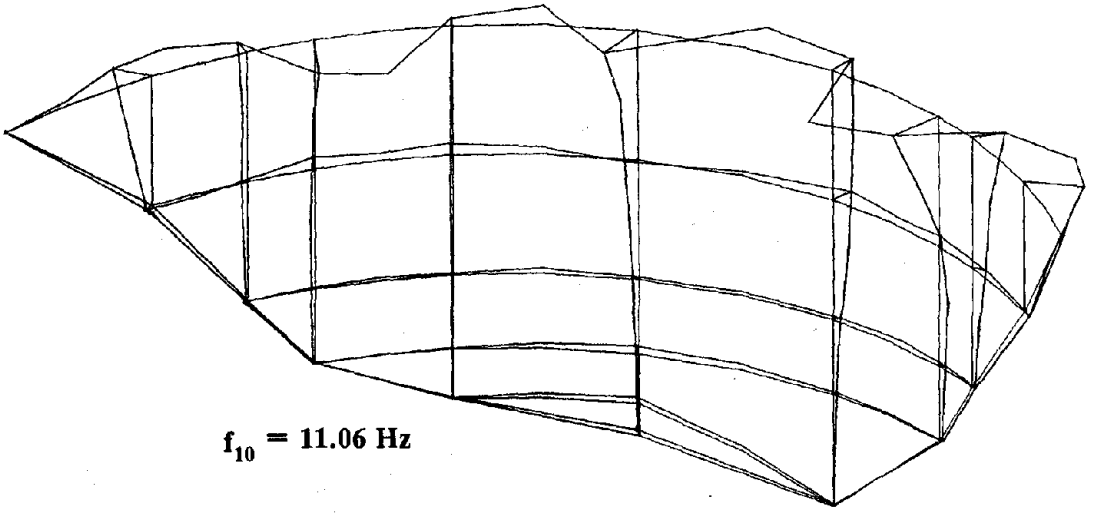

FIG. 3.30 Perspective View Of Upstream Face Displacements: Mode 10

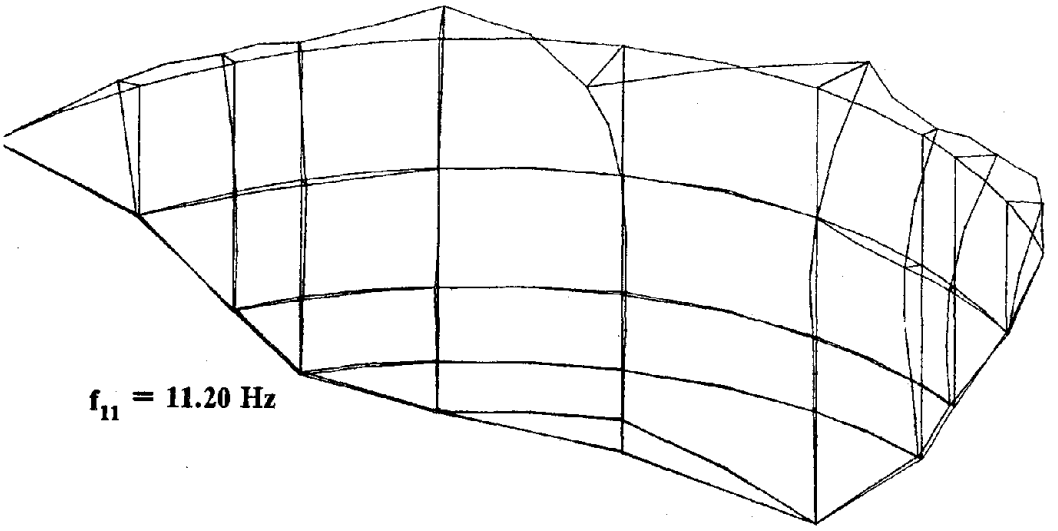

FIG. 3.31 Perspective View Of Upstream Face Displacements: Mode 11

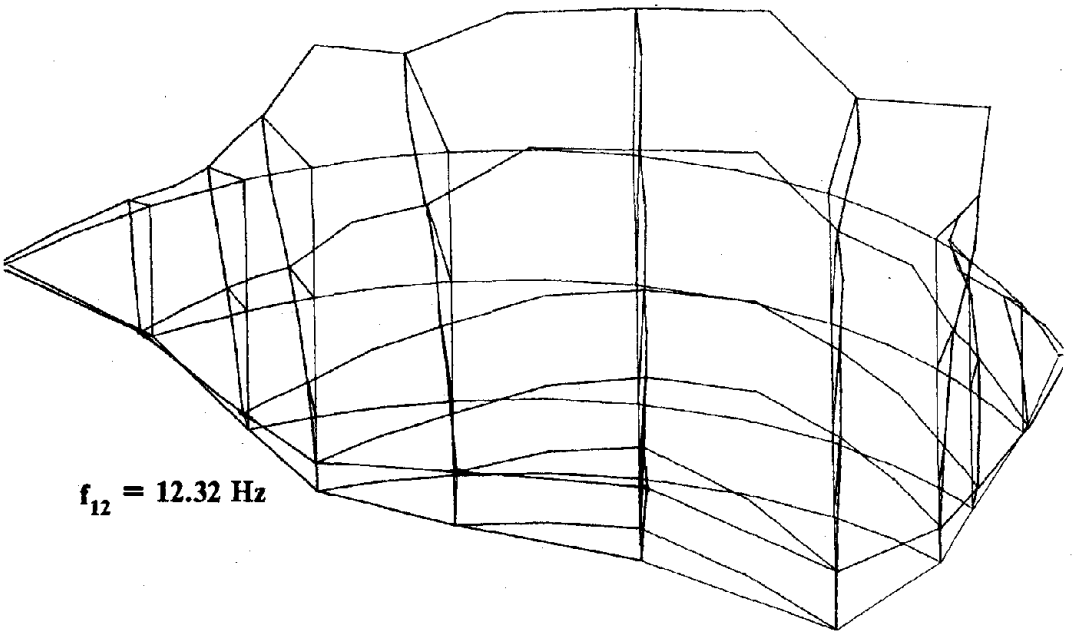

FIG. 3.32 Perspective View Of Upstream Face Displacements: Mode 12

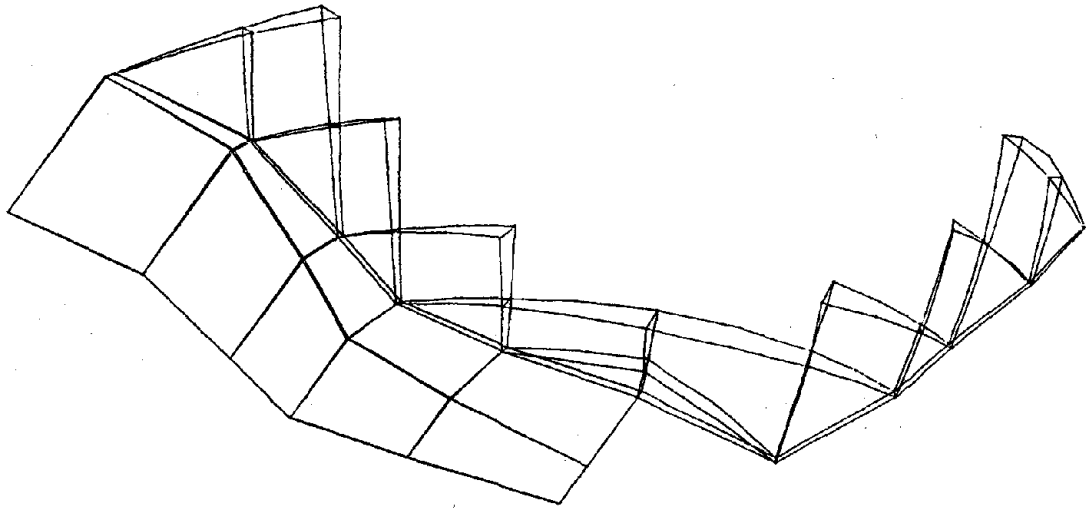

FIG. 3.33 Mode 1, Displacements Of Foundaton Rock And Adjacent Downstream Force Modes

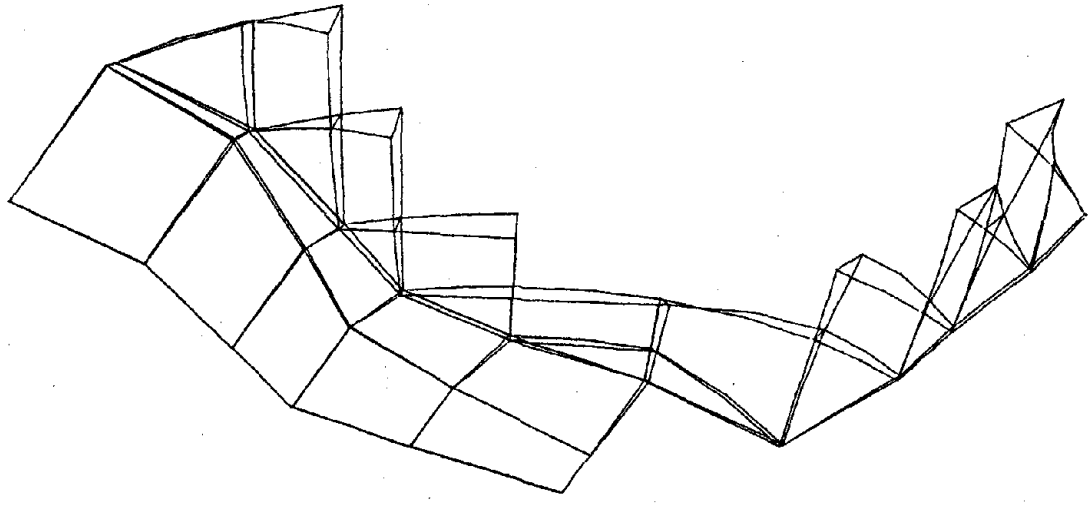

FIG. 3.34 Mode 2, Displacements Of Foundaton Rock And Adjacent Downstream Force Modes

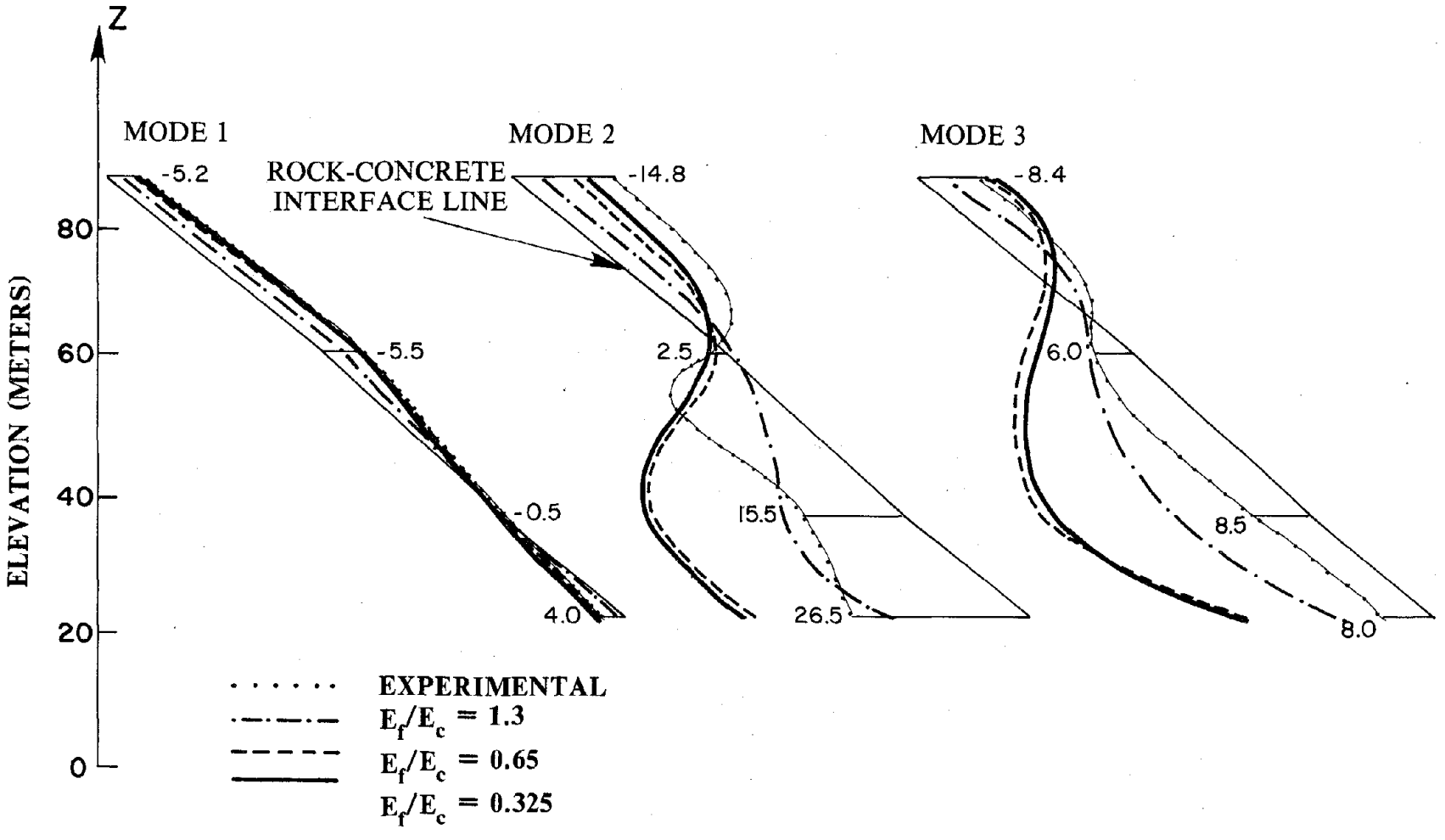

FIG. 4.1 Vibration Shapes At Rock-Concrete Interface: Modes 1,2, and 3

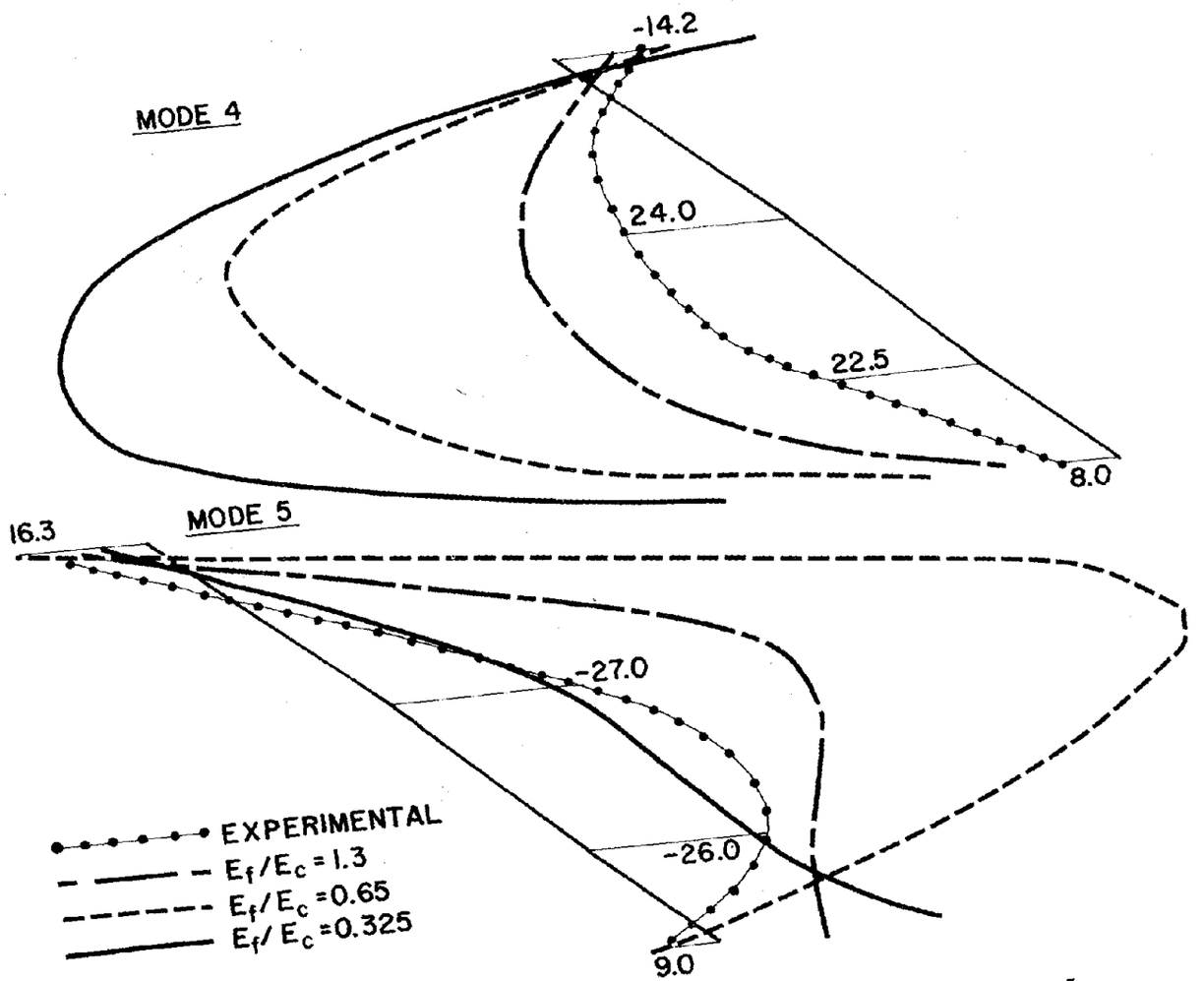

FIG. 4.2 Vibration Shapes At Rock-Concrete Interface: Modes 4 & 5

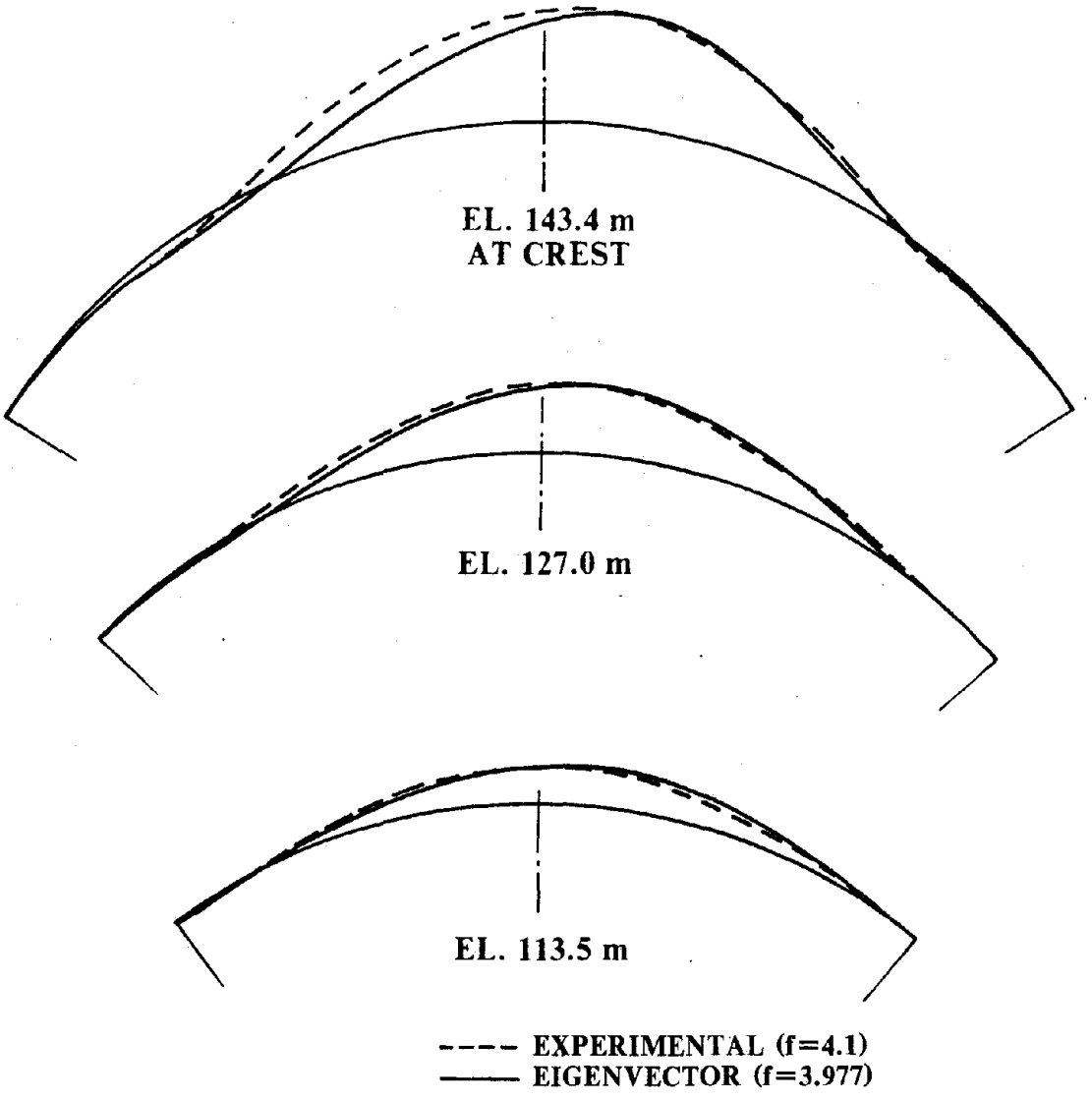

FIG. 4.3 Comparison Of Measured And Calculated Vibration Shapes: Mode 1

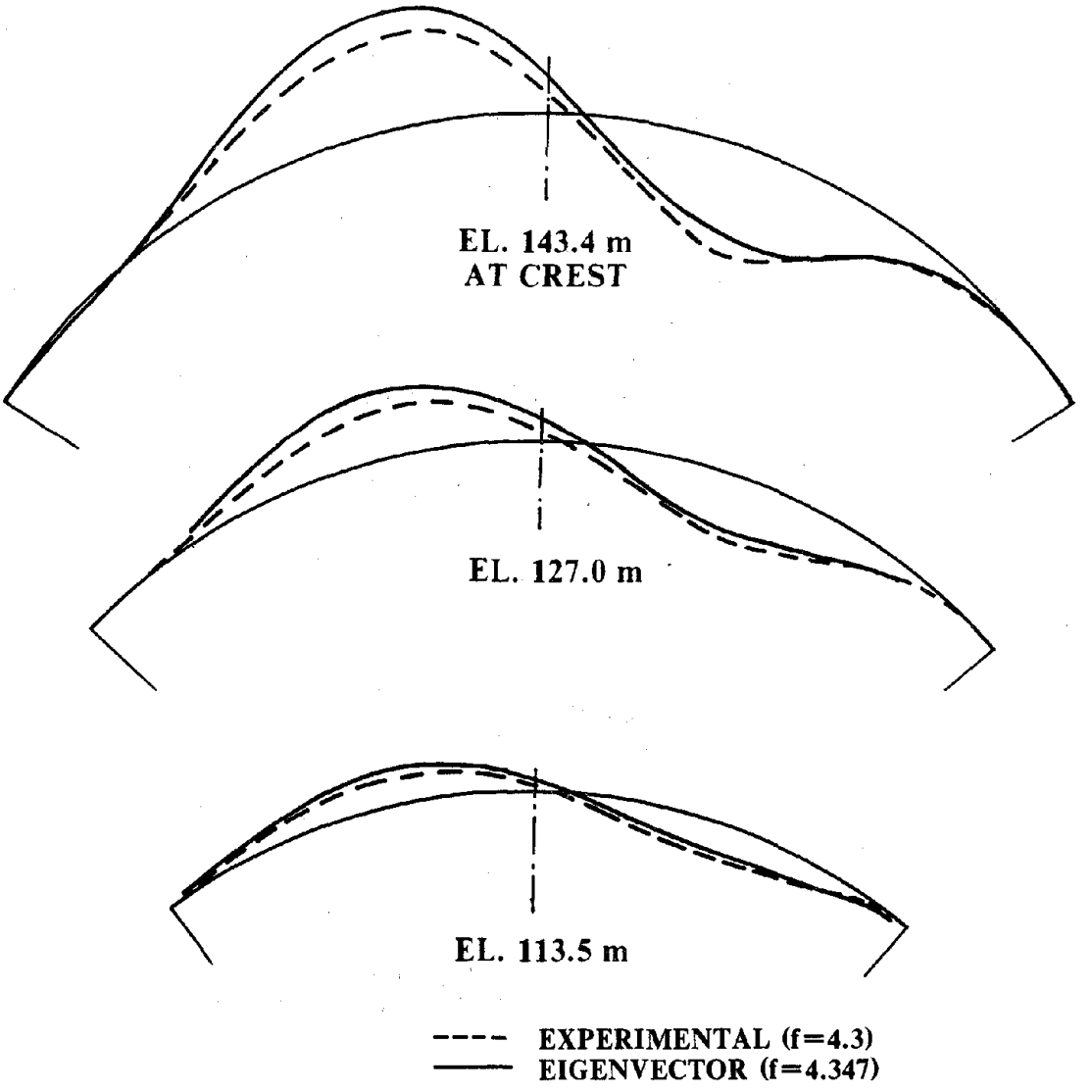

FIG. 4.4 Comparison Of Measured And Calculated Vibration Shapes: Mode 2

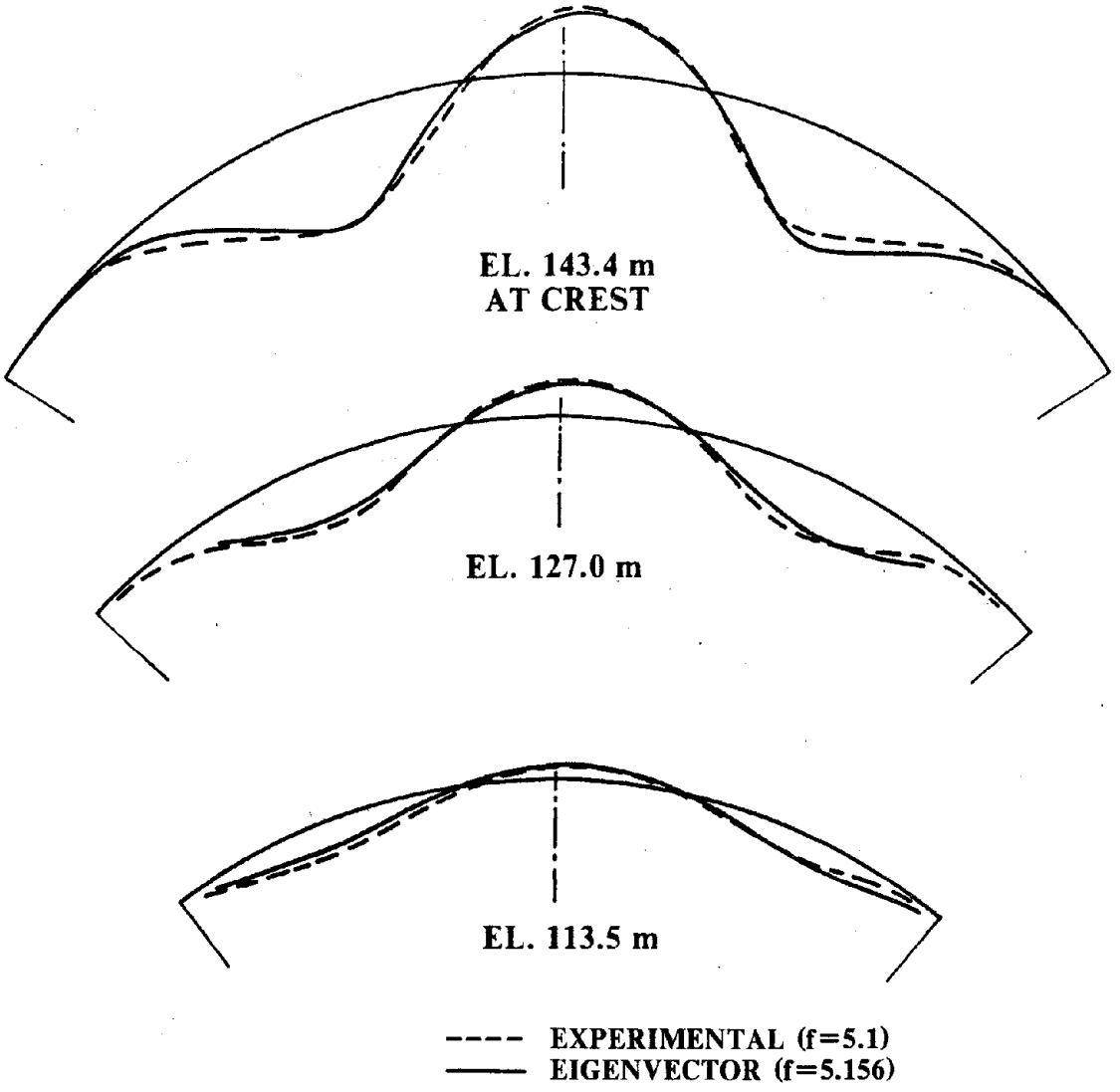

FIG. 4.5 Comparison Of Measured And Calculated Vibration Shapes: Mode 3

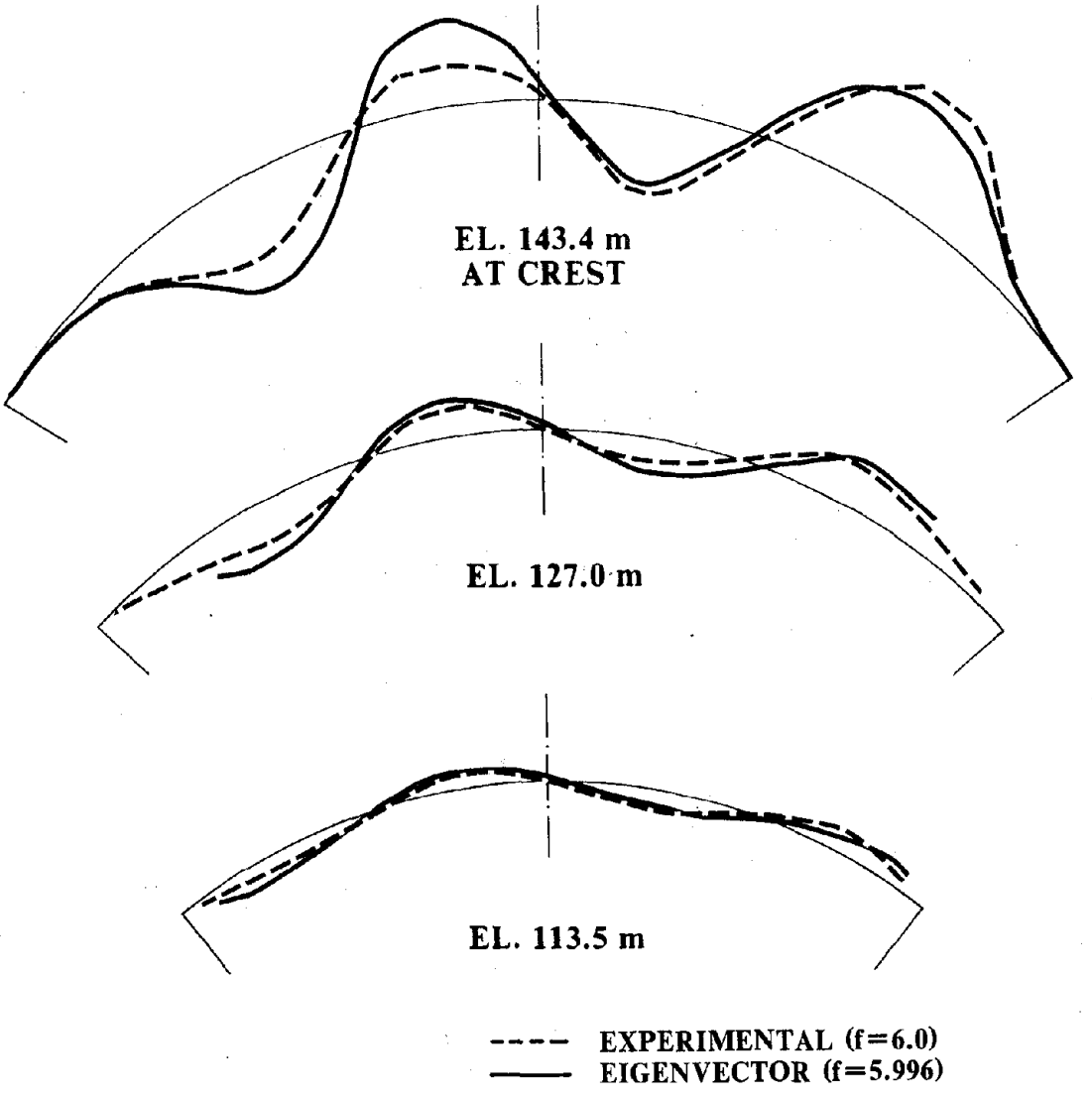

FIG. 4.6 Comparison Of Measured And Calculated Vibration Shapes: Mode 4

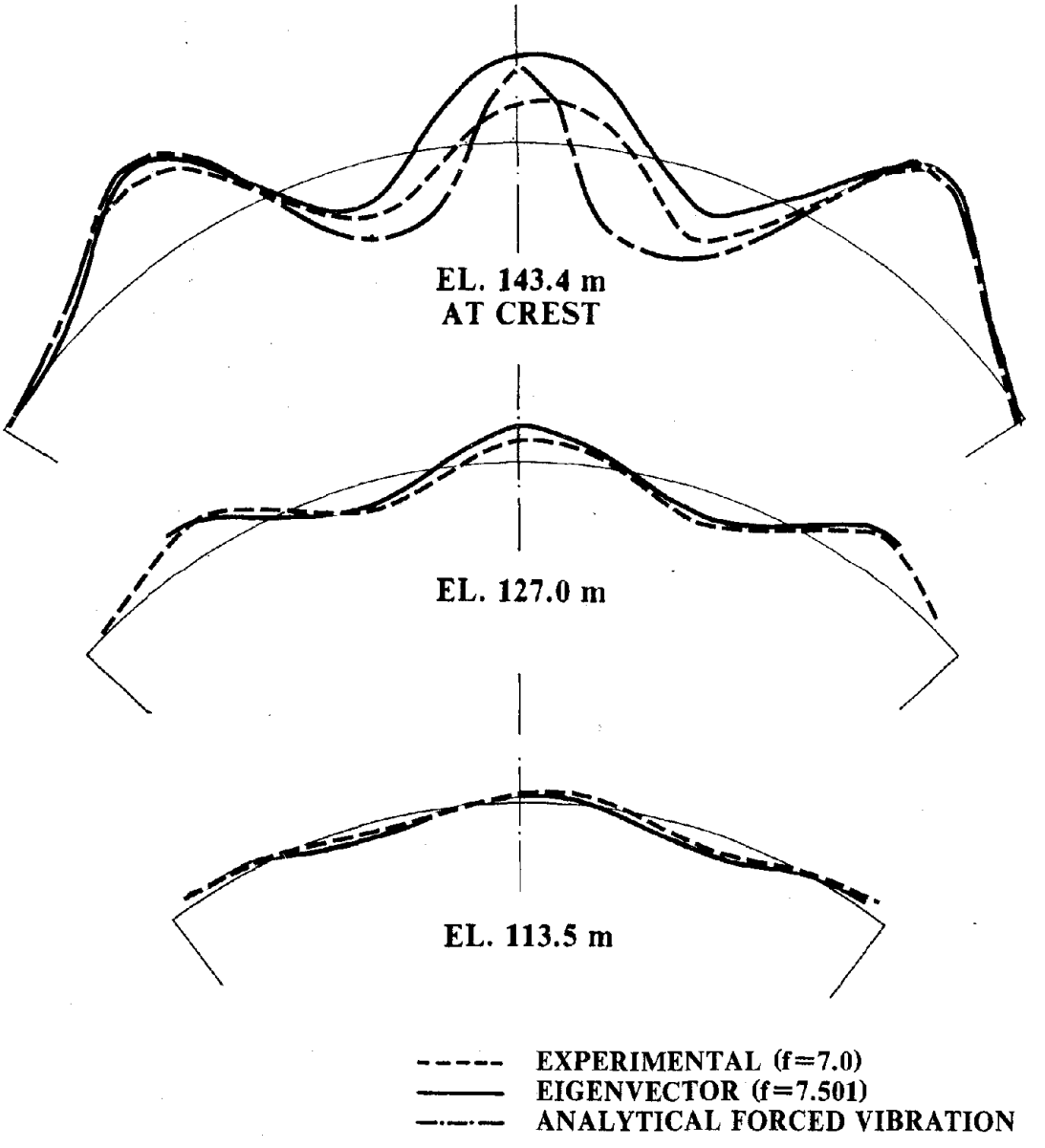

FIG. 4.7 Comparison Of Measured And Calculated Vibration Shapes: Mode 5

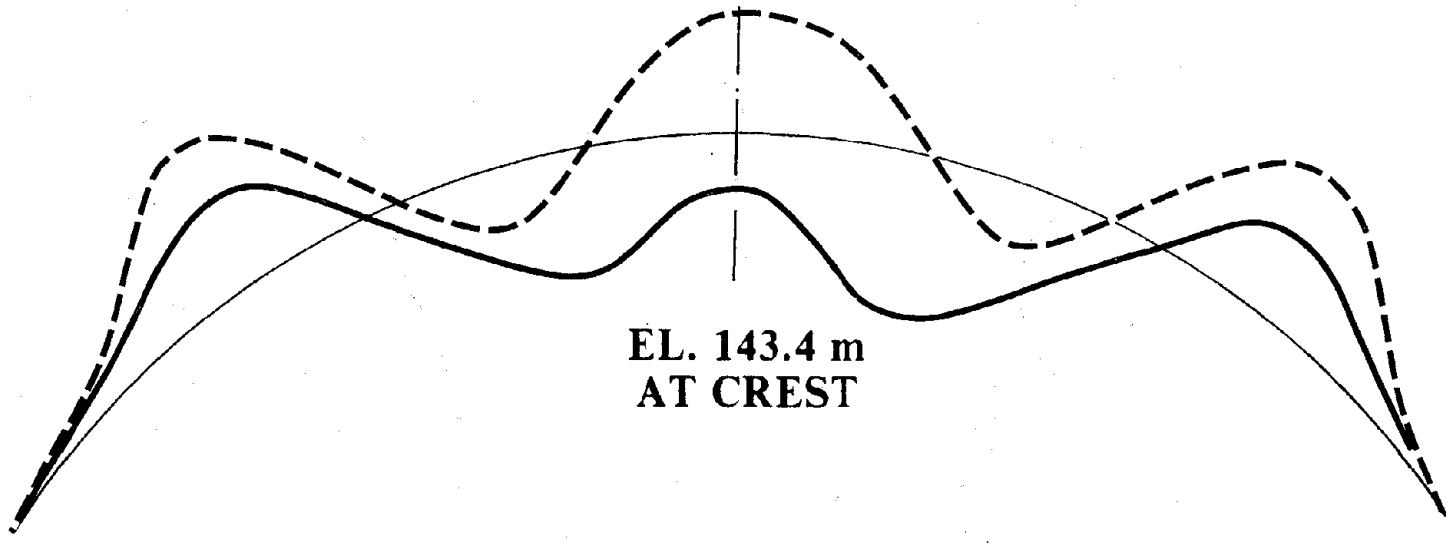

——— EIGENVECTOR (f=7.623)
– – – – ANALYTICAL FORCED VIBRATION
(INCLUDING CONTRIBUTION OF MODES 5 & 7)

FIG. 4.8 Comparison Of Measured And Calculated
Vibration Shapes: Mode 6 (Experimental "Missing Mode")

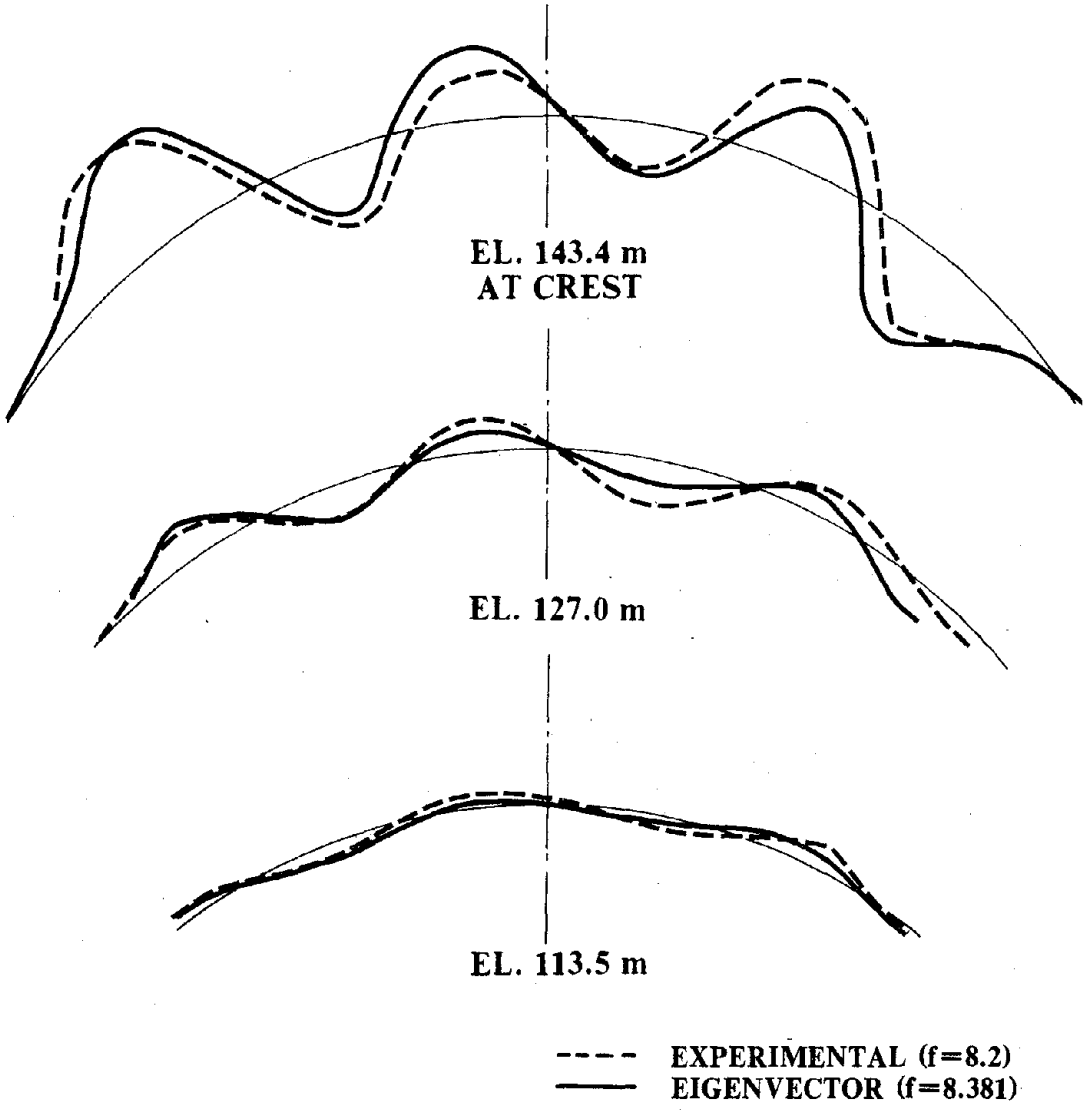

FIG. 4.9 Comparison Of Measured And Calculated Vibration Shapes: Mode 7

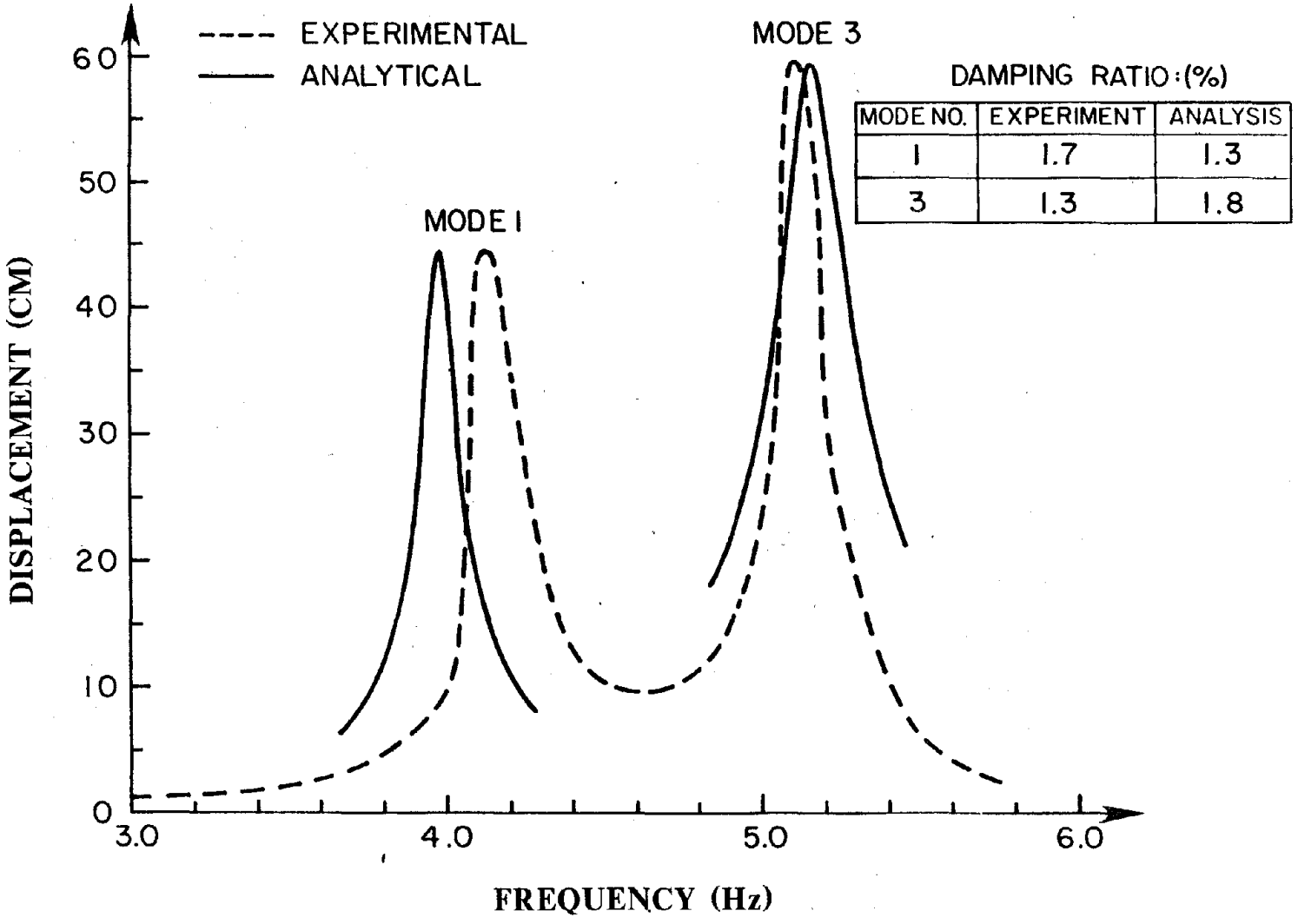

FIG. 4.10 Comparison Of Measured And Calculated Frequency Response Curves - Symmetric Excitation

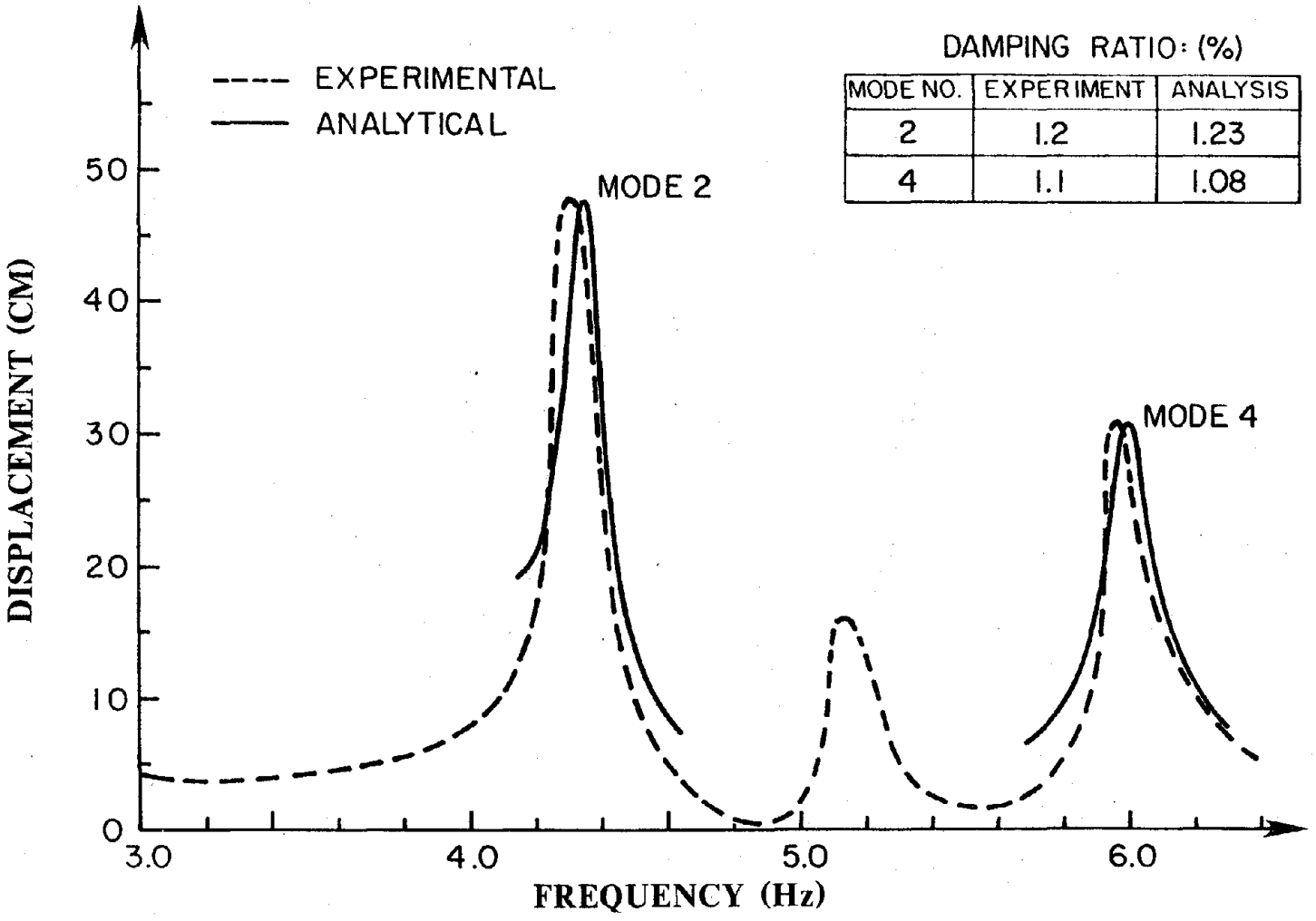

FIG. 4.11 Comparison Of Measured And Calculated Frequency Response Curves - Antisymmetric Excitation

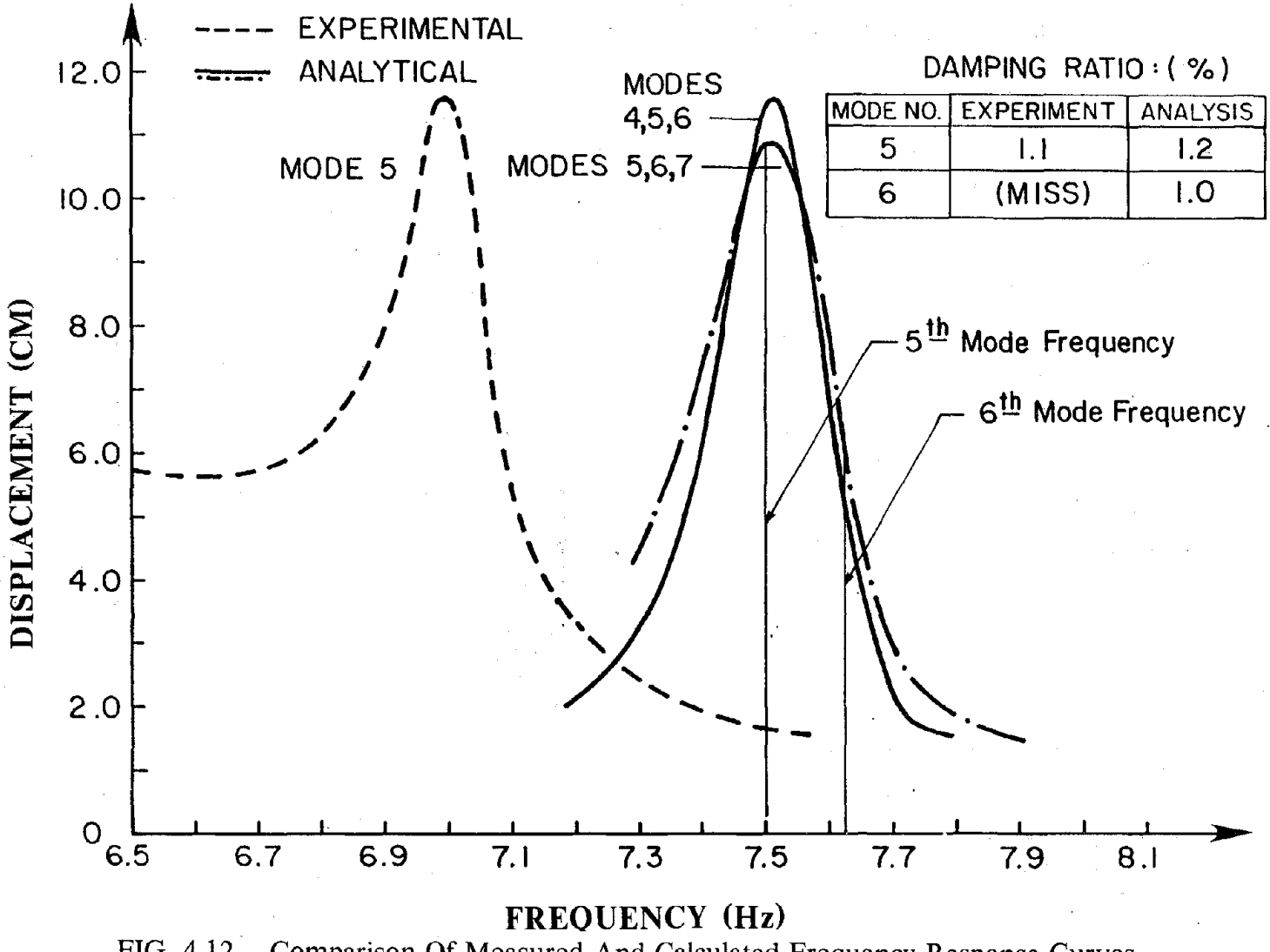

FIG. 4.12 Comparison Of Measured And Calculated Frequency Response Curves - Symmetric Excitation

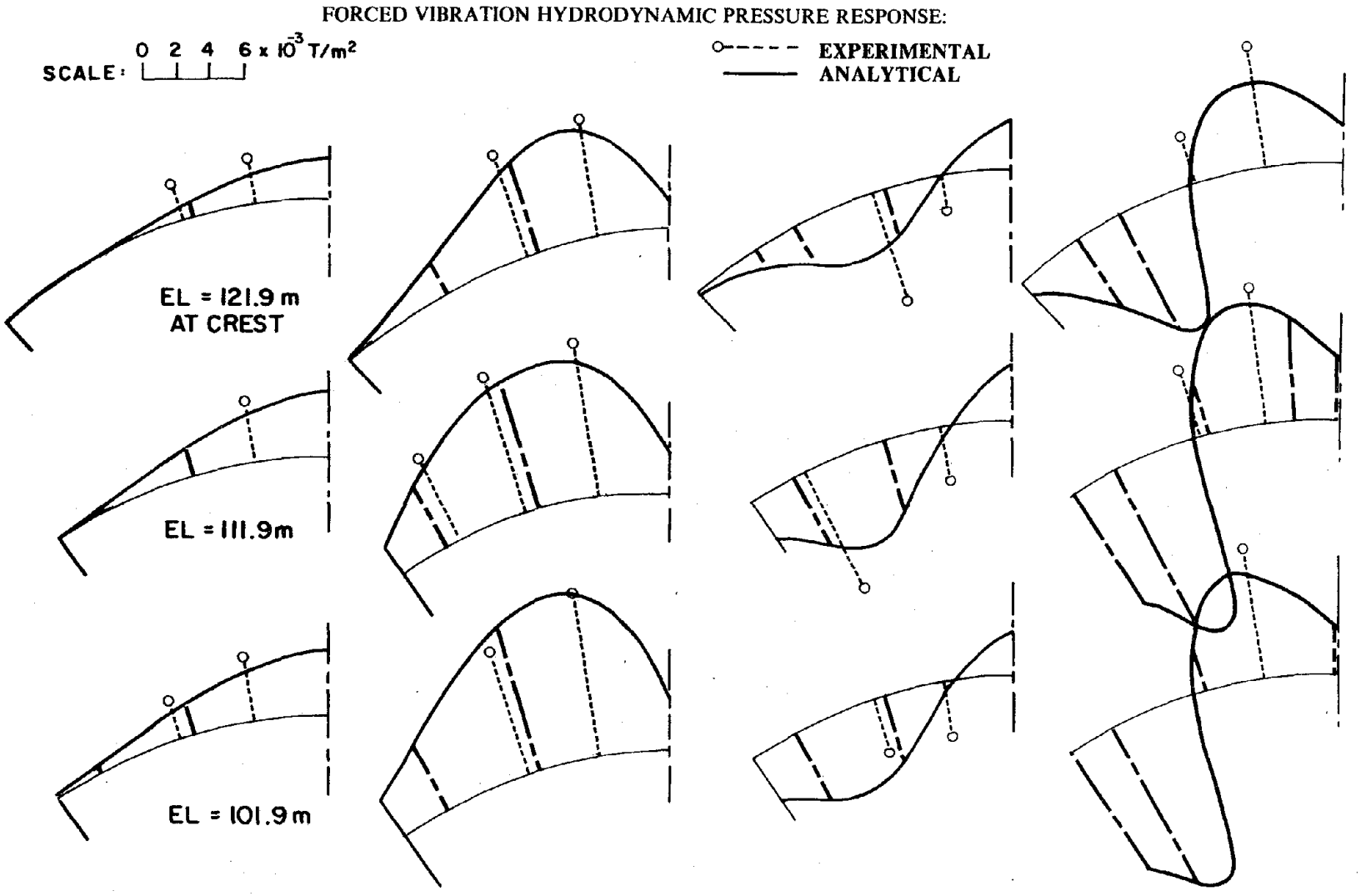

FIG. 4.13 f_1 = 4.1 Hz

FIG. 4.14 f_2 = 4.3 Hz

FIG. 4.15 f_3 = 5.1 Hz

FIG. 4.16 f_4 = 6.0 Hz

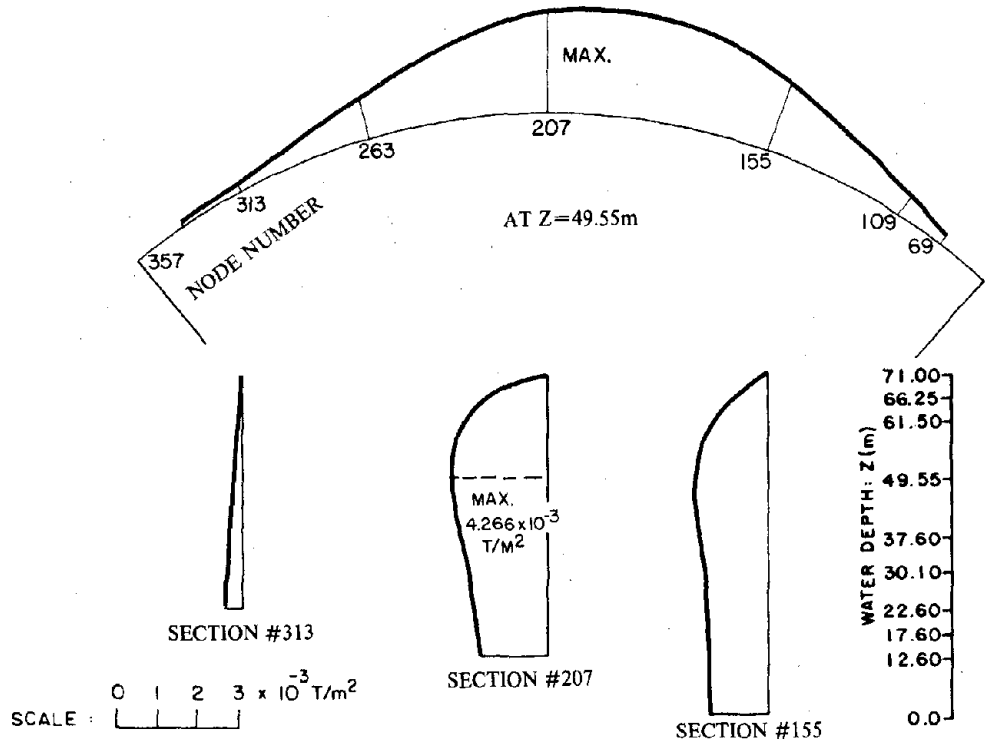

FIG. 4.17 Calculated Forced Vibration Hydrodynamic Pressures: Mode 1

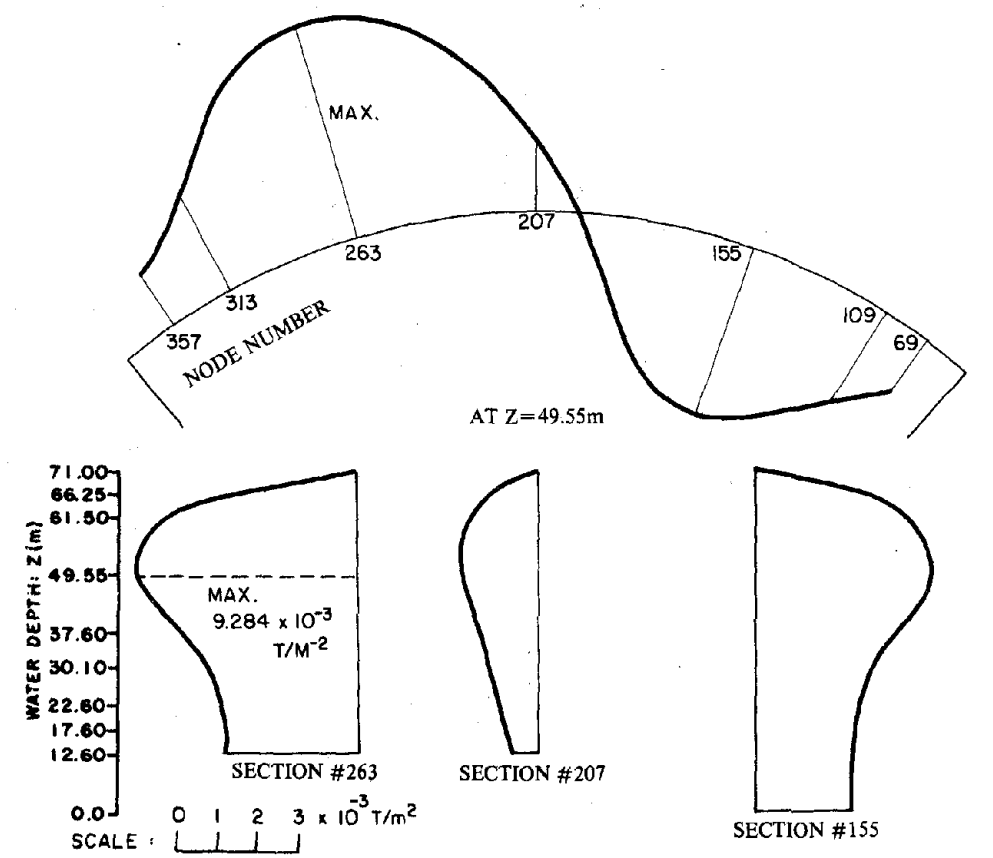

FIG. 4.18 Calculated Forced Vibration Hydrodynamic Pressures: Mode 2

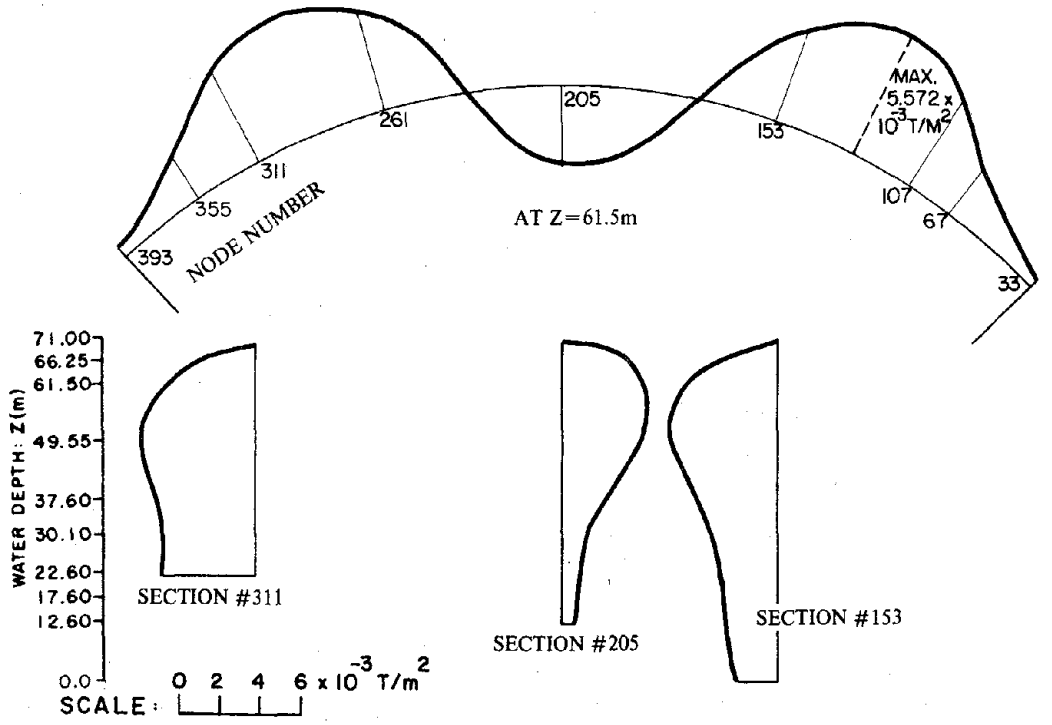

FIG. 4.19 Calculated Forced Vibration Hydrodynamic Pressures: Mode 3

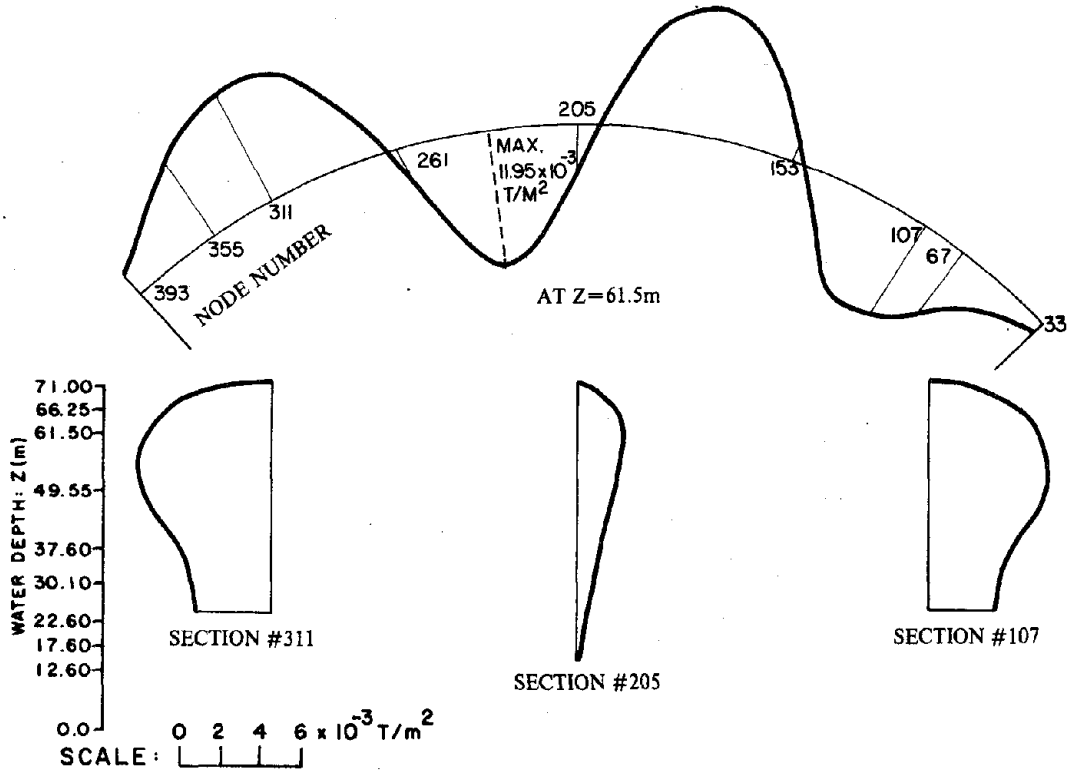

FIG. 4.20 Calculated Forced Vibration Hydrodynamic Pressures: Mode 4

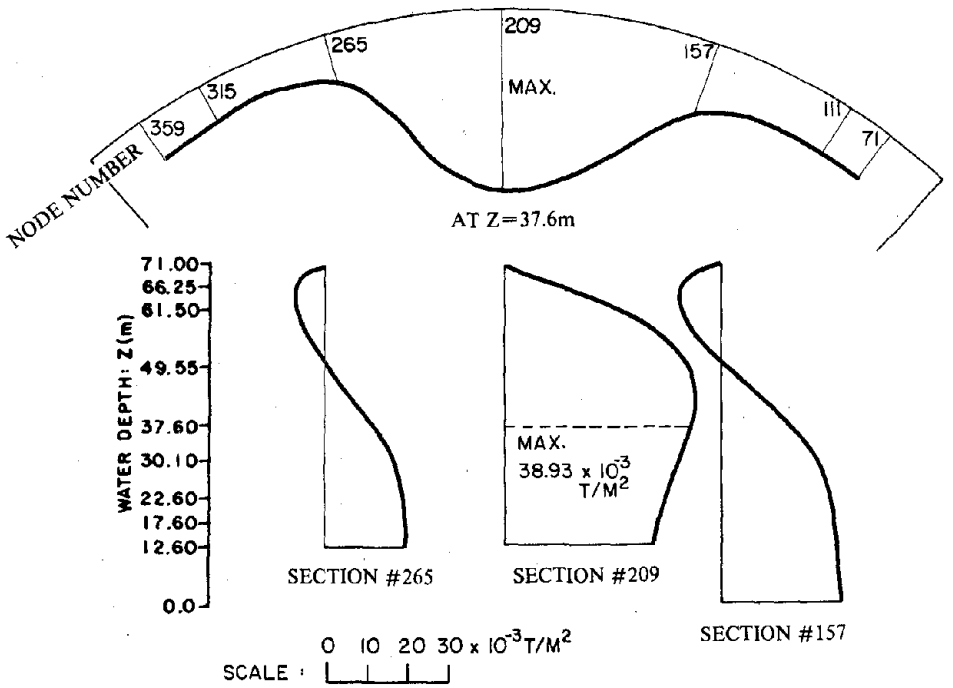

FIG. 4.21 Calculated Forced Vibration Hydrodynamic Pressures: Mode 5

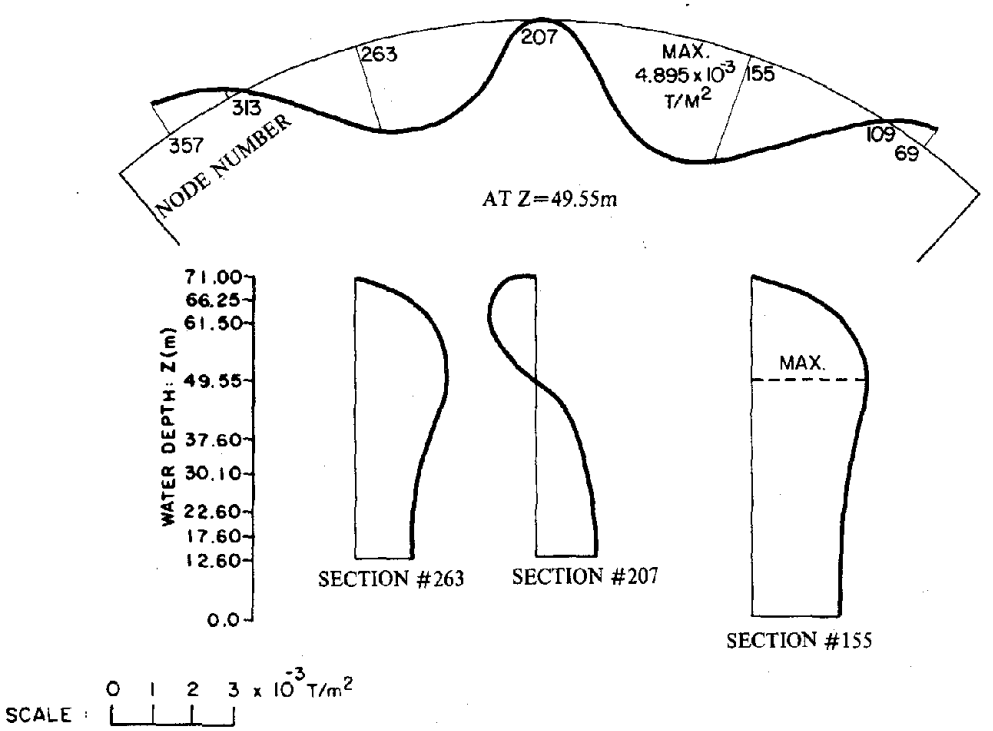

FIG. 4.22 Calculated Forced Vibration Hydrodynamic Pressures: Mode 6

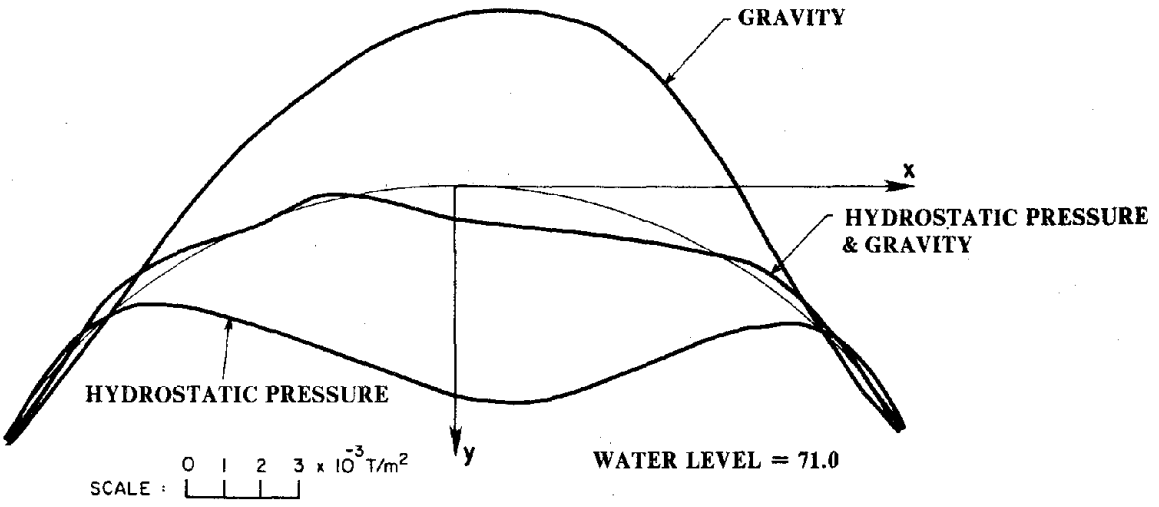

FIG. 5.1 Static Crest Displacements: Gravity, and Hydrostatic Load

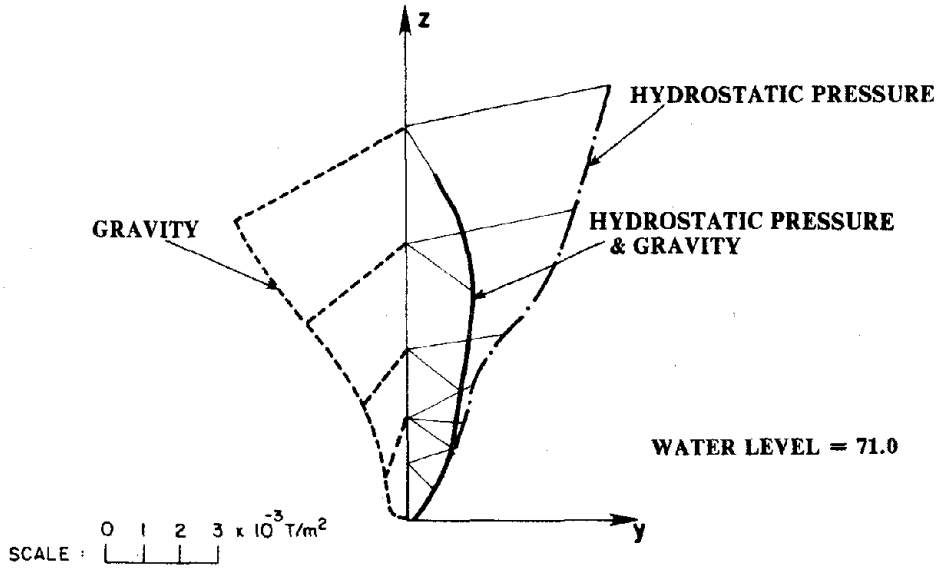

FIG. 5.2 Combined Horizontal Plus Vertical
Static Displacements Of Crown Cantilever

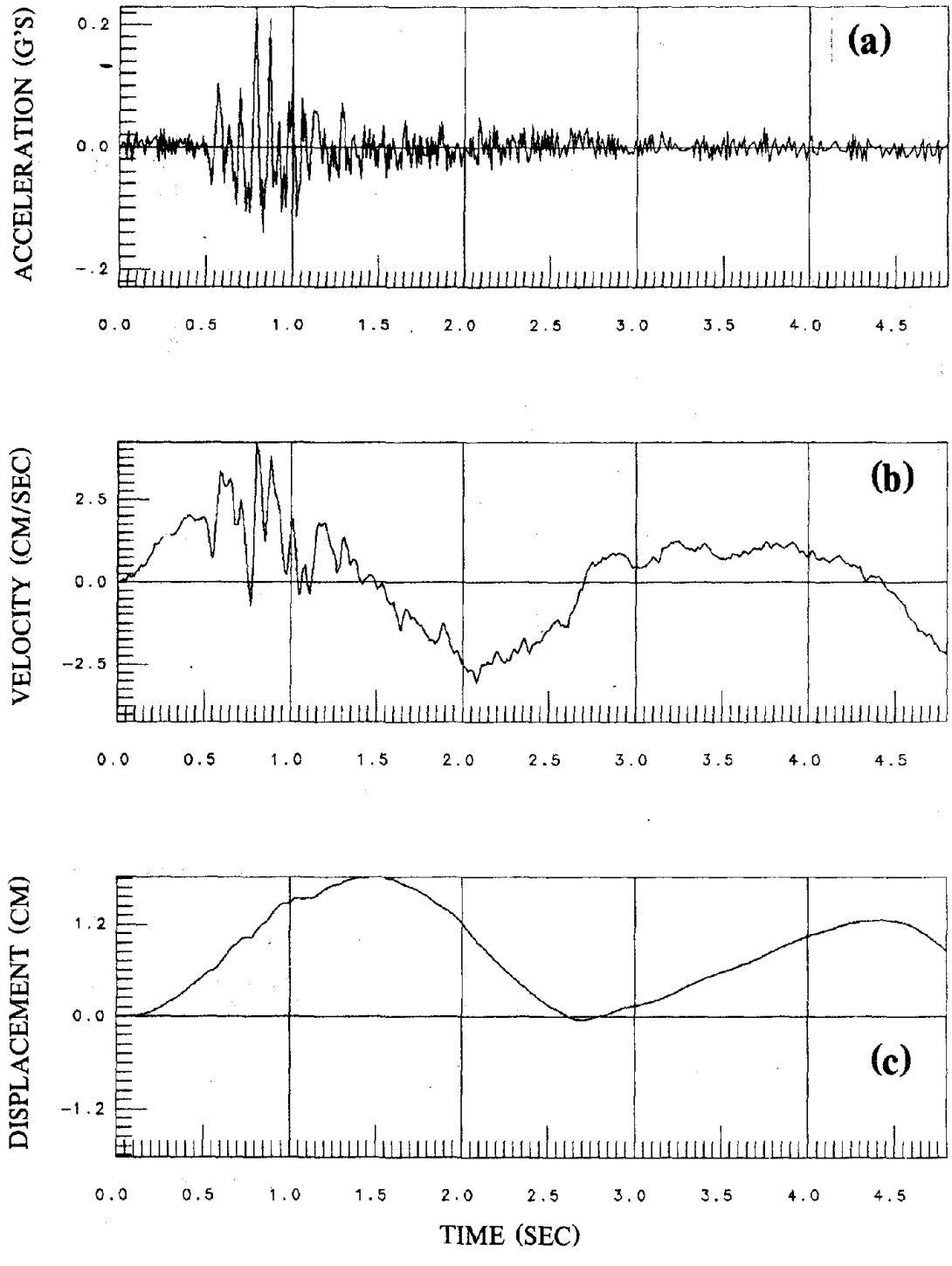

FIG. 5.3A Hsin Feng Jiang Earthquake Motions (Magnified By 5)

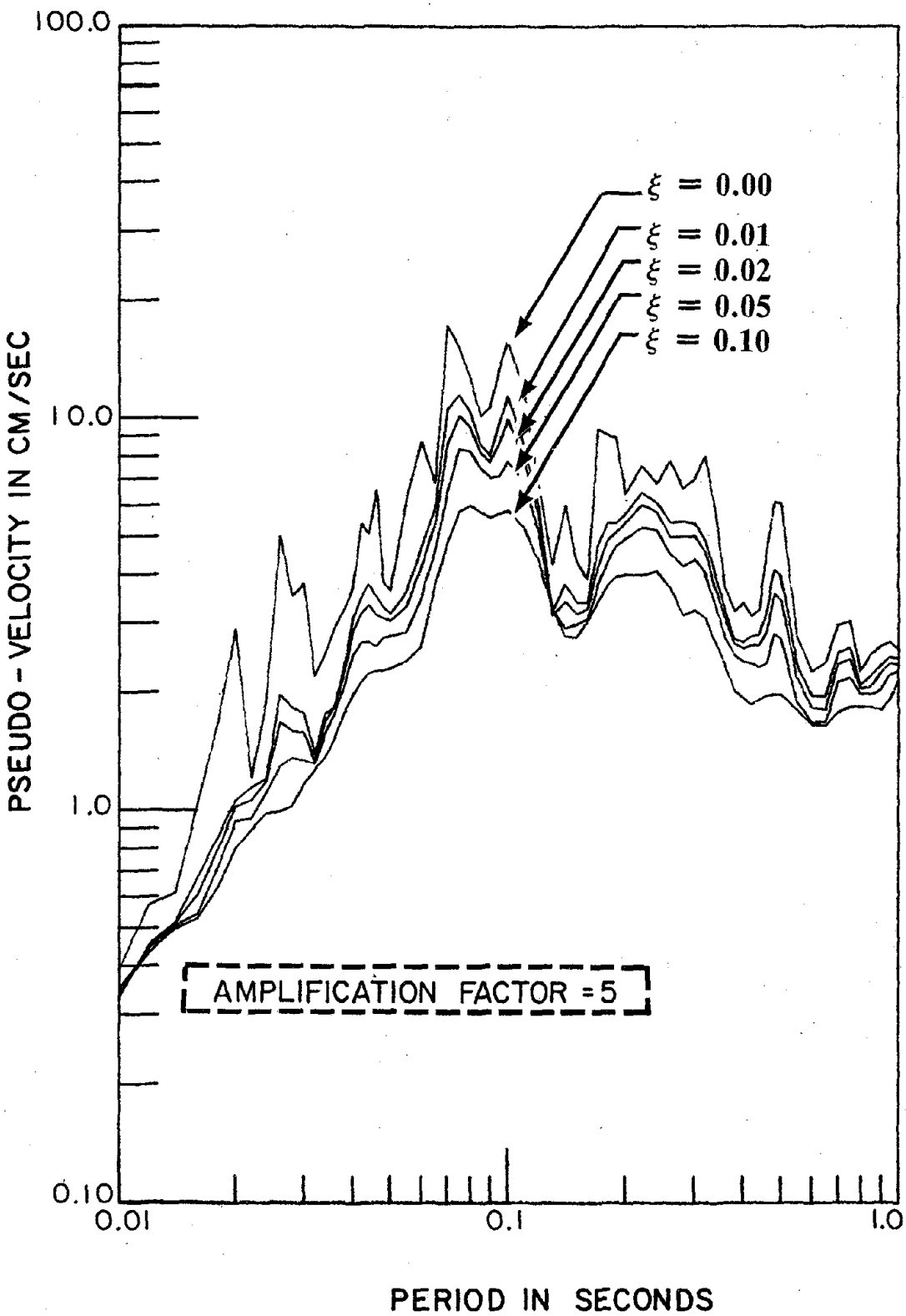

FIG. 5.3B Response Spectrum - Amplified Hsin Feng Jiang Earthquake

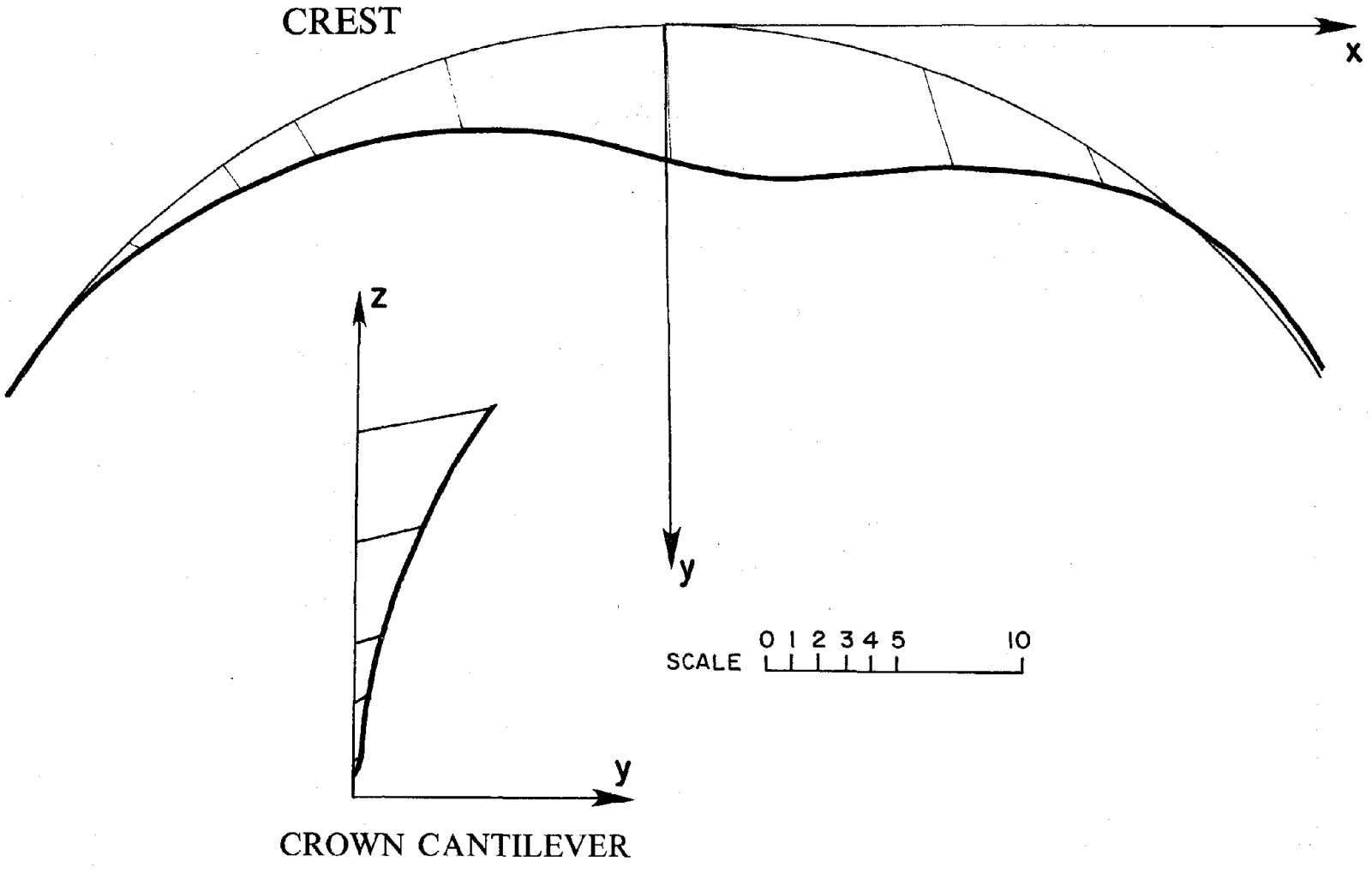

FIG. 5.4 Displacement Envelope Due To Amplified Hsin Feng Jiang Earthquake

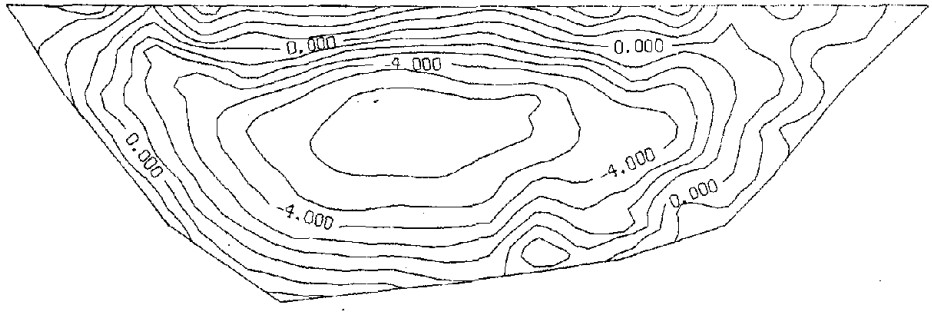

a) MAXIMUM ARCH TENSION STRESS (KG/CM*CM)

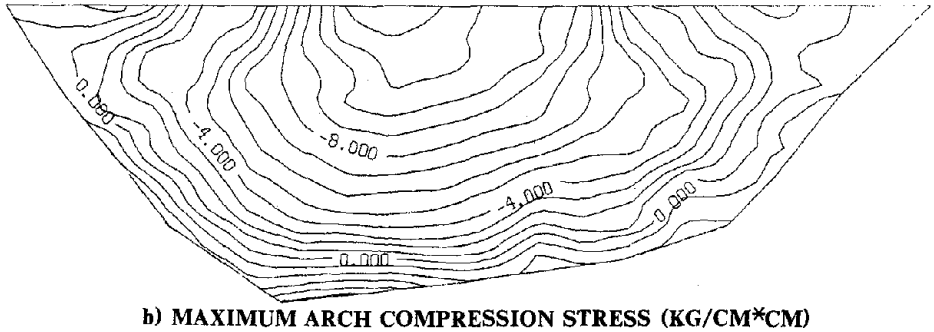

b) MAXIMUM ARCH COMPRESSION STRESS (KG/CM*CM)

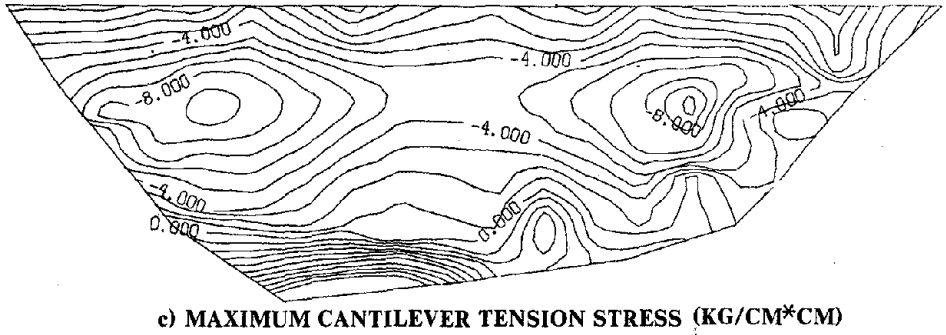

c) MAXIMUM CANTILEVER TENSION STRESS (KG/CM*CM)

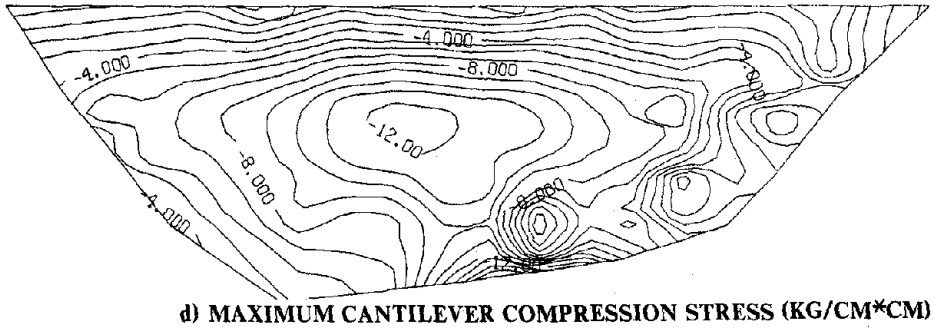

d) MAXIMUM CANTILEVER COMPRESSION STRESS (KG/CM*CM)

FIG. 5.5 Maximum Stresses On Upstream Face
(Static Load Plus Earthquake Response)

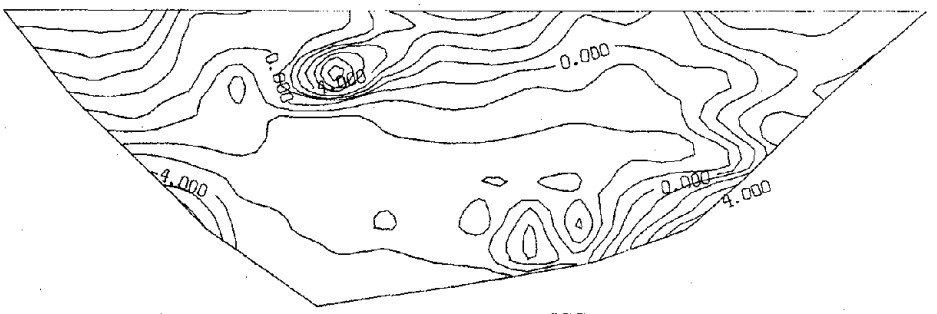

a) MAXIMUM ARCH TENSION STRESS

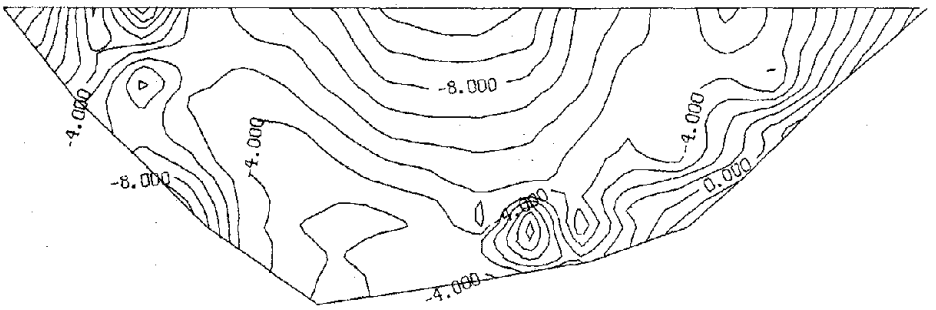

b) MAXIMUM ARCH COMPRESSION STRESS (KG/CM*CM)

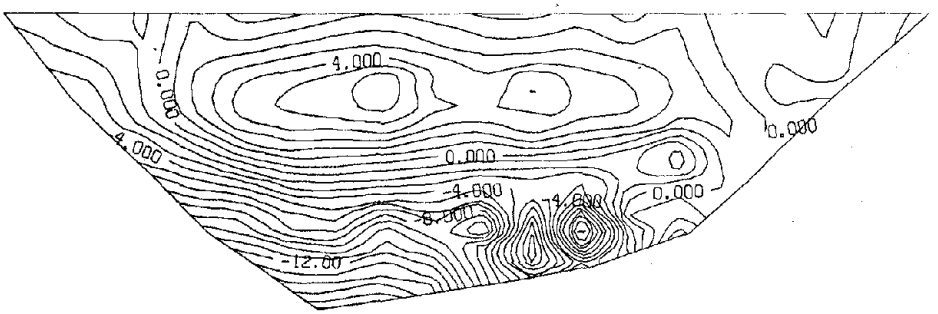

c) MAXIMUM CANTILEVER TENSION STRESS (KG/CM*CM)

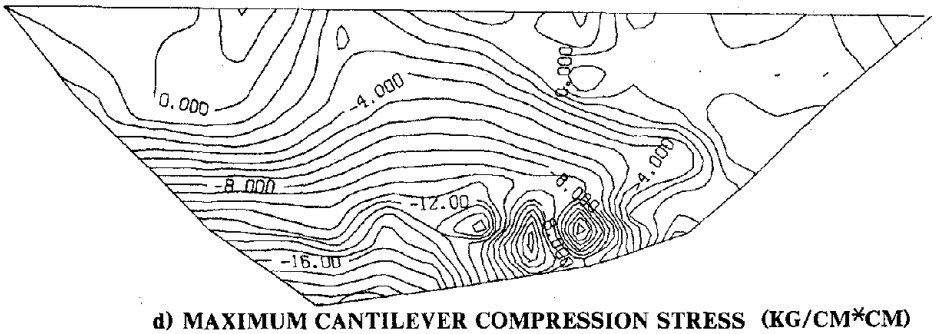

d) MAXIMUM CANTILEVER COMPRESSION STRESS (KG/CM*CM)

FIG. 5.6 Maximum Stresses On Downstream Face (Static Load Plus Earthquake Response)

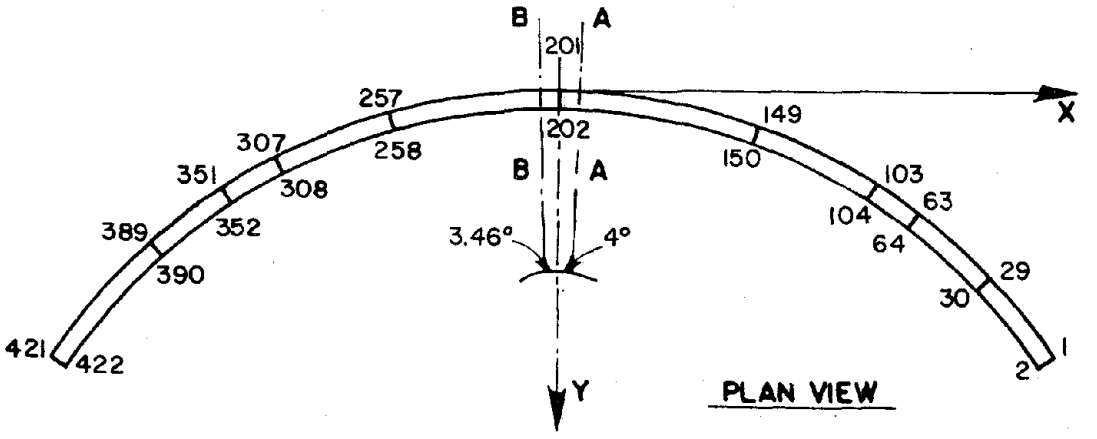

FIG. 5.7 Locations Of Stress Analysis Sections & Crest Nodes

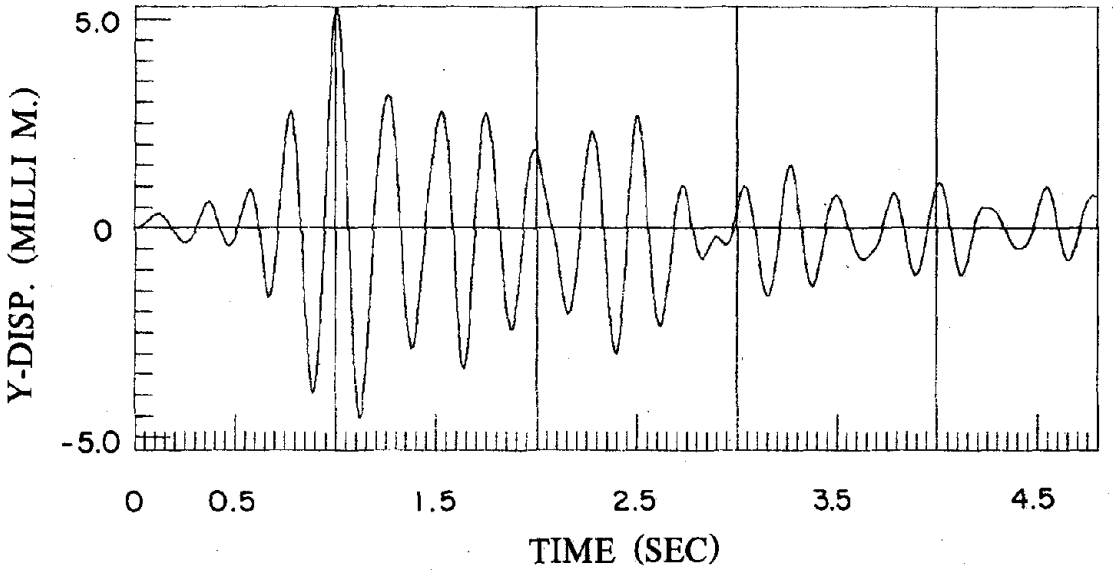

FIG. 5.8 Displacement Response At Center Of Dam Crest

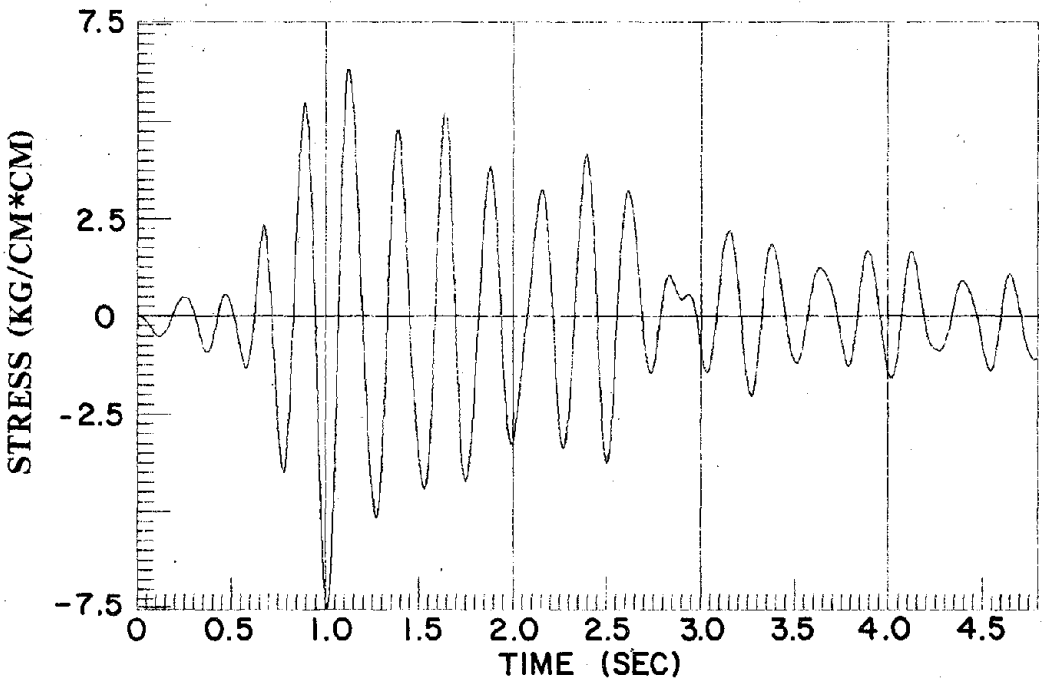

a) ARCH STRESS NEAR TOP OF SECTION A (FIG. 5.7)

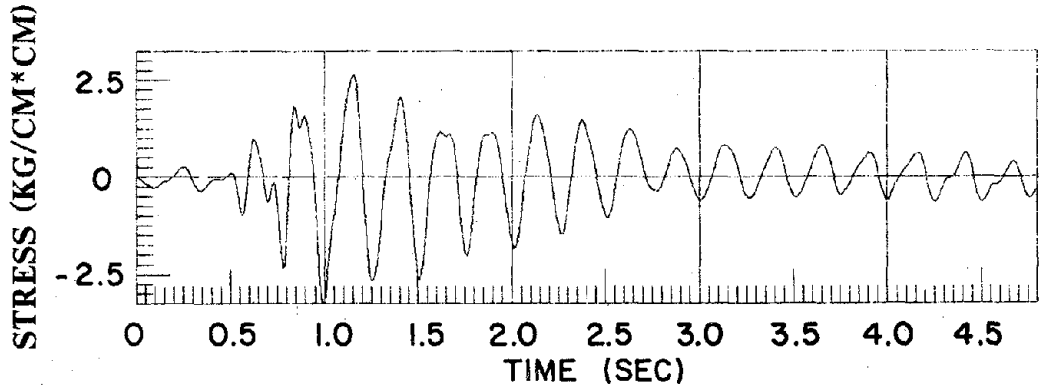

b) CANTILEVER STRESS NEAR BASE OF SECTION A (FIG. 5.7)

FIG. 5.9 Seismic Stress Response At Upstream Face

EARTHQUAKE ENGINEERING RESEARCH CENTER REPORTS

NOTE: Numbers in parentheses are Accession Numbers assigned by the National Technical Information Service; these are followed by a price code. Copies of the reports may be ordered from the National Technical Information Service, 5285 Port Royal Road, Springfield, Virginia, 22161. Accession Numbers should be quoted on orders for reports (PB --- ---) and remittance must accompany each order. Reports without this information were not available at time of printing. The complete list of EERC reports (from EERC 67-1) is available upon request from the Earthquake Engineering Research Center, University of California, Berkeley, 47th Street and Hoffman Boulevard, Richmond, California 94804.

UCB/EERC-77/01 "PLUSH - A Computer Program for Probabilistic Finite Element Analysis of Seismic Soil-Structure Interaction," by M.P. Romo Organista, J. Lysmer and H.B. Seed - 1977 (PB81 177 651)A05

UCB/EERC-77/02 "Soil-Structure Interaction Effects at the Humboldt Bay Power Plant in the Ferndale Earthquake of June 7, 1975," by J.E. Valera, H.B. Seed, C.F. Tsai and J. Lysmer - 1977 (PB 265 795)A04

UCB/EERC-77/03 "Influence of Sample Disturbance on Sand Response to Cyclic Loading," by K. Mori, H.B. Seed and C.K. Chan - 1977 (PB 267 352)A04

UCB/EERC-77/04 "Seismological Studies of Strong Motion Records," by J. Shoja-Taheri - 1977 (PB 269 655)A10

UCB/EERC-77/05 Unassigned

UCB/EERC-77/06 "Developing Methodologies for Evaluating the Earthquake Safety of Existing Buildings," by No. 1 - B. Bresler; No. 2 - B. Bresler, T. Okada and D. Zisling; No. 3 - T. Okada and B. Bresler; No. 4 - V.V. Bertero and B. Bresler - 1977 (PB 267 354)A08

UCB/EERC-77/07 "A Literature Survey - Transverse Strength of Masonry Walls," by Y. Omote, R.L. Mayes, S.W. Chen and R.W. Clough - 1977 (PB 277 933)A07

UCB/EERC-77/08 "DRAIN-TABS: A Computer Program for Inelastic Earthquake Response of Three Dimensional Buildings," by R. Guendelman-Israel and G.H. Powell - 1977 (PB 270 693)A07

UCB/EERC-77/09 "SUBWALL: A Special Purpose Finite Element Computer Program for Practical Elastic Analysis and Design of Structural Walls with Substructure Option," by D.Q. Le, H. Peterson and E.P. Popov - 1977 (PB 270 567)A05

UCB/EERC-77/10 "Experimental Evaluation of Seismic Design Methods for Broad Cylindrical Tanks," by D.P. Clough (PB 272 280)A13

UCB/EERC-77/11 "Earthquake Engineering Research at Berkeley - 1976," - 1977 (PB 273 507)A09

UCB/EERC-77/12 "Automated Design of Earthquake Resistant Multistory Steel Building Frames," by N.D. Walker, Jr. - 1977 (PB 276 526)A09

UCB/EERC-77/13 "Concrete Confined by Rectangular Hoops Subjected to Axial Loads," by J. Vallenas, V.V. Bertero and E.P. Popov - 1977 (PB 275 165)A06

UCB/EERC-77/14 "Seismic Strain Induced in the Ground During Earthquakes," by Y. Sugimura - 1977 (PB 284 201)A04

UCB/EERC-77/15 Unassigned

UCB/EERC-77/16 "Computer Aided Optimum Design of Ductile Reinforced Concrete Moment Resisting Frames," by S.W. Zagajeski and V.V. Bertero - 1977 (PB 280 137)A07

UCB/EERC-77/17 "Earthquake Simulation Testing of a Stepping Frame with Energy-Absorbing Devices," by J.M. Kelly and D.F. Tsztoo - 1977 (PB 273 506)A04

UCB/EERC-77/18 "Inelastic Behavior of Eccentrically Braced Steel Frames under Cyclic Loadings," by C.W. Roeder and E.P. Popov - 1977 (PB 275 526)A15

UCB/EERC-77/19 "A Simplified Procedure for Estimating Earthquake-Induced Deformations in Dams and Embankments," by F.I. Makdisi and H.B. Seed - 1977 (PB 276 820)A04

UCB/EERC-77/20 "The Performance of Earth Dams during Earthquakes," by H.B. Seed, F.I. Makdisi and P. de Alba - 1977 (PB 276 821)A04

UCB/EERC-77/21 "Dynamic Plastic Analysis Using Stress Resultant Finite Element Formulation," by P. Lukkunapvasit and J.M. Kelly - 1977 (PB 275 453)A04

UCB/EERC-77/22 "Preliminary Experimental Study of Seismic Uplift of a Steel Frame," by R.W. Clough and A.A. Huckelbridge 1977 (PB 278 769)A08

UCB/EERC-77/23 "Earthquake Simulator Tests of a Nine-Story Steel Frame with Columns Allowed to Uplift," by A.A. Huckelbridge - 1977 (PB 277 944)A09

UCB/EERC-77/24 "Nonlinear Soil-Structure Interaction of Skew Highway Bridges," by M.-C. Chen and J. Penzien - 1977 (PB 276 176)A07

UCB/EERC-77/25 "Seismic Analysis of an Offshore Structure Supported on Pile Foundations," by D.D.-N. Liou and J. Penzien 1977 (PB 283 180)A06

UCB/EERC-77/26 "Dynamic Stiffness Matrices for Homogeneous Viscoelastic Half-Planes," by G. Dasgupta and A.K. Chopra - 1977 (PB 279 654)A06

UCB/EERC-77/27 "A Practical Soft Story Earthquake Isolation System," by J.M. Kelly, J.M. Eidinger and C.J. Derham - 1977 (PB 276 814)A07

UCB/EERC-77/28 "Seismic Safety of Existing Buildings and Incentives for Hazard Mitigation in San Francisco: An Exploratory Study," by A.J. Meltsner - 1977 (PB 281 970)A05

UCB/EERC-77/29 "Dynamic Analysis of Electrohydraulic Shaking Tables," by D. Rea, S. Abedi-Hayati and Y. Takahashi 1977 (PB 282 569)A04

UCB/EERC-77/30 "An Approach for Improving Seismic - Resistant Behavior of Reinforced Concrete Interior Joints," by B. Galunic, V.V. Bertero and E.P. Popov - 1977 (PB 290 870)A06

UCB/EERC-78/01 "The Development of Energy-Absorbing Devices for Aseismic Base Isolation Systems," by J.M. Kelly and D.F. Tsztoo - 1978 (PB 284 978)A04

UCB/EERC-78/02 "Effect of Tensile Prestrain on the Cyclic Response of Structural Steel Connections, by J.G. Bouwkamp and A. Mukhopadhyay - 1978

UCB/EERC-78/03 "Experimental Results of an Earthquake Isolation System using Natural Rubber Bearings," by J.M. Eidinger and J.M. Kelly - 1978 (PB 281 686)A04

UCB/EERC-78/04 "Seismic Behavior of Tall Liquid Storage Tanks," by A. Niwa - 1978 (PB 284 017)A14

UCB/EERC-78/05 "Hysteretic Behavior of Reinforced Concrete Columns Subjected to High Axial and Cyclic Shear Forces," by S.W. Zagajeski, V.V. Bertero and J.G. Bouwkamp - 1978 (PB 283 858)A13

UCB/EERC-78/06 "Three Dimensional Inelastic Frame Elements for the ANSR-I Program," by A. Riahi, D.G. Row and G.H. Powell - 1978 (PB 295 755)A04

UCB/EERC-78/07 "Studies of Structural Response to Earthquake Ground Motion," by O.A. Lopez and A.K. Chopra - 1978 (PB 282 790)A05

UCB/EERC-78/08 "A Laboratory Study of the Fluid-Structure Interaction of Submerged Tanks and Caissons in Earthquakes," by R.C. Byrd - 1978 (PB 284 957)A08

UCB/EERC-78/09 Unassigned

UCB/EERC-78/10 "Seismic Performance of Nonstructural and Secondary Structural Elements," by I. Sakamoto - 1978 (PB81 154 593)A05

UCB/EERC-78/11 "Mathematical Modelling of Hysteresis Loops for Reinforced Concrete Columns," by S. Nakata, T. Sproul and J. Penzien - 1978 (PB 298 274)A05

UCB/EERC-78/12 "Damageability in Existing Buildings," by T. Blejwas and B. Bresler - 1978 (PB 80 166 978)A05

UCB/EERC-78/13 "Dynamic Behavior of a Pedestal Base Multistory Building," by R.M. Stephen, E.L. Wilson, J.G. Bouwkamp and M. Button - 1978 (PB 286 650)A08

UCB/EERC-78/14 "Seismic Response of Bridges - Case Studies," by R.A. Imbsen, V. Nutt and J. Penzien - 1978 (PB 286 503)A10

UCB/EERC-78/15 "A Substructure Technique for Nonlinear Static and Dynamic Analysis," by D.G. Row and G.H. Powell - 1978 (PB 288 077)A10

UCB/EERC-78/16 "Seismic Risk Studies for San Francisco and for the Greater San Francisco Bay Area," by C.S. Oliveira - 1978 (PB 81 120 115)A07

UCB/EERC-78/17 "Strength of Timber Roof Connections Subjected to Cyclic Loads," by P. Gülkan, R.L. Mayes and R.W. Clough - 1978 (HUD-000 1491)A07

UCB/EERC-78/18 "Response of K-Braced Steel Frame Models to Lateral Loads," by J.G. Bouwkamp, R.M. Stephen and E.P. Popov - 1978

UCB/EERC-78/19 "Rational Design Methods for Light Equipment in Structures Subjected to Ground Motion," by J.L. Sackman and J.M. Kelly - 1978 (PB 292 357)A04

UCB/EERC-78/20 "Testing of a Wind Restraint for Aseismic Base Isolation," by J.M. Kelly and D.E. Chitty - 1978 (PB 292 833)A03

UCB/EERC-78/21 "APOLLO - A Computer Program for the Analysis of Pore Pressure Generation and Dissipation in Horizontal Sand Layers During Cyclic or Earthquake Loading," by P.P. Martin and H.B. Seed - 1978 (PB 292 835)A04

UCB/EERC-78/22 "Optimal Design of an Earthquake Isolation System," by M.A. Bhatti, K.S. Pister and E. Polak - 1978 (PB 294 735)A06

UCB/EERC-78/23 "MASH - A Computer Program for the Non-Linear Analysis of Vertically Propagating Shear Waves in Horizontally Layered Deposits," by P.P. Martin and H.B. Seed - 1978 (PB 293 101)A05

UCB/EERC-78/24 "Investigation of the Elastic Characteristics of a Three Story Steel Frame Using System Identification," by I. Kaya and H.D. McNiven - 1978 (PB 296 225)A06

UCB/EERC-78/25 "Investigation of the Nonlinear Characteristics of a Three-Story Steel Frame Using System Identification," by I. Kaya and H.D. McNiven - 1978 (PB 301 363)A05

UCB/EERC-78/26 "Studies of Strong Ground Motion in Taiwan," by Y.M. Hsiung, B.A. Bolt and J. Penzien - 1978 (PB 298 436)A06

UCB/EERC-78/27 "Cyclic Loading Tests of Masonry Single Piers: Volume 1 - Height to Width Ratio of 2," by P.A. Hidalgo, R.L. Mayes, H.D. McNiven and R.W. Clough - 1978 (PB 296 211)A07

UCB/EERC-78/28 "Cyclic Loading Tests of Masonry Single Piers: Volume 2 - Height to Width Ratio of 1," by S.-W.J. Chen, P.A. Hidalgo, R.L. Mayes, R.W. Clough and H.D. McNiven - 1978 (PB 296 212)A09

UCB/EERC-78/29 "Analytical Procedures in Soil Dynamics," by J. Lysmer - 1978 (PB 298 445)A06

UCB/EERC-79/01 "Hysteretic Behavior of Lightweight Reinforced Concrete Beam-Column Subassemblages," by B. Forzani, E.P. Popov and V.V. Bertero - April 1979(PB 298 267)A06

UCB/EERC-79/02 "The Development of a Mathematical Model to Predict the Flexural Response of Reinforced Concrete Beams to Cyclic Loads, Using System Identification," by J. Stanton & H. McNiven - Jan. 1979(PB 295 875)A10

UCB/EERC-79/03 "Linear and Nonlinear Earthquake Response of Simple Torsionally Coupled Systems," by C.L. Kan and A.K. Chopra - Feb. 1979(PB 298 262)A06

UCB/EERC-79/04 "A Mathematical Model of Masonry for Predicting its Linear Seismic Response Characteristics," by Y. Mengi and H.D. McNiven - Feb. 1979(PB 298 266)A06

UCB/EERC-79/05 "Mechanical Behavior of Lightweight Concrete Confined by Different Types of Lateral Reinforcement," by M.A. Manrique, V.V. Bertero and E.P. Popov - May 1979(PB 301 114)A06

UCB/EERC-79/06 "Static Tilt Tests of a Tall Cylindrical Liquid Storage Tank," by R.W. Clough and A. Niwa - Feb. 1979 (PB 301 167)A06

UCB/EERC-79/07 "The Design of Steel Energy Absorbing Restrainers and Their Incorporation into Nuclear Power Plants for Enhanced Safety: Volume 1 - Summary Report," by P.N. Spencer, V.F. Zackay, and E.R. Parker - Feb. 1979(UCB/EERC-79/07)A09

UCB/EERC-79/08 "The Design of Steel Energy Absorbing Restrainers and Their Incorporation into Nuclear Power Plants for Enhanced Safety: Volume 2 - The Development of Analyses for Reactor System Piping,""Simple Systems" by M.C. Lee, J. Penzien, A.K. Chopra and K. Suzuki "Complex Systems" by G.H. Powell, E.L. Wilson, R.W. Clough and D.G. Row - Feb. 1979(UCB/EERC-79/08)A10

UCB/EERC-79/09 "The Design of Steel Energy Absorbing Restrainers and Their Incorporation into Nuclear Power Plants for Enhanced Safety: Volume 3 - Evaluation of Commercial Steels," by W.S. Owen, R.M.N. Pelloux, R.O. Ritchie, M. Faral, T. Ohhashi, J. Toplosky, S.J. Hartman, V.F. Zackay and E.R. Parker - Feb. 1979(UCB/EERC-79/09)A04

UCB/EERC-79/10 "The Design of Steel Energy Absorbing Restrainers and Their Incorporation into Nuclear Power Plants for Enhanced Safety: Volume 4 - A Review of Energy-Absorbing Devices," by J.M. Kelly and M.S. Skinner - Feb. 1979(UCB/EERC-79/10)A04

UCB/EERC-79/11 "Conservatism In Summation Rules for Closely Spaced Modes," by J.M. Kelly and J.L. Sackman - May 1979(PB 301 328)A03

UCB/EERC-79/12 "Cyclic Loading Tests of Masonry Single Piers; Volume 3 - Height to Width Ratio of 0.5," by P.A. Hidalgo, R.L. Mayes, H.D. McNiven and R.W. Clough - May 1979(PB 301 321)A08

UCB/EERC-79/13 "Cyclic Behavior of Dense Course-Grained Materials in Relation to the Seismic Stability of Dams," by N.G. Banerjee, H.B. Seed and C.K. Chan - June 1979(PB 301 373)A13

UCB/EERC-79/14 "Seismic Behavior of Reinforced Concrete Interior Beam-Column Subassemblages," by S. Viwathanatepa, E.P. Popov and V.V. Bertero - June 1979(PB 301 326)A10

UCB/EERC-79/15 "Optimal Design of Localized Nonlinear Systems with Dual Performance Criteria Under Earthquake Excitations," by M.A. Bhatti - July 1979(PB 80 167 109)A06

UCB/EERC-79/16 "OPTDYN - A General Purpose Optimization Program for Problems with or without Dynamic Constraints," by M.A. Bhatti, E. Polak and K.S. Pister - July 1979(PB 80 167 091)A05

UCB/EERC-79/17 "ANSR-II, Analysis of Nonlinear Structural Response, Users Manual," by D.P. Mondkar and G.H. Powell July 1979(PB 80 113 301)A05

UCB/EERC-79/18 "Soil Structure Interaction in Different Seismic Environments," A. Gomez-Masso, J. Lysmer, J.-C. Chen and H.B. Seed - August 1979(PB 80 101 520)A04

UCB/EERC-79/19 "ARMA Models for Earthquake Ground Motions," by M.K. Chang, J.W. Kwiatkowski, R.F. Nau, R.M. Oliver and K.S. Pister - July 1979(PB 301 166)A05

UCB/EERC-79/20 "Hysteretic Behavior of Reinforced Concrete Structural Walls," by J.M. Vallenas, V.V. Bertero and E.P. Popov - August 1979(PB 80 165 905)A12

UCB/EERC-79/21 "Studies on High-Frequency Vibrations of Buildings - 1: The Column Effect," by J. Lubliner - August 1979 (PB 80 158 553)A03

UCB/EERC-79/22 "Effects of Generalized Loadings on Bond Reinforcing Bars Embedded in Confined Concrete Blocks," by S. Viwathanatepa, E.P. Popov and V.V. Bertero - August 1979(PB 81 124 018)A14

UCB/EERC-79/23 "Shaking Table Study of Single-Story Masonry Houses, Volume 1: Test Structures 1 and 2," by P. Gülkan, R.L. Mayes and R.W. Clough - Sept. 1979 (HUD-000 1763)A12

UCB/EERC-79/24 "Shaking Table Study of Single-Story Masonry Houses, Volume 2: Test Structures 3 and 4," by P. Gülkan, R.L. Mayes and R.W. Clough - Sept. 1979 (HUD-000 1836)A12

UCB/EERC-79/25 "Shaking Table Study of Single-Story Masonry Houses, Volume 3: Summary, Conclusions and Recommendations," by R.W. Clough, R.L. Mayes and P. Gülkan - Sept. 1979 (HUD-000 1837)A06

UCB/EERC-79/26 "Recommendations for a U.S.-Japan Cooperative Research Program Utilizing Large-Scale Testing Facilities," by U.S.-Japan Planning Group - Sept. 1979(PB 301 407)A06

UCB/EERC-79/27 "Earthquake-Induced Liquefaction Near Lake Amatitlan, Guatemala," by H.B. Seed, I. Arango, C.K. Chan, A. Gomez-Masso and R. Grant de Ascoli - Sept. 1979(NUREG-CR1341)A03

UCB/EERC-79/28 "Infill Panels: Their Influence on Seismic Response of Buildings," by J.W. Axley and V.V. Bertero Sept. 1979(PB 80 163 371)A10

UCB/EERC-79/29 "3D Truss Bar Element (Type 1) for the ANSR-II Program," by D.P. Mondkar and G.H. Powell - Nov. 1979 (PB 80 169 709)A02

UCB/EERC-79/30 "2D Beam-Column Element (Type 5 - Parallel Element Theory) for the ANSR-II Program," by D.G. Row, G.H. Powell and D.P. Mondkar - Dec. 1979(PB 80 167 224)A03

UCB/EERC-79/31 "3D Beam-Column Element (Type 2 - Parallel Element Theory) for the ANSR-II Program," by A. Riahi, G.H. Powell and D.P. Mondkar - Dec. 1979(PB 80 167 216)A03

UCB/EERC-79/32 "On Response of Structures to Stationary Excitation," by A. Der Kiureghian - Dec. 1979(PB 80166 929)A03

UCB/EERC-79/33 "Undisturbed Sampling and Cyclic Load Testing of Sands," by S. Singh, H.B. Seed and C.K. Chan Dec. 1979(ADA 087 298)A07

UCB/EERC-79/34 "Interaction Effects of Simultaneous Torsional and Compressional Cyclic Loading of Sand," by P.M. Griffin and W.N. Houston - Dec. 1979(ADA 092 352)A15

UCB/EERC-80/01 "Earthquake Response of Concrete Gravity Dams Including Hydrodynamic and Foundation Interaction Effects," by A.K. Chopra, P. Chakrabarti and S. Gupta - Jan. 1980(AD-A087297)A10

UCB/EERC-80/02 "Rocking Response of Rigid Blocks to Earthquakes," by C.S. Yim, A.K. Chopra and J. Penzien - Jan. 1980 (PB80 166 002)A04

UCB/EERC-80/03 "Optimum Inelastic Design of Seismic-Resistant Reinforced Concrete Frame Structures," by S.W. Zagajeski and V.V. Bertero - Jan. 1980(PB80 164 635)A06

UCB/EERC-80/04 "Effects of Amount and Arrangement of Wall-Panel Reinforcement on Hysteretic Behavior of Reinforced Concrete Walls," by R. Iliya and V.V. Bertero - Feb. 1980(PB81 122 525)A09

UCB/EERC-80/05 "Shaking Table Research on Concrete Dam Models," by A. Niwa and R.W. Clough - Sept. 1980(PB81 122 368)A06

UCB/EERC-80/06 "The Design of Steel Energy-Absorbing Restrainers and their Incorporation into Nuclear Power Plants for Enhanced Safety (Vol 1A): Piping with Energy Absorbing Restrainers: Parameter Study on Small Systems," by G.H. Powell, C. Oughourlian and J. Simons - June 1980

UCB/EERC-80/07 "Inelastic Torsional Response of Structures Subjected to Earthquake Ground Motions," by Y. Yamazaki April 1980(PB81 122 327)A08

UCB/EERC-80/08 "Study of X-Braced Steel Frame Structures Under Earthquake Simulation," by Y. Ghanaat - April 1980 (PB81 122 335)A11

UCB/EERC-80/09 "Hybrid Modelling of Soil-Structure Interaction," by S. Gupta, T.W. Lin, J. Penzien and C.S. Yeh May 1980(PB81 122 319)A07

UCB/EERC-80/10 "General Applicability of a Nonlinear Model of a One Story Steel Frame," by B.I. Sveinsson and H.D. McNiven - May 1980(PB81 124 877)A06

UCB/EERC-80/11 "A Green-Function Method for Wave Interaction with a Submerged Body," by W. Kioka - April 1980 (PB81 122 269)A07

UCB/EERC-80/12 "Hydrodynamic Pressure and Added Mass for Axisymmetric Bodies," by F. Nilrat - May 1980(PB81 122 343)A08

UCB/EERC-80/13 "Treatment of Non-Linear Drag Forces Acting on Offshore Platforms," by B.V. Dao and J. Penzien May 1980(PB81 153 413)A07

UCB/EERC-80/14 "2D Plane/Axisymmetric Solid Element (Type 3 - Elastic or Elastic-Perfectly Plastic) for the ANSR-II Program," by D.P. Mondkar and G.H. Powell - July 1980(PB81 122 350)A03

UCB/EERC-80/15 "A Response Spectrum Method for Random Vibrations," by A. Der Kiureghian - June 1980(PB81 122 301)A03

UCB/EERC-80/16 "Cyclic Inelastic Buckling of Tubular Steel Braces," by V.A. Zayas, E.P. Popov and S.A. Mahin June 1980(PB81 124 985)A10

UCB/EERC-80/17 "Dynamic Response of Simple Arch Dams Including Hydrodynamic Interaction," by C.S. Porter and A.K. Chopra - July 1980(PB81 124 000)A13

UCB/EERC-80/18 "Experimental Testing of a Friction Damped Aseismic Base Isolation System with Fail-Safe Characteristics," by J.M. Kelly, K.E. Beucke and M.S. Skinner - July 1980(PB81 148 595)A04

UCB/EERC-80/19 "The Design of Steel Energy-Absorbing Restrainers and their Incorporation into Nuclear Power Plants for Enhanced Safety (Vol 1B): Stochastic Seismic Analyses of Nuclear Power Plant Structures and Piping Systems Subjected to Multiple Support Excitations," by M.C. Lee and J. Penzien - June 1980

UCB/EERC-80/20 "The Design of Steel Energy-Absorbing Restrainers and their Incorporation into Nuclear Power Plants for Enhanced Safety (Vol 1C): Numerical Method for Dynamic Substructure Analysis," by J.M. Dickens and E.L. Wilson - June 1980

UCB/EERC-80/21 "The Design of Steel Energy-Absorbing Restrainers and their Incorporation into Nuclear Power Plants for Enhanced Safety (Vol 2): Development and Testing of Restraints for Nuclear Piping Systems," by J.M. Kelly and M.S. Skinner - June 1980

UCB/EERC-80/22 "3D Solid Element (Type 4-Elastic or Elastic-Perfectly-Plastic) for the ANSR-II Program," by D.P. Mondkar and G.H. Powell - July 1980(PB81 123 242)A03

UCB/EERC-80/23 "Gap-Friction Element (Type 5) for the ANSR-II Program," by D.P. Mondkar and G.H. Powell - July 1980 (PB81 122 285)A03

UCB/EERC-80/24 "U-Bar Restraint Element (Type 11) for the ANSR-II Program," by C. Oughourlian and G.H. Powell July 1980(PB81 122 293)A03

UCB/EERC-80/25 "Testing of a Natural Rubber Base Isolation System by an Explosively Simulated Earthquake," by J.M. Kelly - August 1980(PB81 201 360)A04

UCB/EERC-80/26 "Input Identification from Structural Vibrational Response," by Y. Hu - August 1980(PB81 152 308)A05

UCB/EERC-80/27 "Cyclic Inelastic Behavior of Steel Offshore Structures," by V.A. Zayas, S.A. Mahin and E.P. Popov August 1980(PB81 196 180)A15

UCB/EERC-80/28 "Shaking Table Testing of a Reinforced Concrete Frame with Biaxial Response," by M.G. Oliva October 1980(PB81 154 304)A10

UCB/EERC-80/29 "Dynamic Properties of a Twelve-Story Prefabricated Panel Building," by J.G. Bouwkamp, J.P. Kollegger and R.M. Stephen - October 1980(PB82 117 128)A06

UCB/EERC-80/30 "Dynamic Properties of an Eight-Story Prefabricated Panel Building," by J.G. Bouwkamp, J.P. Kollegger and R.M. Stephen - October 1980(PB81 200 313)A05

UCB/EERC-80/31 "Predictive Dynamic Response of Panel Type Structures Under Earthquakes," by J.P. Kollegger and J.G. Bouwkamp - October 1980(PB81 152 316)A04

UCB/EERC-80/32 "The Design of Steel Energy-Absorbing Restrainers and their Incorporation into Nuclear Power Plants for Enhanced Safety (Vol 3): Testing of Commercial Steels in Low-Cycle Torsional Fatigue," by P. Spencer, E.R. Parker, E. Jongewaard and M. Drory

UCB/EERC-80/33 "The Design of Steel Energy-Absorbing Restrainers and their Incorporation into Nuclear Power Plants for Enhanced Safety (Vol 4): Shaking Table Tests of Piping Systems with Energy-Absorbing Restrainers," by S.F. Stiemer and W.G. Godden - Sept. 1980

UCB/EERC-80/34 "The Design of Steel Energy-Absorbing Restrainers and their Incorporation into Nuclear Power Plants for Enhanced Safety (Vol 5): Summary Report," by P. Spencer

UCB/EERC-80/35 "Experimental Testing of an Energy-Absorbing Base Isolation System," by J.M. Kelly, M.S. Skinner and K.E. Beucke - October 1980(PB81 154 072)A04

UCB/EERC-80/36 "Simulating and Analyzing Artificial Non-Stationary Earthquake Ground Motions," by R.F. Nau, R.M. Oliver and K.S. Pister - October 1980(PB81 153 397)A04

UCB/EERC-80/37 "Earthquake Engineering at Berkeley - 1980," - Sept. 1980(PB81 205 874)A09

UCB/EERC-80/38 "Inelastic Seismic Analysis of Large Panel Buildings," by V. Schricker and G.H. Powell - Sept. 1980 (PB81 154 338)A13

UCB/EERC-80/39 "Dynamic Response of Embankment, Concrete-Gravity and Arch Dams Including Hydrodynamic Interaction," by J.F. Hall and A.K. Chopra - October 1980(PB81 152 324)A11

UCB/EERC-80/40 "Inelastic Buckling of Steel Struts Under Cyclic Load Reversal," by R.G. Black, W.A. Wenger and E.P. Popov - October 1980(PB81 154 312)A08

UCB/EERC-80/41 "Influence of Site Characteristics on Building Damage During the October 3, 1974 Lima Earthquake," by P. Repetto, I. Arango and H.B. Seed - Sept. 1980(PB81 161 739)A05

UCB/EERC-80/42 "Evaluation of a Shaking Table Test Program on Response Behavior of a Two Story Reinforced Concrete Frame," by J.M. Blondet, R.W. Clough and S.A. Mahin

UCB/EERC-80/43 "Modelling of Soil-Structure Interaction by Finite and Infinite Elements," by F. Medina - December 1980(PB81 229 270)A04

UCB/EERC-81/01 "Control of Seismic Response of Piping Systems and Other Structures by Base Isolation," edited by J.M. Kelly - January 1981 (PB81 200 735)A05

UCB/EERC-81/02 "OPTNSR - An Interactive Software System for Optimal Design of Statically and Dynamically Loaded Structures with Nonlinear Response," by M.A. Bhatti, V. Ciampi and K.S. Pister - January 1981 (PB81 218 851)A09

UCB/EERC-81/03 "Analysis of Local Variations in Free Field Seismic Ground Motions," by J.-C. Chen, J. Lysmer and H.B. Seed - January 1981 (AD-A099508)A13

UCB/EERC-81/04 "Inelastic Structural Modeling of Braced Offshore Platforms for Seismic Loading," by V.A. Zayas, P.-S.B. Shing, S.A. Mahin and E.P. Popov - January 1981(PB82 138 777)A07

UCB/EERC-81/05 "Dynamic Response of Light Equipment in Structures," by A. Der Kiureghian, J.L. Sackman and B. Nour-Omid - April 1981 (PB81 218 497)A04

UCB/EERC-81/06 "Preliminary Experimental Investigation of a Broad Base Liquid Storage Tank," by J.G. Bouwkamp, J.P. Kollegger and R.M. Stephen - May 1981(PB82 140 385)A03

UCB/EERC-81/07 "The Seismic Resistant Design of Reinforced Concrete Coupled Structural Walls," by A.E. Aktan and V.V. Bertero - June 1981(PB82 113 358)A11

UCB/EERC-81/08 "The Undrained Shearing Resistance of Cohesive Soils at Large Deformations," by M.R. Pyles and H.B. Seed - August 1981

UCB/EERC-81/09 "Experimental Behavior of a Spatial Piping System with Steel Energy Absorbers Subjected to a Simulated Differential Seismic Input," by S.F. Stiemer, W.G. Godden and J.M. Kelly - July 1981

UCB/EERC-81/10 "Evaluation of Seismic Design Provisions for Masonry in the United States," by B.I. Sveinsson, R.L. Mayes and H.D. McNiven - August 1981 (PB82 166 075)A08

UCB/EERC-81/11 "Two-Dimensional Hybrid Modelling of Soil-Structure Interaction," by T.-J. Tzong, S. Gupta and J. Penzien - August 1981(PB82 142 118)A04

UCB/EERC-81/12 "Studies on Effects of Infills in Seismic Resistant R/C Construction," by S. Brokken and V.V. Bertero - September 1981 (PB82 166 190)A09

UCB/EERC-81/13 "Linear Models to Predict the Nonlinear Seismic Behavior of a One-Story Steel Frame," by H. Valdimarsson, A.H. Shah and H.D. McNiven - September 1981(PB82 138 793)A07

UCB/EERC-81/14 "TLUSH: A Computer Program for the Three-Dimensional Dynamic Analysis of Earth Dams," by T. Kagawa, L.H. Mejia, H.B. Seed and J. Lysmer - September 1981(PB82 139 940)A06

UCB/EERC-81/15 "Three Dimensional Dynamic Response Analysis of Earth Dams," by L.H. Mejia and H.B. Seed - September 1981 (PB82 137 274)A12

UCB/EERC-81/16 "Experimental Study of Lead and Elastomeric Dampers for Base Isolation Systems," by J.M. Kelly and S.B. Hodder - October 1981 (PB82 166 182)A05

UCB/EERC-81/17 "The Influence of Base Isolation on the Seismic Response of Light Secondary Equipment," by J.M. Kelly - April 1981 (PB82 255 266)A04

UCB/EERC-81/18 "Studies on Evaluation of Shaking Table Response Analysis Procedures," by J. Marcial Blondet - November 1981 (PB82 197 278)A10

UCB/EERC-81/19 "DELIGHT.STRUCT: A Computer-Aided Design Environment for Structural Engineering," by R.J. Balling, K.S. Pister and E. Polak - December 1981 (PB82 218 496)A07

UCB/EERC-81/20 "Optimal Design of Seismic-Resistant Planar Steel Frames," by R.J. Balling, V. Ciampi, K.S. Pister and E. Polak - December 1981 (PB82 220 179)A07

UCB/EERC-82/01 "Dynamic Behavior of Ground for Seismic Analysis of Lifeline Systems," by T. Sato and A. Der Kiureghian - January 1982 (PB82 218 926)A05

UCB/EERC-82/02 "Shaking Table Tests of a Tubular Steel Frame Model," by Y. Ghanaat and R. W. Clough - January 1982 (PB82 220 161)A07

UCB/EERC-82/03 "Behavior of a Piping System under Seismic Excitation: Experimental Investigations of a Spatial Piping System supported by Mechanical Shock Arrestors and Steel Energy Absorbing Devices under Seismic Excitation," by S. Schneider, H.-M. Lee and W. G. Godden - May 1982 (PB83 172 544)A09

UCB/EERC-82/04 "New Approaches for the Dynamic Analysis of Large Structural Systems," by E. L. Wilson - June 1982 (PB83 148 080)A05

UCB/EERC-82/05 "Model Study of Effects of Damage on the Vibration Properties of Steel Offshore Platforms," by F. Shahrivar and J. G. Bouwkamp - June 1982 (PB83 148 742)A10

UCB/EERC-82/06 "States of the Art and Practice in the Optimum Seismic Design and Analytical Response Prediction of R/C Frame-Wall Structures," by A. E. Aktan and V. V. Bertero - July 1982 (PB83 147 736)A05

UCB/EERC-82/07 "Further Study of the Earthquake Response of a Broad Cylindrical Liquid-Storage Tank Model," by G. C. Manos and R. W. Clough - July 1982 (PB83 147 744)A11

UCB/EERC-82/08 "An Evaluation of the Design and Analytical Seismic Response of a Seven Story Reinforced Concrete Frame - Wall Structure," by F. A. Charney and V. V. Bertero - July 1982(PB83 157 628)A09

UCB/EERC-82/09 "Fluid-Structure Interactions: Added Mass Computations for Incompressible Fluid," by J. S.-H. Kuo - August 1982 (PB83 156 281)A07

UCB/EERC-82/10 "Joint-Opening Nonlinear Mechanism: Interface Smeared Crack Model," by J. S.-H. Kuo - August 1982 (PB83 149 195)A05

UCB/EERC-82/11 "Dynamic Response Analysis of Techi Dam," by R. W. Clough, R. M. Stephen and J. S.-H. Kuo - August 1982 (PB83 147 496)A06

UCB/EERC-82/12 "Prediction of the Seismic Responses of R/C Frame-Coupled Wall Structures," by A. E. Aktan, V. V. Bertero and M. Piazza - August 1982 (PB83 149 203)A09

UCB/EERC-82/13 "Preliminary Report on the SMART 1 Strong Motion Array in Taiwan," by B. A. Bolt, C. H. Loh, J. Penzien, Y. B. Tsai and Y. T. Yeh - August 1982 (PB83 159 400)A10

UCB/EERC-82/14 "Shaking-Table Studies of an Eccentrically X-Braced Steel Structure," by M. S. Yang - September 1982 (PB83 260 778)A12

UCB/EERC-82/15 "The Performance of Stairways in Earthquakes," by C. Roha, J. W. Axley and V. V. Bertero - September 1982 (PB83 157 693)A07

UCB/EERC-82/16 "The Behavior of Submerged Multiple Bodies in Earthquakes," by W.-G. Liao - Sept. 1982 (PB83 158 709)A07

UCB/EERC-82/17 "Effects of Concrete Types and Loading Conditions on Local Bond-Slip Relationships," by A. D. Cowell, E. P. Popov and V. V. Bertero - September 1982 (PB83 153 577)A04

UCB/EERC-82/18 "Mechanical Behavior of Shear Wall Vertical Boundary Members: An Experimental Investigation," by M. T. Wagner and V. V. Bertero - October 1982 (PB83 159 764)A05

UCB/EERC-82/19 "Experimental Studies of Multi-support Seismic Loading on Piping Systems," by J. M. Kelly and A. D. Cowell - November 1982

UCB/EERC-82/20 "Generalized Plastic Hinge Concepts for 3D Beam-Column Elements," by P. F.-S. Chen and G. H. Powell - November 1982 (PB83 247 981)A13

UCB/EERC-82/21 "ANSR-III: General Purpose Computer Program for Nonlinear Structural Analysis," by C. V. Oughourlian and G. H. Powell - November 1982 (PB83 251 330)A12

UCB/EERC-82/22 "Solution Strategies for Statically Loaded Nonlinear Structures," by J. W. Simons and G. H. Powell - November 1982 (PB83 197 970)A06

UCB/EERC-82/23 "Analytical Model of Deformed Bar Anchorages under Generalized Excitations," by V. Ciampi, R. Eligehausen, V. V. Bertero and E. P. Popov - November 1982 (PB83 169 532)A06

UCB/EERC-82/24 "A Mathematical Model for the Response of Masonry Walls to Dynamic Excitations," by H. Sucuoğlu, Y. Mengi and H. D. McNiven - November 1982 (PB83 169 011)A07

UCB/EERC-82/25 "Earthquake Response Considerations of Broad Liquid Storage Tanks," by F. J. Cambra - November 1982 (PB83 251 215)A09

UCB/EERC-82/26 "Computational Models for Cyclic Plasticity, Rate Dependence and Creep," by B. Mosaddad and G. H. Powell - November 1982 (PB83 245 829)A08

UCB/EERC-82/27 "Inelastic Analysis of Piping and Tubular Structures," by M. Mahasuverachai and G. H. Powell - November 1982 (PB83 249 987)A07

UCB/EERC-83/01 "The Economic Feasibility of Seismic Rehabilitation of Buildings by Base Isolation," by J. M. Kelly - January 1983 (PB83 197 988)A05

UCB/EERC-83/02 "Seismic Moment Connections for Moment-Resisting Steel Frames," by E. P. Popov - January 1983 (PB83 195 412)A04

UCB/EERC-83/03 "Design of Links and Beam-to-Column Connections for Eccentrically Braced Steel Frames," by E. P. Popov and J. O. Malley - January 1983 (PB83 194 811)A04

UCB/EERC-83/04 "Numerical Techniques for the Evaluation of Soil-Structure Interaction Effects in the Time Domain," by E. Bayo and E. L. Wilson - February 1983 (PB83 245 605)A09

UCB/EERC-83/05 "A Transducer for Measuring the Internal Forces in the Columns of a Frame-Wall Reinforced Concrete Structure," by R. Sause and V. V. Bertero - May 1983 (PB84 119 494)A06

UCB/EERC-83/06 "Dynamic Interactions between Floating Ice and Offshore Structures," by P. Croteau - May 1983 (PB84 119 486)A16

UCB/EERC-83/07 "Dynamic Analysis of Multiply Tuned and Arbitrarily Supported Secondary Systems," by T. Igusa and A. Der Kiureghian - June 1983 (PB84 118 272)A11

UCB/EERC-83/08 "A Laboratory Study of Submerged Multi-body Systems in Earthquakes," by G. R. Ansari - June 1983 (PB83 261 842)A17

UCB/EERC-83/09 "Effects of Transient Foundation Uplift on Earthquake Response of Structures," by C.-S. Yim and A. K. Chopra - June 1983 (PB83 261 396)A07

UCB/EERC-83/10 "Optimal Design of Friction-Braced Frames under Seismic Loading," by M. A. Austin and K. S. Pister - June 1983 (PB84 119 288)A06

UCB/EERC-83/11 "Shaking Table Study of Single-Story Masonry Houses: Dynamic Performance under Three Component Seismic Input and Recommendations," by G. C. Manos, R. W. Clough and R. L. Mayes - June 1983

UCB/EERC-83/12 "Experimental Error Propagation in Pseudodynamic Testing," by P. B. Shing and S. A. Mahin - June 1983 (PB84 119 270)A09

UCB/EERC-83/13 "Experimental and Analytical Predictions of the Mechanical Characteristics of a 1/5-scale Model of a 7-story R/C Frame-Wall Building Structure," by A. E. Aktan, V. V. Bertero, A. A. Chowdhury and T. Nagashima - August 1983 (PB84 119 213)A07

UCB/EERC-83/14 "Shaking Table Tests of Large-Panel Precast Concrete Building System Assemblages," by M. G. Oliva and R. W. Clough - August 1983

UCB/EERC-83/15 "Seismic Behavior of Active Beam Links in Eccentrically Braced Frames," by K. D. Hjelmstad and E. P. Popov - July 1983 (PB84 119 676)A09

UCB/EERC-83/16 "System Identification of Structures with Joint Rotation," by J. S. Dimsdale and H. D. McNiven - July 1983

UCB/EERC-83/17 "Construction of Inelastic Response Spectra for Single-Degree-of-Freedom Systems," by S. Mahin and J. Lin - July 1983

UCB/EERC-83/18 "Interactive Computer Analysis Methods for Predicting the Inelastic Cyclic Behaviour of Structural Sections," by S. Kaba and S. Mahin - July 1983

UCB/EERC-83/19 "Effects of Bond Deterioration on Hysteretic Behavior of Reinforced Concrete Joints," by F.C. Filippou, E.P. Popov and V.V. Bertero - August 1983

UCB/EERC-83/20 "Analytical and Experimental Correlation of Large-Panel Precast Building System Performance," by M.G. Oliva, R.W. Clough, M. Velkov, P. Gavrilovic and J. Petrovski - November 1983

UCB/EERC-83/21 "Mechanical Characteristics of Materials Used in a 1/5 Scale Model of a 7-Story Reinforced Concrete Test Structure," by V.V. Bertero, A.E. Aktan, H.G. Harris and A.A. Chowdhury - September 1983

UCB/EERC-83/22 "Hybrid Modelling of Soil-Structure Interaction in Layered Media," by T.-J. Tzong and J. Penzien - October 1983

UCB/EERC-83/23 "Local Bond Stress-Slip Relationships of Deformed Bars under Generalized Excitations," by R. Eligehausen, E.P. Popov and V.V. Bertero - October 1983

UCB/EERC-83/24 "Design Considerations for Shear Links in Eccentrically Braced Frames," by J.O. Malley and E.P. Popov - November 1983

UCB/EERC-84/01 "Pseudodynamic Test Method for Seismic Performance Evaluation: Theory and Implementation," by P.-S. Shing and S.A. Mahin - January 1984

UCB/EERC-84/02 "Dynamic Response Behavior of Xiang Hong Dian Dam," by R. W. Clough, K.-T. Chang, H.-Q. Chen, R. M. Stephen, G.-L. Wang and Y. Ghanaat - April 1984